ENGINEERED MATERIALS FOR SPATIOTEMPORAL REGULATION OF MONOCYTE AND MACROPHAGE RECRUITMENT

A Dissertation
Presented to
The Academic Faculty

by

Claire E. Olingy

In Partial Fulfillment
of the Requirements for the Degree
Doctor of Philosophy in the
Wallace H. Coulter Department of Biomedical Engineering

Georgia Institute of Technology
Emory University
August 2017

ENGINEERED MATERIALS FOR SPATIOTEMPORAL REGULATION OF MONOCYTE AND MACROPHAGE RECRUITMENT

Approved by:

Edward A. Botchwey, PhD
Wallce H. Coulter Department of Biomedical Engineering
Georgia Institute of Technology

Krishnendu Roy, PhD
Wallce H. Coulter Department of Biomedical Engineering
Georgia Institute of Technology

Luke P. Brewster, MD
Division of Vascular Surgery, Department of Surgery
Emory University

Philip J. Santangelo, PhD
Wallce H. Coulter Department of Biomedical Engineering
Georgia Institute of Technology

Andrés J. García, PhD
Woodruff School of Mechanical Engineering
Petite Institute for Bioengineering and Bioscience
Georgia Institute of Technology

Date Approved: May 15, 2017

ACKNOWLEDGEMENTS

If there is one thing I have learned, it is that a PhD cannot be done in isolation. My family, mentors, friends, and colleagues have been extremely supportive over the course of my graduate education. I would like to begin my thanking my advisor, Edward Botchwey, who has pushed me to be the best I can be throughout the course of my PhD. On my first day in Ed's lab, I was immediately at the bench and assisting other graduate students. These memories remind me that being in the Botchwey lab has meant you're a part of a team from the very beginning. I remember early conversations with Ed, where I was extremely intimidated and did a lot of nodding in agreement. Since then, Ed has taught me to have confidence, both in my work and my opinions. Perhaps most importantly, Ed has taught me how to communicate science in a way that gets people excited, and makes them want to hear more (or fund you). He has taught me not to undervalue myself, to be less risk averse, and to treat every exercise or experiment as though it were the final version. While Ed and I have very different styles and personalities, this contrast has enabled me to become a better scientist and a better thinker. In short, Ed has made me feel like I can tackle any problem, and to me, that is what a PhD is truly about.

I am extremely grateful for the expertise and insight my thesis committee has provided, which includes Drs. Luke Brewster, Andrés García, Krishnendu Roy, and Phil Santangelo. Their constructive feedback and guidance has focused my thesis work and made it better. In particular, I'd like to thank Dr. García for his willingness to provide advice, his valuable insight on science and science careers, and encouraging me in ongoing collaboration with his lab. I'd also like to thank the professors who I had the opportunity

to work with during my teaching assistantship, Dr. Johnna Temenoff and James Rains. Dr. Temenoff taught me many of the traditional aspects of great teaching, while Professor Rains taught me the valuable lesson of how to give students good feedback. Both of these experiences reinforced my love for teaching.

My labmates are the primary reason that I consider my time as a PhD student to have been both a successful and joyful time in my life. When I joined the Botchwey lab at the University of Virginia, Cynthia Huang was the person who first recruited me to join the lab. I am extremely grateful for her early guidance and friendship. Dr. Anusuya Das was my first mentor in the lab, and I thank her for helping me transition from an inexperience undergraduate to an independent graduate student. I can't imagine where I would be today without the mentorship and friendship of Dr. Molly Ogle. I have worked collaboratively with Molly more than anyone else in the lab, and I think we make a pretty great team. Molly has been one of the most influential people during my PhD, teaching me everything from molecular biology techniques and mouse work, to how to be a better writer and keep a lab running. She is the best person to provide gentle critique before a talk, gives compliments when they are most needed, and provides support to everyone in the lab. I'd also like to thank Cheryl San Emeterio, for being both my closest friend in graduate school, but also a great co-worker and fellow scientist. She is one of the best listeners I have ever met, and always sympathizes and provides great advice. Thanks to Nathan Chiappa for all of his help around the lab, broadening my exposure to other fields during my PhD, and being a good friend. Thanks to Caitlin Sok for sitting next to me and never making me feel like I'm distracting her when I talk to her. Thanks to Jack Krieger for the numerous conversations on troubleshooting, experimental design, and data analysis, and also for

always being the first person to take a second slice of cake. Thanks to Jada Selma, Tiffany Wang, Dr. Tony Awojoodu, Dan Bowers, and Dr. Hannah Song who have made the lab a better place to work. When your co-workers are also your friends, work feels a little bit less like work. I would also like to acknowledge Jose Garcia and other members of the García lab who I worked collaboratively with throughout my thesis research. I can't imagine what graduate school would have been like without my friends outside the lab, particularly Betsy Campbell, Candice Hovell, and Giuli Salazar-Noratto, who provided the welcome occasional distraction from work, including oyster happy hours, craft nights, and frequent lunches. I will always treasure the memories I made with these friends during graduate school.

I have worked with many great undergraduates during the course of my PhD, who have given me the reward of mentorship and helped me accomplish more than I could have alone. Chris Jreige had the best attitude and made friends with everyone in the lab. Brett Jordan's attention to detail, especially when editing our manuscript, was greatly appreciated. Shane Chu's work ethic and independence made him very successful in the lab and I appreciated his willingness to help out with anything. Jerrell Fang has been extremely helpful during the last few months of my PhD. He is always willing to contribute in whatever way possible, including performing extremely repetitive (but important!) tasks. I have also had the opportunity to mentor two high school students, Jovanay Carter and Amadou Bah. Watching their development as critical thinkers and young scientists was extremely rewarding, especially now that they are attending some of the best colleges in the country.

Georgia Tech is one of the best places to do research, and that is in no small part due to the staff that support our research. I would like to thank Dr. Laura O'Farrell, Dr. Richard Noel, Kim Benjamin, Andrea Gibson, Altair Rivas, Ogeda Blue, and all of the Physiological Research Lab staff for providing care to the animals that help make our research possible. Their expertise and passion for ensuring animal welfare makes the work of all Georgia Tech researchers using the PRL easier and more enjoyable. I would also like to thank the core facilities staff for their limitless expertise and willingness to be of help. In particular, Andrew Shaw is always willing to go above and beyond to help. Additionally, thank you Nadia Boguslavsky for her flexibility and always helping me accomplish what I need to, as well as Steve Woodard for the support he provides and continuing to make the core facilities even better. I'd like to thank the many members of the BME and IBB staff who help our community run, as well as make it an enjoyable place to work. In particular, Colly Mitchell has been a welcoming resource throughout my time in the Petit Institute and during my leadership of BBUGS. Shannon Sullivan has been endlessly supportive, both in making BME a better program over the course of PhD, but also in helping me with administrative tasks, even when I didn't do things correctly. I have always appreciated Karen Ethier's willingness to help me with anything I needed, and Michelle Wong's enthusiasm for getting to know the students within the Petit Institute. Other staff including Floyd Wood, Allen Echols, Tracy Dinkins, Sandra Powell, Laura Paige, Maria Pinto, and Leilani Burkhead have generously helped me during my time at Georgia Tech.

I have been extremely fortunate to have received external funding that has supported my thesis research, including a National Science Foundation Graduate Research Fellowship and an American Heart Association Predoctoral Fellowship. Additionally, I

was honored with a P.E.O. Scholar Award, which was a great support for my studies. This scholarship also introduced me to the women of P.E.O. Chapter B, who have been my greatest cheerleaders and shown me so much support, particularly Ruth Anne Paradice, Jan Metcalf, Pat Holbrook, and Becky Battle.

There are many people in my life who I will be forever grateful to for the love and support they have shown me throughout my many years of schooling. My dad inspired me from an early age to love math and science, and encouraged me to pursue biomedical engineering, even when everyone told me they had never heard of it. My mom has been a constant source of love and support, always making me feel like I can do anything and encouraging me every step of the way. My sister has always been my best friend and loves to brag to others about me or tell me how proud she is. My family has shaped who I am today and what I've been able to accomplish, for which I am extremely grateful. My new in-laws, Jeff and Julie Olingy, have been exceedingly supportive, particularly as my husband and I move from our home in Atlanta that is two hours away from them, to our new home in California. They have embraced me as one of their own and been extremely supportive of my career. Other new family, including Matt Olingy, Autumn Rosser, and Jessica, Brian, Jackson, and Brayden Hay have given me many great memories over the past 5 years, and I look forward to many more.

The last person who I would like to thank is my husband, Mike Olingy. Mike has supported me since the beginning of my studies in biomedical engineering when we met at Washington University in St. Louis. Mike is my biggest supporter and makes me feel like I can accomplish anything. Most importantly, he is my constant reminder of what truly matters in life. I also can't end without saying how grateful I am for my hound dog, Vesper,

who is both the cutest and most strong-willed dog I have ever met, but who has provided much-needed laughs, playtime, and cuddles during the course of my PhD. Our little family makes me excited for the future and I can't wait to see what the next step holds.

TABLE OF CONTENTS

LIST OF TABLES

LIST OF FIGURES

LIST OF SYMBOLS AND ABBREVIATIONS

ANOVA	Analysis of variance
BSA	Bovine serum albumin
BMP	Bone morphogenetic protein
CCL	CC-chemokine ligand
CCR	CC-chemokine receptor
cMoP	Common monocyte progenitor
CD	Cluster of differentiation
CO_2	Carbon dioxide
CXCL	C-X-C ligand
CXCR4	C-X-C chemokine receptor 4
CX3CR1	C-X3-C chemokine receptor 1
$CX3CR1^{GFP/+}$	B6.129P-Cx3cr1tm1Litt/J mice
DC	Dendritic cell
DMEM	Dulbecco's Modified Eagle Media
DWC	Dorsal skinfold window chamber
ECM	Extracellular matrix
FBGC	Foreign body giant cells
FBS	Fetal bovine serum
FGF	Fibroblast growth factor
GFP	Green fluorescent protein
GM-CSF	Granulocyte-macrophage colony stimulating factor
GTP	Guanosine triphosphate

IACUC	Institutional Animal Care and Use Committee
IGF	Insulin-like growth factor
IHC	Immunohistochemistry
IL	Interleukin
iNOS	Inducible nitric oxide synthase
IFN	interferon
i.p.	Intraperitoneally
LFA-1	Lymphocyte function-associated antigen 1
LPS	Lipopolysaccharide
kDa	Kilodalton
kPa	Kilopascal
Mafia	Macrophage fas-induced apoptosis transgenic mice
MCP-1	Monocyte chemoattractant protein-1
M-CSF	Macrophage colony stimulating factor
MDP	Macrophage-dendritic cell precursor
MerTK	Mer receptor tyrosine kinase
mg/kg	Milogram per kilogram
MMP	Matrix metalloproteinase
M1	Classically activated inflammatory macrophage
M2	Alternatively activated macrophages
NIH	National Institutes of Health
NR4A1	Nuclear receptor subfamily 4 group A member 1
PBS	Phosphate buffered saline
PCA	Principle component analysis
PEG	Poly(ethylene glycol)

PEG-MAL	4-arm poly(ethylene glycol)-maleimide
PLGA	Poly(lactic-co-glycolic acid)
PDGF	Platelet-derived growth factor
RDG	(Argine-aspartic acid-glycine) scrambled peptide
RELMα	Resistin-like molecular alpha
RGD	(Arginine-glycine-aspartic acid) peptide
ROS	Radical oxygen species
SSC	Side scatter
SDF-1	Stromal cell-derived factor-1
S.E.M.	Standard error of the mean
S1P	Sphingosine-1-phosphate
S1PR	Sphingosine-1-phosphate receptor
SPHK	Sphingosine kinase
TIMP	Tissue inhibitor of matrix metalloproteinase
TGF-ß	Transforming growth factor-beta
T_H	T helper
TNF- α	Tumor necrosis factor-alpha
VCAM-1	Vascular cell adhesion molecule 1
VEGF	Vascular endothelial growth factor
VPM	Valine-proline-methionine peptide
WT	Wildtype
3D	Three-dimensional
2D	Two-dimensional

SUMMARY

Significant advances have been made in the development of materials that better mimic native tissues through incorporation of biofunctionality, transplantation of exogenous cells, and recapitulation of host tissue mechanical and structural properties. While these advances have generated promising pre-clinical results, biomaterial implantation still faces several challenges, including proper integration into host tissue, vascularization, and circumventing fibrosis and the foreign body response. Successful tissue repair requires the activities of myeloid cells such as monocytes and macrophages that guide the progression of inflammation and healing outcome. Materials that balance the reparative and inflammatory functions of endogenous immune cells represent a promising strategy to enhance the efficacy of biomaterial-based regenerative strategies. A deeper understanding of innate immune cell function in inflamed tissues and their subsequent interactions with implanted materials is necessary to guide the design of these materials.

Monocytes and macrophages display significant heterogeneity *in vivo*, enabling them to perform extremely varied and tissue-specific functions. Blood monocytes are composed of classical and non-classical subsets, while macrophages display many phenotypes in response to a wide variety of polarizing cues. Alternatively activated macrophages that produce anti-inflammatory mediators and growth factors have been associated with repair of muscle, bone, nerve, and skin, as well as with favorable host response to material implantation. In the current work, we expanded understanding of the relationship between blood monocyte subsets and alternatively activated macrophages, as well as identified potential targets by which to modulate monocyte recruitment.

Subsequently, we explored how biomolecule release and adhesive ligand presentation from materials impact myeloid cell recruitment and contributions to post-injury vascularization.

We demonstrated that circulating non-classical monocytes are directly recruited to polymer films implanted in skin injuries, where they generate alternatively activated, wound healing macrophages. These results highlight non-classical monocytes as key regulators of inflammatory response and motivated the use of materials that selectively target their recruitment. Subsequently, we examined the effect of FTY720 delivery from poly(lactic-*co*-glycolic acid) materials on accumulation of monocyte and macrophage subsets within injured skin and muscle. We found that local FTY720 delivery promotes accumulation of alternatively activated macrophages that are derived at least in part from circulating non-classical monocytes. FTY720-mediated immunomodulation enhanced vascularization, collagen matrix deposition, and non-fibrotic muscle regeneration in a mouse model of volumetric muscle loss.

We also explored the kinetics of myeloid cell recruitment in response to adhesive ligand functionalization and angiogenic growth factor delivery from degradable poly(ethylene glycol) hydrogels. The temporal progression of inflammation around subcutaneously implanted hydrogels was not significantly affected by the presence of RGD adhesive ligand; however real-time intravital imaging revealed that myeloid cells migrate faster in the presence of RGD-functionalized materials. Delivery of vascular endothelial growth factor (VEGF) enhanced recruitment of monocytes and dendritic cells, but decreased the frequency of macrophages. In the presence of RGD, VEGF promoted vascular network expansion. Taken together, these findings identify therapeutic targets within the innate immune system for overcoming challenges in the field of biomaterials,

including proper integration into host tissue, vascularization, and minimizing fibrosis. These results provide previously unknown insight into the value of leveraging endogenous populations of pro-regenerative monocytes and macrophages during tissue repair.

1. INTRODUCTION AND SPECIFIC AIMS

Introduction

Successful tissue repair requires the activities of myeloid cells such as monocytes and macrophages that guide the progression of inflammation and healing outcome. Materials that leverage the function of endogenous immune cells to orchestrate mechanisms of repair represents a promising strategy to enhance the efficacy of biomaterial-based regenerative strategies; however, a deeper understanding of the trafficking of immune cells and their subsequent interactions with implanted materials is necessary to guide the design of these materials.

The *objective* of this work is to engineer materials that tune myeloid cell recruitment and function to improve post-injury revascularization and tissue repair. Myeloid cells are the primary responders to material implantation and are critical to processes such as vascularization, extracellular matrix remodeling, and stimulating local progenitor cell activities. By dynamically modulating monocyte/macrophages recruitment, novel roles for these cells in repair of damaged tissues can be revealed. In this work, we first expanded understanding of the relationship between blood monocyte subsets and alternatively activated macrophages, as well as identified potential targets by which to modulate monocyte recruitment. Subsequently, we explored how biomolecule release and adhesive ligand presentation impact myeloid cell recruitment and contributions to post-injury vascularization.

Aim 1: Investigate the contribution of circulating monocyte subsets to the pool of alternatively activated wound macrophages during traumatic skin injury.

Alternatively activated macrophages have been associated with improved functional outcomes in a variety of injury contexts, including myocardial infarction, peripheral nerve injury, and dermal wounds. With these observations in mind, this aim sought to identify monocytic precursors of pro-regenerative macrophage populations to inform the design of materials that better leverage endogenous immune cell populations. We *hypothesized* that circulation-derived non-classical monocytes selectively differentiate into alternatively activated macrophages during soft tissue injury. Using a murine model of excisional skin injury, the relationship between circulating monocyte subsets and wound macrophages was evaluated. The trafficking and fate of monocyte subsets was tracked using complementary *in situ* bead-based labeling, adoptive transfer of sorted monocyte subsets, and monocyte depletion techniques. Flow cytometry-based immunophenotyping was used to characterize expression of chemokine receptors on monocyte subsets to identify potential therapeutic targets for enhancing recruitment of specific myeloid cell populations.

Aim 2: Examine the effects of biomaterial-based FTY720 delivery on wound monocyte/macrophage accumulation, revascularization, and muscle repair.

Targeting the recruitment and function of endogenous immune cell populations represents a promising strategy to enhance the efficacy of biomaterial-guided soft tissue repair. We have demonstrated that incorporation of molecules that target sphingosine-1-phosphate receptor (S1PR) signaling such as FTY720 modulate the inflammatory response

and promote microvascular remodeling. We *hypothesized* that FTY720 delivery from a poly(lactic-co-glycolic acid) implant would enhance accumulation of alternatively activated macrophages in ischemic and traumatic muscle injuries. Also, we hypothesized that FTY720 delivery would promote revascularization and muscle repair. To address these hypotheses, we examined the effect of FTY720 delivery on accumulation of pro-regenerative myeloid subsets after skin and muscle injury, and whether these cells are associated with subsequent processes of repair. We utilized a novel mouse model of volumetric muscle injury to more closely study tissue repair and investigate vascularization, matrix deposition, and muscle fiber regeneration using high power confocal microscopy.

Aim 3: Investigate the impact of adhesive ligand functionalization and vascular endothelial growth factor delivery on myeloid cell recruitment to degradable poly(ethylene glycol) hydrogels.

Significant advances have been made in the development of materials that better mimic native tissues; however how these materials interact with the host immune system after implantation remains incompletely understood. We *hypothesized* that incorporation of bioadhesive ligands and vascular endothelial growth factor (VEGF) into poly(ethylene glycol) (PEG) hydrogels would enhance myeloid cell recruitment and promote vascularization. To test this hypothesis, we characterized the progression of inflammation around protease-degradable PEG hydrogels functionalized with Arg-Gly-Asp (RGD) peptide and covalently-tethered VEGF using high-dimensional flow cytometry data paired with real-time intravital image acquisition. Using a mouse subcutaneous implantation model, the inflammatory response was characterized using flow cytometry-based

immunophenotyping. Real-time interactions of myeloid cells with the hydrogel surface were visualized using intravital confocal microscopy in mouse dorsal skinfold window chambers.

Significance

The work presented in this thesis represents a *significant* contribution to the fields of biomaterials and regenerative medicine by demonstrating that modulation of mononuclear phagocyte accumulation around biomaterial implants can enhance vascularization and tissue repair. By investigating the recruitment of myeloid cells to implanted biomaterials, we revealed several key findings: 1) Non-classical monocytes differentiate into wound healing macrophages within cutaneous wounds, 2) Biomaterial-delivered FTY720 enhances wound healing macrophage accumulation, vascularization, and non-fibrotic repair during muscle injury, 3) Both PEG hydrogel implantation and RGD functionalization enhance the speed of myeloid cells migrating within skin injuries, and 4) Degradable PEG hydrogels promote accumulation of alternatively activated macrophages, which is further enhanced by VEGF delivery. These findings identify non-classical monocytes and alternatively activated macrophages as therapeutic targets for strategies attempting to overcome challenges facing biomaterials, including proper integration into host tissue, vascularization, and circumventing fibrosis. Taken together, these results provide previously unknown insight into the value of leveraging endogenous populations of pro-regenerative monocytes and macrophages during soft tissue repair.

2. THE ROLE OF MONOCYTES AND MACROPHAGES IN TISSUE REPAIR: IMPLICATIONS FOR IMMUNOREGENERATIVE BIOMATERIAL DESIGN[1]

2.1 The mononuclear phagocyte system

2.1.1 Development of the mononuclear phagocyte system

The innate immune system plays a critical role in tissue development, homeostasis, and repair of injured tissues. Monocytes and macrophages are among the first responders to tissue injury and are required for successful tissue regeneration [1-7]. The striking evolutionary examples of complex tissue regeneration in the salamander limb and zebrafish tailfin require the presence of myeloid cells and regeneration fails when macrophages are depleted prior to injury [2, 3]. Increasing evidence suggests that division of labor among subpopulations of monocytes and macrophages could allow for harnessing regenerative functions over inflammatory functions of myeloid cells [7-11]; however, the complex balance between necessary functions of inflammatory versus regenerative myeloid cells remains to be fully understood [12].

Monocytes (immunophenotyped as $CD115^{+}CD11b^{+}SSC^{low}$ cells) differentiate from hematopoietic stem and progenitor cells in the bone marrow, and traffic to the blood and spleen of vertebrates during homeostasis. Monocytes are robustly recruited to tissue injury

[1]Adapted from: Ogle ME, Segar CE, Sridhar S, Botchwey EA, Monocytes and macrophages in tissue repair: Implications for immunoregenerative biomaterial design. Exp Biol Med (241) pp. 1084-97. Copyright © 2016. Reprinted by permission of SAGE publications.

or infection as effector cells and as progenitors of macrophages and dendritic cells [1, 13, 14]. As effectors, monocytes participate in coordinating efforts between the innate and adaptive immune response [10, 11, 15, 16], killing microbial pathogens and parasites such as *Leishmania major* [17], and promoting repair of damaged tissues [4, 8, 18, 19]. Myeloid cells responding to injuries typically secrete inflammatory cytokines and chemokines, phagocytose necrotic debris, secrete proteolytic and matrix remodeling proteins, and produce growth factors upon entry to the tissue [1, 20].

Macrophages ($MerTK^{+}CD64^{+}$) [21] have many important tissue functions in development, homeostasis, and tissue repair [22-25]. Some macrophages are the descendants of circulating monocytes and are replenished at steady state and during inflammation by blood-derived monocytes [13, 26]. Considerable evidence also supports a model of multiple origins for macrophages, where some macrophages are derived from embryonic sources and self-maintain locally in tissues throughout adulthood [14, 27, 28]. Specifically, populations of tissue macrophages of the heart, lung, brain, skin, and liver are derived prenatally [14, 29-31]. Some injury contexts, such as T_H2-linked infection, can increase local tissue macrophage populations specifically through proliferation as opposed to monocyte recruitment from the blood [27]. Characterization of gene expression signatures among macrophage populations from different tissues, species, and activation states reveal marked heterogeneity based on these factors [21, 32]. These studies suggest that "macrophage" is an umbrella term covering cells that have remarkable diversity in gene and protein expression and function [21, 26, 32, 33] (**Table 1**). Despite the diversity of macrophage origin [26], tissue environment [34], and secondary pathologies [12], macrophages (tissue resident and monocyte-derived) seem to share the common expression

signature of MerTK and CD64 across populations [21]. Like monocytes, macrophage functional diversity is described as a continuum from inflammatory to anti-inflammatory macrophages and plasticity is believed to be retained in order to rapidly respond to microenvironmental changes [33]. As current dogma continues to evolve concerning the origin of tissue macrophages, evidence suggests the diversity in macrophage phenotypes likely extends beyond stimulating factors to cell ontogeny, tissue residence, and other environmental factors.

2.1.2 Monocyte heterogeneity

Cell surface markers and functional activities distinguish multiple subsets of monocytes that include classical inflammatory and non-classical or patrolling (**Table 1**). Each monocyte subset responds to distinct chemotactic and trophic cues and equivalent subsets have been identified across multiple vertebrate species, including human, mouse, and rat [16, 35-37]. Dynamic and biphasic recruitment of monocyte subsets is a key feature of the early inflammatory response. Monocytes either persist in tissue as monocytes, repolarize to a different monocyte subset, or differentiate into macrophages [19]. Heterogeneity in the function and differentiation potential of monocyte subsets is important to consider in designing therapies to manipulate the innate immune microenvironment, particularly which subset to recruit and how to educate the cells upon recruitment to perform a desired function.

Classical monocytes are characterized by high surface expression of Ly6C and CCR2, but low expression of CX3CR1 in mice [16]. Low expression of CD43 in rat indicates an equivalent population [36]. The human classical inflammatory subset is

$CD14^+CD16^-$ [16, 35] and an intermediate population expressing both CD14 and CD16 [1]. Classical monocytes are derived from a dividing macrophage-dendritic cell precursor (MDP) or common monocyte progenitor (cMoP) in the bone marrow [38, 39] and have a half-life of about 20 hours in the blood during homeostasis [14]. They are elevated in circulation following inflammatory injury with a peak concentration near 48 hours, and the magnitude of mobilization scales with the severity of the inflammatory injury [40].

Table 1. Monocyte and macrophage subset characteristics.

Subset	Polarizing cues	Common surface markers	Distinguishing surface markers	Protein/gene expression	Reference
Classical monocyte	Unknown	$CD115^+$ $CD11b^+$ CX3CR1+	Mouse: $Ly6C^{hi}$, $CX3CR1^{lo}$, $CCR2^{hi}$ Human: $CD14^+CD16^-$ Rat: $CD43^{lo}$	TNFα, IL1β	[4, 16]
Non-classical monocyte	Unknown		Mouse: $Ly6C^{lo}$, $CX3CR1^{hi}$, $CCR2^-$ Human: $CD14^{lo/-}CD16^+$ Rat: $CD43^{hi}$	TGFβ, IL10	[4, 16]
M1	IFNγ, LPS, TNFα, GM-CSF	$MerTK^+$ $CD64^+$ [21]	CCR7, CD80, MHC II	IL1β, TNFα, IL6, IL8, IL12, IL23, iNOS, CXCL10 (IP-10), CXCL11 (IP-9), IFNγ, CCL1, CCL5, VEGF, FGF	[10, 32, 41-43]
M2a	IL-4, IL-13		CD206	CCL17, CCL18, CCL22, PDGF-BB, TIMP-3, Arginase 1, YM1, Fizz1/RELMα, IL-27Rα, CXCR4, IGF1	[10, 32, 41-44]
M2b	Immune complexes plus TLR or IL-1 agonist		CD86, MHCII	IL10, CCL1, CXCL3, IL6, TNFα, SPHK1, iNOS	[11, 42, 44]
M2c	IL-10, glucocorticoid hormones		CD163, MHCII	IL10, MMP9, IL1β,	[32, 41, 42, 45]

TNF, Tumor necrosis factor; IL, interleukin; iNOS, inducible nitric oxide synthase; CCL, CC-chemokine ligand; CXCL, C-X-C motif ligand; IFN, interferon; VEGF, vascular endothelial growth factor; FGF, fibroblast growth factor; PDGF-BB, platelet-derived growth factor; TIMP, tissue inhibitor of metalloproteinase; YM1, chitinase-like 3; Fizz1/RELMα, resistin-like molecule alpha1; IGF1, insulin-like growth factor 1; SPHK1, sphingosine kinase 1; MMP9, matrix metalloproteinase 9

The source of this increase is likely mobilization from primary reservoirs in the bone marrow and spleen [46] and requires expression of CCR2 [14]. Early during the innate immune response, classical monocytes are recruited from blood to sites of inflammation utilizing integrin $\alpha_4\beta_1$ and L-selectin (CD62L) to arrest on the endothelium [47-49] and chemokine receptors CCR2 and CCR5 to migrate toward gradients of inflammatory cytokines such as monocyte chemoattractant protein-1 (MCP-1) [1, 50]. While classical monocytes are sparsely adherent and motile on the endothelium during steady-state, they rapidly adhere and transmigrate through the endothelium when the vessel is activated with inflammatory cytokines such as tumor necrosis factor α (TNF-α) or interferon gamma (IFN-γ) [48]. The MCP-1/CCR2 signaling axis is a major experimental tool for exploring the role of classical monocytes in tissue injury and could be utilized in biomaterials to specifically target classical monocyte recruitment.

Non-classical monocytes have recently emerged as pro-regenerative cells that support activities such as matrix remodeling, arteriogenesis, and prevention of fibrosis [1, 8, 9, 20]. Non-classical monocytes are characteristically $Ly6C^{lo}$, $CCR2^{-}$ and $CX3CR1^{hi}$ in mice, $CD14^{lo}CD16^{+}$ and $CX3CR1^{+}$ in human, and $CD43^{hi}$ in rat [16, 35, 36] (**Table 1**). In addition, these monocytes express a particular signature of adhesion molecules, including high lymphocyte function-associated antigen 1 (LFA-1 or $\alpha_L\beta_2$ integrin) and low CD62L [1] that allow them to "patrol" or crawl on blood vessel walls during homeostasis [48, 49]. At steady-state, non-classical monocytes maintain a half-life in the blood of greater than two days, which is more than double the half-life of their classical counterparts [14]. Interestingly, knockout of CCR2 reduces increases the circulation half-life of non-classical monocytes to approximately 11 days, suggesting that classical monocytes limit

their lifespan of at steady state [14]. Two models exist for the origin of non-classical monocytes in blood circulation: they may differentiate from classical monocytes or directly from a MDP in the bone marrow [14, 38, 51]. Fate mapping, adoptive transfer, and new intravital imaging studies have elegantly shown transition of labeled classical monocytes to non-classical monocytes; however, these studies do not exclude the possibility that some are derived directly from progenitors in the bone marrow [4, 14, 16, 19, 38, 51]. Further evidence suggests that this differentiation is unidirectional [16]. The signals controlling the switch from classical to non-classical monocyte are not clear, although recent work suggests the transcription factor NR4A1 controls the development of non-classical monocytes and NR4A1 knockout mice have fewer non-classical monocytes in blood [51].

Chemokine receptors that distinguish monocyte subsets may be particularly useful in impacting selective recruitment or activity of this subset. Non-classical monocytes exhibit higher migration to gradients of CX3CL1 due their higher expression of the cognate receptor CX3CR1 than classical monocytes [16, 52]. Additional chemotactic receptors, including the sphingosine-1-phosphate receptor 3 (S1PR3) and C-X-C chemokine receptor 4 (CXCR4), are higher on non-classical monocytes and may contribute to enhanced sensitization to regenerative chemotactic signals [9, 16, 53, 54]. We have recently shown that localized release of SDF-1α, a CXCR4 ligand, or the S1PR3-targeting small molecule FTY720 can increase the recruitment of non-classical monocytes into injured skin tissue and position the cells along a gradient from the biomaterial source [9, 53, 54]. SDF-1α may also work in tandem with vascular endothelial growth factor (VEGF) to position monocytes in a perivascular niche in order to facilitate their role in vascular repair [55, 56]. Localized signals from biomaterials provide a powerful *in situ* opportunity to recruit cells along an

engineered gradient and also "educate" or modulate the response of recruited cells without impacting systemic inflammatory responses [9, 53, 54, 56, 57]. A clearer understanding of the signals that different monocytes respond to *in vivo* could provide valuable tools for engineering their recruitment and activity within injured tissues and biomaterial implants.

2.1.3 Macrophage heterogeneity

Inflammatory macrophages (M1) are the classically activated subset of macrophage. *In vitro*, naïve macrophages can be polarized to an M1 phenotype by treatment with IFN-γ, microbial stimuli such as lipopolysaccharide (LPS), and/or inflammatory cytokines such as TNF-α [42]. These cells produce many inflammatory cytokines, reactive oxygen species (ROS), and growth factors such as VEGF and FGF2 [41, 58] upon stimulation (**Table 1**). IFN-γ can be provided in inflamed tissue by natural killer cells and T helper 1 (T_H1) cells to activate or polarize macrophages [10]. The inflammatory cytokines produced by M1 macrophages support host defense through pathogen clearance, necrotic tissue clearance and activation of additional immune populations. Over-stimulation or failure to resolve the M1 response can be detrimental through activation and propagation of T_H17 cells, which can contribute to tissue damage and autoimmune disease pathologies when not properly regulated [10].

Anti-inflammatory macrophages (M2) are also known as "alternatively activated" macrophages due to a different set of activation signals compared to the M1 subset. This group of macrophages can be further subdivided into M2a, M2b, and M2c based on activation signals, cell surface receptors, and functional diversity (**Table 1**). *In vitro*, naïve macrophages can be polarized to an M2a phenotype by treatment with IL-4 receptor ligands

IL-4 and/or IL-13; an M2b phenotype can be achieved by treatment with immune complexes combined with toll-like receptor (TLR) or IL-1R ligands; and M2c macrophages are generated by IL-10 stimulation [42]. M2a macrophages, also called wound healing macrophages, express high levels of arginase 1 in response to IL-4, which allows them to generate precursors for collagen and fibroblast stimulating factors, thus supporting their role in extracellular matrix deposition and wound closure [10]. This matrix-remodeling role of M2a cells allows them to contribute to wound stabilization; however, must be carefully coordinated to avoid creating undesirable fibrotic changes in an injured tissue or surrounding a biomaterial implant [10, 45]. M2b and M2c macrophages contribute to suppressing inflammation through secretion of IL-10 [10]. M2 macrophages retain a great deal of plasticity and are thought to be able to shift through various transition states between M2a-c. A greater understanding of their specific functions *in vivo* has been difficult due to the complexity of signal integration and the lack of defined set of distinguishing markers for each class of macrophage.

The monocyte to macrophage transition, particularly the phenotypes each monocyte subset produces and under what circumstances is the target of much recent investigation. Most studies support a model where classical monocytes are recruited to tissues and convert to non-classical monocytes and then to macrophages [4]. Some studies contend that non-classical monocytes are directly recruited from blood to supply monocyte-derived macrophages [8, 9, 59]. This distinction could be attributed to differences in tissue injury context; however, experiments to directly test this idea in injury models have not been performed [26]. Additionally, tissue monocytes that are

phenotypically similar to non-classical monocytes in terms of surface marker expression may differ significantly in function.

2.2 Functions of monocytes and macrophages in tissue repair

The site of tissue injury can be functionally equated to a niche, or "injury niche," based on localized complex signaling that orchestrates the progression of inflammation and healing. After injury, rapid, spatially-controlled changes occur within the tissue through the evolutionarily-conserved endogenous program of clean-up, repair, and regeneration. The tissue microenvironment becomes rich with signals to recruit, position, and functionally instruct cells of the inflammatory system to program repair and inflammation resolution. Recruited cells further propagate the response by releasing their own paracrine signals that continue to guide inflammation even after their apoptotic clearance, as well as guide the activities of stem and progenitor cells present in the damaged tissue.

Each tissue injury niche has a unique set of damage, recruitment, and education signals coordinating the repair response that arise from specialization within the tissue composition and the type of injury. Unique microenvironmental cues are created by sterile inflammation versus pathogen-mediated inflammation due to the damage-associated molecular patterns recognized by inflammatory cells rather than pathogen-associated molecular patterns. Similarly, ischemic injury can activate signaling divergent from traumatic injury based on induction of hypoxia signaling and ROS. Upon recruitment from the vasculature, monocytes differentiate into macrophages based on signals they encounter within the injury niche. Physiology/biology of the particular tissue also significantly impacts the way the injury niche orchestrates repair. For example, repair of a bony structure

requires vastly different activities than regeneration of skeletal muscle. The local stromal cell and tissue resident macrophage populations, mechanical properties and organization of the tissue, and extent of vascularization and oxygenation could all contribute to differential engagement of immune cell populations *in situ*.

2.2.1 Monocytes/macrophages in vascular remodelling

Vasculature is a universal necessity for the delivery of oxygen and nutrients to tissue and vascular damage is a common feature of many injury sites. Ischemic and traumatic injuries produce vascular damage and induce the two major processes of post-developmental vascular remodeling: angiogenesis and arteriogenesis. Regenerative therapies, including biomaterials or tissue engineered constructs, similarly must ensure proper oxygen and nutrient supply through remodeling or expansion of existing vascular networks [60]. Monocytes and macrophages have been implicated in supporting vascular network remodeling and growth in development, homeostasis, and repair [7, 23, 53-55, 61-63] (**Figure 1**). During development, embryonic macrophages similar to an M2 phenotype physically associate with sprouting angiogenic tip cells to guide connections between fusing vessels in both murine and zebrafish models [23]. This direct association of macrophage and endothelial cell suggests that the positioning of myeloid cells relative to vessels is important for their pro-angiogenic function and highlights the potential importance of spatially guiding recruited myeloid cells with immunoregenerative material strategies. Genetic mutation of colony stimulating factor receptor 1 (CSFR1) in the osteopetrotic (op/op) mouse, which is essential to normal myeloid development, causes not only a reduction in circulating monocytes and tissue macrophages, but also aberrant and immature vascular networks [7, 23].

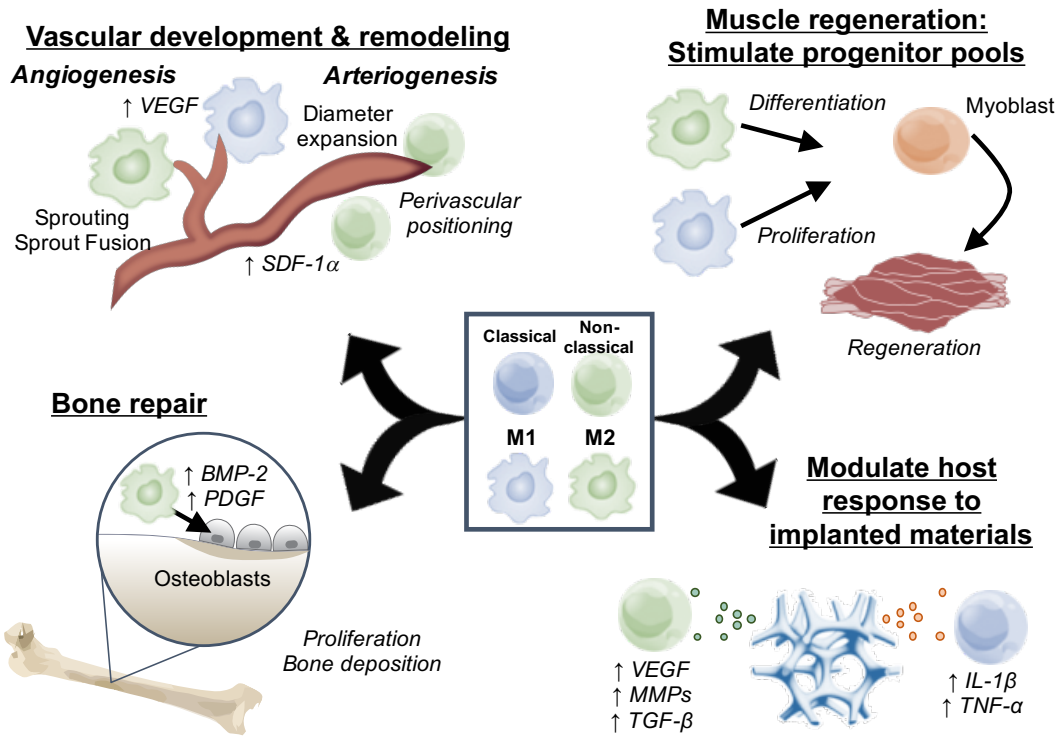

Figure 1. Mononuclear phagocytes in regenerative medicine. During injury, subpopulations of monocytes (classical and non-classical) are recruited from circulation, where they can persist transiently as monocytes or differentiate into macrophages ranging in phenotype from M1-type to M2-type. Within the specific injury niche, monocytes and macrophages can guide tissue repair by promoting angiogenesis and arteriogenesis, secreting growth factors that guide progenitor cell differentiation and proliferation, regulating the secretome of parenchymal cells, and releasing inflammatory mediators that guide other immune cells.

Monocyte recruitment to sites of vessel injury and their ability to adhere to the endothelium [64] have been correlated with the extent of collateral arterial growth [9, 54, 62, 65] and effective angiogenesis [66]. In a typical biphasic injury response, classical monocytes are the first monocytic responders, followed by the appearance of non-classical monocytes around 3 days later. Loss of CCR2, which leads to removal of classical monocytes from the blood and decreased tissue myeloid cells [14], impairs the development of collateral arteriogenesis in mice after ischemic hindlimb occlusion [67].

MCP-1 infusion into the ischemic hindlimb increases total monocyte accumulation in parallel with increased density of collateral arteries and number of sprouting capillaries [63]. MCP-1 is a key chemotactic molecule for classical monocytes, so this suggests a role in arteriogenesis following ischemic damage. Constitutive overexpression of MCP-1 in heart tissue leads to severe damage to the myocardium that is related to persistent monocyte infiltration and macrophage tunneling within cardiac tissue [68]. Collectively these studies suggest that pro-inflammatory mononuclear cells may be essential for effective vascularization, although overzealous activation of these cells can lead to tissue damage.

The precise roles of classical and non-classical monocyte subsets during vascular remodeling remains unknown; however, some studies suggest that inflammatory myeloid cells are the primary producers of VEGF [41, 69]. Pathologically, VEGF can be upregulated by endothelial cells or pericytes in a stress response to hypoxia to stimulate angiogenesis. Transgenic organ-specific VEGF induction causes robust tissue infiltration of circulating monocytes [55]. Increased transgenic VEGF expression causes perivascular cells to produce the chemotactic factor SDF-1α, which positions monocytes in close proximity to vascular structures, allowing for reciprocal paracrine signaling between the monocytes and the vasculature [55]. While this study did not characterize the subset of monocyte that was recruited, the expression of CX3CR1 and CXCR4 suggest that these cells may be non-classical monocytes [54]. Release of SDF-1α from a biomaterial implant in a dermal inflammatory wound causes an increase in the early recruitment of non-classical monocytes, which correlated with later parameters of vascular network expansion [54]. Intravascularly, non-classical monocytes patrol the endothelial layer for signs of damage and assist in clearing apoptotic endothelial cells [18]. Loss of IL-4 receptor α,

which plays a major role in M2a polarization, leads to massive hemorrhage and delayed epithelialization in a skin injury model, highlighting the critical role these cells play in supporting repair [45]. Monocyte/macrophage subset discrimination analysis has suggested that enhancing the number of anti-inflammatory monocytes/macrophages correlates with increased vascular remodeling [9, 54]. The precise mechanisms by which each subset of myeloid cell contributes to vessel development and stabilization remains to be fully elucidated; however, secretion of soluble factors [4], matrix deposition/remodeling [70], and stabilization of nascent endothelial sprouts [23] are likely to mediate the process.

2.2.2 Monocytes/macrophages in musculoskeletal repair

Repair of the damaged musculoskeletal system has been a major focus in tissue engineering and regenerative medicine, which can be broadly divided into therapies that target injured muscle and those that target bone repair. Muscle tissue maintains the ability to regenerate in the adult through maintenance of a quiescent resident stem cell population known as satellite cells or myogenic precursor cells. Macrophages in injured muscle can produce pro-regenerative growth factors such as IGF-1 to stimulate the activity of muscle-resident stem cell population- satellite cells (**Figure 1**). CCR2-deficient muscle displays a significant healing defect accompanied by a dampened macrophage response, which can be partially rescued by exogenous IGF-1 [25]. During skeletal muscle toxin-induced injury, the myeloid response is characterized by an early infiltration of inflammatory monocytes/macrophages for the first 4 days after injury, followed by the appearance of anti-inflammatory monocytes/macrophages beginning around 4 days after injury [4]. This switch appears to be due to *in situ* differentiation of classical monocytes into anti-inflammatory monocytes/macrophages [4]. Similar biphasic kinetics of early M1 cells

followed by M2 cells in the muscle tissue have been observed in other skeletal muscle injury models [71, 72]. *In vitro*, M1 macrophages stimulate proliferation of myogenic precursor cells, while M2a and M2c cells increase myotube formation [4, 73]. Blockade of M2 polarization by transgenic knockout of IL-10 causes an increased/sustained M1 response and poor regeneration in an injured muscle [71]. Most work exploring the role of myeloid cells in skeletal muscle repair has not been performed using traumatic models of muscle loss; consequently, additional studies are needed to determine whether the cellular immune response is similar across different types of muscle injuries.

While a role for monocytes and macrophages in bone repair is just beginning to be appreciated [74], bone has received significant attention in the field of regenerative medicine. During homeostasis, osteal macrophages form a canopy structure along the endosteal bone surface, and their depletion either with clodronate liposomes or macrophage-Fas-induced apoptosis (Mafia) transgenic mice rapidly eliminates bone-forming osteoblasts [75, 76]. Macrophages appear to directly signal to osteogenic cells, as they promote mineralization during *in vitro* co-culture through soluble cues [75]. Long-term depletion of macrophages in the Mafia mouse results in severe osteopenia [77], and genetic depletion of macrophages results in shorter bone length and reduced bone density by three months of age [78]. During bone injury, monocytes and macrophages play diverse roles in repair, modulating the acute inflammatory response [22], producing growth factors such as bone morphogenetic protein (BMP)-2 [79] and PDGF-BB [80], and inducing ostegeonesis of mesenchymal progenitor cells [75, 78] (**Figure 1**). Impaired monocyte trafficking induced by genetic knockout of CCR2 does not affect osteoclast numbers, but impairs vascular remodeling and delays bone repair [81]. Macrophages are also required

for callous formation after fracture and they localize to regions undergoing early endochondral ossification [82]. Depletion of macrophages significantly impairs intramembranous bone repair [83] and prevents fracture repair, resulting in fibrotic tissue formation instead of endochondral bone [78]. These studies indicate that monocytes and macrophages are multi-faceted cellular regulators of the healing response after bone injury, and likely represent a powerful target for immunoregenerative therapies.

2.3 Innate immune response to engineered materials

Biomaterials afford many advantages as a system to exploit the repair functions of monocytes/macrophages; however, foreign materials unavoidably elicit a biological response when implanted *in vivo.* The immune response must be carefully considered in the material design in order to avoid unwanted cell recruitment/adhesion, excessive secretion of inflammatory cytokines, fibrous encapsulation, or chronic inflammation [84, 85]. Immunomodulatory or immunoregenerative materials seek to tune this inflammatory response typically through biomolecule or small molecule delivery. As the innate immune response is highly dynamic, spatial and temporal control over delivery may be critical to target specific phases of inflammation and repair *in vivo*. Localized release can be utilized to generate a gradient of a particular compound, which is important for providing spatial information to innate immune cells in order to recruit them to the desired site. Materials can also be used to provide a substrate or scaffold to organize complex tissue reconstruction, however, can face challenges such as proper integration into host tissue, vascularization, and circumventing fibrosis and the foreign body response [85]. By engineering material properties and biomolecule delivery, the biological response can be controlled to maximally promote repair, but not prolong the inflammatory response.

2.3.1 Passive inflammatory response to material implantation

Implantation of a foreign material induces a physiological response that is both spatially and temporally regulated, and varies widely depending on the material properties [86]. Within 5 seconds of contact with whole blood, protein adsorption and platelet activation occurs on titanium oxide surfaces [87]. The composition and bioactivity of adsorbed proteins evolves over time and depends on the concentration of proteins in the surrounding microenvironment, their affinity for the material surface, and their conformation on the surface [88]. Adsorbed plasma proteins include albumin, extracellular matrix proteins such as fibronectin and vitronectin, and complement proteins. While *in vivo* studies on the precise composition and magnitude of adsorbed proteins are limited, some measurements have been made. Mass spectrometry analysis of adsorbed proteins collected from PEG hydrogels revealed that albumin is the most abundant protein after 30 minutes of subcutaneous implantation in mice [89].

Implantation of a material is believed to induce an inflammatory response that mimics many of the cell recruitment patterns observed in response to other inflammatory stimuli, but may also represent a unique context. Neutrophils are recruited within 16 hours after material implantation during the acute inflammatory phase [90] and may persist for as long as two weeks, as is the case for non-degradable microparticles implanted in the mouse peritoneum [91]. Neutrophil recruitment may be mediated by histamine released during mast cell degranulation in response to material implantation [90]; however, damage-associated molecular patterns recognized by tissue resident macrophages are also known to initiate neutrophil recruitment by producing inflammatory mediators such as TNF-α and IL-6 [92]. Neutrophil activation and degranulation results in the release of proteolytic

enzymes and ROS that may contribute to material degradation [93], as well as initiate subsequent phases of inflammation [92].

Monocytes are recruited from circulation in response to mediators released from neutrophil granules that alter local chemokine production by endothelial cells and resident macrophages, as well as induce expression of intercellular adhesion molecules. For example, proteinase-3 release from neutrophil secondary granules induces MCP-1 production by endothelial and upregulates ICAM-1 and VCAM-1 [94]. Extravasated monocytes differentiate into macrophages or dendritic cells in response to M-CSF or GM-CSF, respectively [95]. Crosstalk with other immune cells, including apoptotic neutrophils [96] and paracrine signals derived from T helper cells [97], regulate the phenotype of macrophages. Macroscale biomaterials induce a unique response in macrophages that involves cell fusion and formation of foreign body giant cells (FBGC) that are believed to be the result of frustrated phagocytosis [85]. While these cells are not fully characterized at the transcriptional and protein level, they are induced by IL-4 and IL-13 signaling [98], similar to alternatively activated macrophages, but can also produce both TNF-α and TGF-β [99]. The role of FBGC in the inflammatory response to degradable materials such as natural matrices or synthetic matrices with engineered degradation sites remains unknown.

Immune cells recruited to the material interact with the surface through integrin ligation to adsorbed proteins such as complement proteins, fibrinogen, and fibronectin [100, 101]. Integrins are heterodimeric proteins composed of an alpha and beta chain that pair in a cell type-specific manner to enable cell-matrix and cell-cell interactions [102]. Phagocytes (including neutrophils, monocytes, and macrophages) can express the β_1, β_2, and β_3 chains, which dimerize to form integrins that include $\alpha_L\beta_2$ (LFA-1), $\alpha_M\beta_2$ (Mac-1),

$\alpha_5\beta_1$, and $\alpha_V\beta_3$ [102]. The affinity of specific integrins for their ligand may be dependent on cell activation, as is the case for α_4, which undergoes a conformational change after exposure to SDF-1 or the complement protein C5a that enhances subsequent binding to VCAM-1 [103]. Integrin expression can also be activation-dependent, as local administration of TNF- α to the vasculature increases expression of Mac-1, but not LFA-1, on neutrophils and monocytes [104]. Integrin signaling typically modulates Rho GTPase activity, which subsequently induces cytoskeletal remodeling [105]. While formation of focal adhesions and cell migration are initiated on short time scales (minutes to hours), integrin signaling can alter transcriptional programs that impact longer-term processes such as cell survival and differentiation [106, 107].

Integrin signaling appears to play different roles in leukocyte migration, depending on the context in which the cell is migrating. For example, monocytes utilize integrins (particularly LFA-1) to crawl along the endothelium and extravasate across the endothelial barrier [49, 108]. Conversely, leukocyte migration through interstitial space that does not involve interactions with 2D surfaces is not integrin-dependent and instead involves amoeboid-like flowing and squeezing motions [108]. Integrins (particularly Mac-1) are required for macrophage adhesion to complement proteins adsorbed to biomaterial surfaces [100]. Additionally, integrins appear to play key roles in mediating the function of biomaterial-associated leukocytes, as blockade of Mac-1 in macrophages reduces pro-inflammatory cytokine production and reduces fibrous encapsulation [109]. Mac-1 signaling is also critical for macrophage fusion and subsequent FBGC formation [110, 111]. Consequently, integrins appear to be the key molecular tool that leukocytes use to

interact with a material surface, and integrin signaling can significantly impact inflammatory cascade.

While many steps in the inflammatory cascade are conserved across tissues, the precise host response is also dictated by the implantation site. For example, PEG hydrogels displayed differences in the magnitude and composition of the inflammatory cells when implanted subcutaneously versus in the abdominal cavity or muscle [112]. The properties of the material, either those inherent to the selected material or those introduced by design, significantly alter the behavior of immune cells interacting with the material [101]. Physical properties such as geometry, topography, and porosity and biochemical properties such as surface chemistry, ligand functionalization, and degradation mode are critical factors in the host response to the material (**Figure 2**).

2.3.2 Physical properties

Material geometry on the bulk, micro, and nano scale, can greatly impact material-host interactions and presents an opportunity to design features of a material to best hone the inflammatory response. Phagocytic cells like monocytes and macrophages are primary responders to foreign materials and the ability of these cells to interact with the material is greatly impacted by the shape and size. Pathophysiologically, myeloid cells use size and shape of microbes they encounter to dictate the immune response they signal [113]. Geometry can influence the ability of cells to adhere to a surface, phagocytose, or align with one another. Spherical materials appear to induce far less fibrous encapsulation than cylindrical or materials containing sharp angles [114]. Moreover, a spherical diameter around 1.5mm is superior to smaller spheres across a wide range of materials (including

alginate hydrogels, stainless steel, and glass) for reducing foreign body response perhaps due to reduced cell attachment to the particle surface [114]. Macrophages are most able to phagocytose microspheres around 2μm in diameter, both in terms of the number of microspheres internalized and their total volume [115]. Microsphere shape is equally important, as macrophages detect a "local shape" at the initial point of contact that determines whether they will spread along or initiate phagocytosis of the material [116]. Interestingly, a wide range of shapes can be engulfed by macrophages if the initial orientation is correct and total size primarily affects completion of phagocytosis. Further, the sub-micron size of particles can determine whether a particle is engulfed by endocytosis (~150nm) versus phagocytosis (~500nm), a distinction that could impact the extent of macrophage activation [117]. Liposomal material strategies can take advantage of the phagocytic nature of monocytes and macrophages to specifically target drug delivery to myeloid cells. Phagocytosis of unilamellar nano-liposomes (~200nm) has been exploited experimentally as a tool to specifically deplete mononuclear phagocytes with clodronate-loaded liposomes [2].

Topographical cues at the micro or nano scale direct macrophage responses to materials after implantation, including adhesion, spreading, migration, and activation. Murine macrophages appear unable to detect nano-topographical features less than 150nm, whereas cells such as fibroblasts and endothelial cells are able to detect smaller topographies and display decreased spreading as feature size increases from 55nm to 200nm [118]. Parallel gratings made of different polymers ranging from 250-2000 nm promote spreading and elongation of unpolarized macrophages and impact secretion of M1-associated cytokines such as TNF-α, MCP-1, and VEGF [119]. Electrospun fibers,

which can create scaffolds mimicking natural extracellular matrix, support differing macrophage responses based on diameter, packing, and alignment features [120-122]. The topographical orientation appears to also be important, as randomly-oriented nanofibers reduce fibrous encapsulation *in vivo* compared to aligned nanofibers or non-patterned substrates [122]. Material geometry and topography can be used to engineer desired inflammatory outcomes. For example, micro-patterned lines of fibronectin (20μm in width) promote macrophage elongation, reduce inflammatory cytokine production, and prime these cells for differentiation into M2 macrophages compared to larger patterns or no patterning [123]. Generally, porous implants are more readily vascularized and can exhibit lower fibrous encapsulation than their non-porous counterparts [124, 125]. Polytetrafluoroethylene materials with pores 4.4μm in width increase secretion of IL-1β by human monocytes *in vitro* compared to non-porous materials or those with smaller pores (1.2 or 3.0μm), but reduce fibrous encapsulation *in vivo* [126]. Consequently, single outputs measured during *in vitro* screens may not directly correlate with *in vivo* outcomes, particularly due to the complexity of the inflammatory response.

2.3.3 Surface properties

The chemical makeup of the material impacts properties such as surface charge and hydrophobicity. For small cellulose microspheres, macrophages are less able to phagocytose non-ionic hydrophilic particles, demonstrating an 8-fold increase in phagocytosis for particles that are highly anionic or a 4-fold increase for highly cationic particles [115]. Negatively charged particles induce apoptotic clearance of classical monocytes following scavenger receptor-dependent uptake in the circulation. A negative charge was required for therapeutic efficacy in preventing classical monocyte

accumulation and reducing disease symptoms during myocardial infarction, encephalitis, colitis, and other experimental inflammatory diseases [127]. The surface properties of macro-materials impact the foreign body response, with hydrophilic or anionic surfaces causing macrophage apoptosis and inhibiting macrophage fusion *in vivo* compared to unmodified, cationic, or hydrophobic surfaces [128]. Effects on macrophage function by surface properties of the material may be due to variations in the type [129] and conformation [107] of adsorbed proteins or related to the charged regions on macrophage membranes [130].

2.3.4 Mechanical properties

Like many other cell types, macrophages are able to detect mechanical properties of their substrate such as stiffness [131-133]. Soft PEG hydrogels (modulus of 130 kilopascals (kPa)) prevent macrophage spreading and formation of actin stress fibers, as well as prevent inflammatory gene expression *in vitro* and fibrous encapsulation *in vivo* [132]. Stiffer hydrogels (up to 840 kPa) prime macrophages for higher expression of IL-1β and IL-6, and promote generation of thicker fibrous capsules *in vivo*. A decrease in inflammatory response with decreasing material stiffness applies to even softer substrates such as polyacrylamide hydrogels below 150 kPa [131]. Interestingly, inflammatory mediators such as IFN-γ or LPS increase the elasticity of the macrophages [131]. Consequently, cellular mechanics can be regulated both by substrate properties and through biochemical cues in macrophages.

2.3.5 Incorporation of adhesion sites

The emergence of chemical conjugation strategies that enable biomaterials scientists to have precise control over material bioactivity has paved the way for the next generation of biomaterials. For example, bioorthogonal click chemistry has increased opportunities to develop diverse and complex materials that are both biocompatible and biofunctional. Hydrogels have been increasingly utilized in tissue engineering for their ease of tunability to specific applications, relative inertness *in vivo*, and compatibility for cell and biomolecule delivery. Inflammatory cell interactions with materials are mediated by adsorption of proteins such as albumin, fibrinogen, and components of the complement system [89, 134], which is dictated by properties such as surface chemistry and hydrophobicity. Due to their protein-fouling nature, hydrogels often must be functionalized with adhesive ligands such as the integrin recognition site arginylglycylaspartic acid (RGD) to induce cell attachment to their surface. Poly(ethylene glycol) (PEG) hydrogels with functionalized with RGD adsorb less protein than unfunctionalized hydrogels following subcutaneous implantation *in vivo*, although the relative composition of adsorbed protein remains approximately 90% the same [89]. Functionalization with RGD reduces inflammatory gene expression by macrophages *in vitro* [135], and reduces the inflammatory response to non-degradable PEG hydrogels *in vivo* [136]. Interestingly, a delay in RGD presentation via *in vivo* light-triggered activation reduces the fibrous capsule thickness surrounding implanted PEG hydrogels [61], highlighting the potential importance of spatiotemporal control of biomaterial features. Components of the extracellular matrix may inherently be immunomodulatory, as coating polypropylene meshes with various types of extracellular matrices shifts the macrophage response from

M1 to M2 and reduces the foreign body response [137]. Taken together, adhesive ligands enable better integration with surrounding tissue, which may reduce the material-mediated inflammatory response.

2.3.6 Degradation

Incorporation of degradation sites has enabled more precise control over the kinetics and mechanism of degradation, as well as release rates of embedded biomolecules that are diffusion-limited. Protease-sensitive linkers allow a material to be environmentally-responsive in the sense that degradation depends on the abundance of proteases surrounding the material. Proteases such as MMP-2, MMP-9, and cathepsins are upregulated during the early stages of inflammation. Materials that degrade in response to MMP activity promote better integration with host tissue and healing compared to non-degradable materials [138]. The rate of degradation can be further controlled by tuning the affinity, avidity, and protease specificity of crosslinkers used [139]. Growth factor delivery can be engineered to be environmentally-responsive through conjugation to PEG monomers with a protease-sensitive linker [140]. While protease-sensitive materials, as well as similar pH-sensitive materials, are able to dynamically respond to their environment, they are not able to respond to user-defined stimuli. Consequently, an emerging field in biomaterials that will likely be a critical component of immunoregenerative therapies, is the application of materials that can be regulated temporally be external stimuli such as light, ultrasound, and heat [141]. For example, macrophage and neutrophil adhesion to hydrogels can be activated by transdermal application of ultraviolet light due to functionalization with “caged” adhesive ligands. Non-

invasive adhesive ligand activation 7 days post-implantation reduces fibrous encapsulation, providing control over the inflammatory response in both space and time [61].

2.3.7 Biomolecule delivery

Delivery of synthetic and natural molecules from implanted materials can be used to further modulate the host response. Generally, biomolecules embedded to regulate monocyte and macrophage function can target the following biological processes: 1) recruitment of monocytes and macrophages from blood or surrounding tissue, 2) monocyte/macrophage polarization state, and 3) macrophage proliferation. Recruitment can be controlled by locally delivery of chemokines that selectively target monocytes and macrophages, such as MCP-1, SDF-1, CX3CL1, or bioactive sphingolipids. This strategy can be further fine-tuned by selecting biomolecules that target monocyte/macrophage subsets. For example, SDF-1 delivery from heparin-PEG hydrogels can selectively enhance recruitment of non-classical monocytes, but not classical monocytes, by exploiting their relative overexpression of CXCR4 [54]. Delivery of MCP-1, which broadly recruits monocytes through CCR2, increased the frequency of arginase-positive M2 macrophages and improved endothelial cell transplantation [142]. Delivery of M-CSF from PEG hydrogels enhances macrophage accumulation in the cornea and better supports vascularization than VEGF [143], further indicating that targeting macrophages can improve repair. Polarizing cytokines can also be released to condition the local macrophages to a particular phenotype. Delivery of IL-4 from an agarose-based scaffold enhanced M2 macrophage bias in the local tissue and correlated with increase in peripheral nerve regeneration [144]. Sequential delivery of IFN-γ and IL-4 can be used to guide the kinetics of macrophage polarization on decellularized bone matrices to achieve a biphasic

inflammatory to regenerative macrophage profile [57]. Delivery of macrophage polarizing factors has been investigated silk matrices, either through adsorption or direct conjugation [145]. Inflammation-induced macrophage proliferation has only recently been appreciated and may provide a new therapeutic target, given that tissue macrophage expansion depends on IL-4 and M-CSF [146]. Material-based biomolecule delivery has the unique advantage of the ability to control both the spatial and temporal profiles of released molecules, both of which are critical aspects of the immunological response after injury.

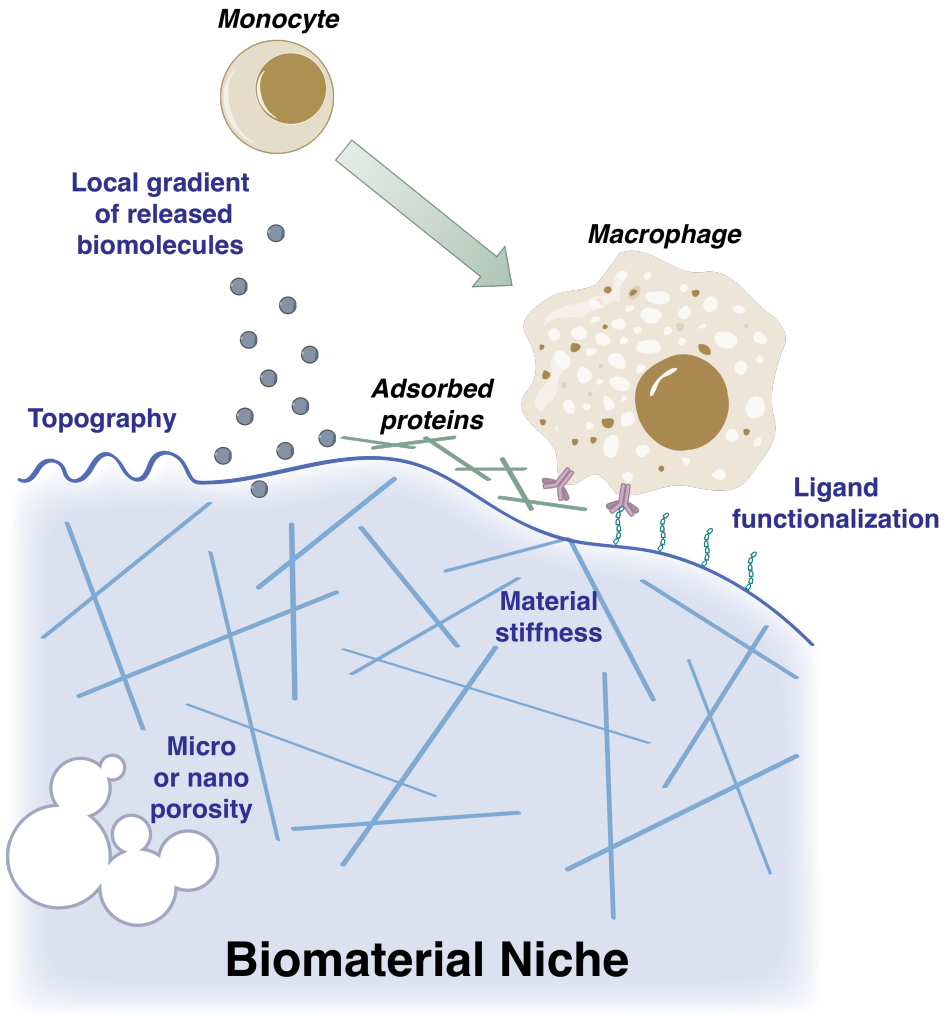

Figure 2. Biomaterial properties that affect monocytes/macrophages. The fate of monocytes and macrophages surrounding implants can be greatly affected by material properties, both those inherent to the selected material and those engineered to confer

additional functionality. Properties with effects on macrophages include topographical cues, mechanical properties such as elasticity and stiffness, porosity, functionalization with adhesive ligands, and release of biomolecules.

2.4 Conclusions and future directions

Proof-of-principle experiments have demonstrated that changes to specific material properties alter the biological response to implanted materials, but this may become more complicated when multiple parameters are simultaneously varied. For example, the foreign body response to materials varying significantly in surface chemistry, stiffness, and topography (polymers, ceramics, metals, and plastics) is most controlled by the material size [114], despite previous studies demonstrating that each of these properties can impact the inflammatory response. Consequently, high-throughput and empirical studies may be required when optimizing material design. While a set of unified principles describing the impact that material properties have on inflammatory cell response have yet to be developed, the design of next-generation immunomodulatory materials will likely rely on a deeper understanding of how specific material properties impact immune cell function *in vivo*.

3. NON-CLASSICAL MONOCYTES ARE BIASED PROGENITORS OF WOUND HEALING MACROPHAGES[2]

3.1 Abstract

Successful tissue repair requires the activities of myeloid cells such as monocytes and macrophages that guide the progression of inflammation and healing outcome. Immunoregenerative materials leverage the function of endogenous immune cells to orchestrate complex mechanisms of repair; however, a deeper understanding of innate immune cell function in inflamed tissues and their subsequent interactions with implanted materials is necessary to guide the design of these materials. Blood monocytes exist in two primary subpopulations, characterized as classical inflammatory or non-classical. While classical monocytes extravasate into inflamed tissue and give rise to macrophages, the recruitment kinetics and functional role of non-classical monocytes remains unclear. Here, we demonstrate that circulating non-classical monocytes are directly recruited to polymer films within skin injuries, where they generate alternatively activated, wound healing macrophages. Utilizing selective labeling of blood monocyte subsets, we demonstrate that that non-classical monocytes are directly recruited to soft tissue injury and selectively give rise to alternatively activated macrophages. Reduction of non-classical monocytes with clodronate liposomes impairs generation of alternatively activated macrophages, while adoptive transfer of non-classical monocytes increases the frequency of donor-derived

[2] Adapted from: Olingy CE, San Emeterio CL, Ogle ME, Krieger JR, Bruce AC, Pfau DD, et al. Non-classical monocytes are biased progenitors of wound healing macrophages during soft tissue injury. Sci Rep. 2017;7:447. Published under Creative Commons license.

wound healing macrophages compared to adoptive transfer of classical monocytes. These results elucidate a previously unknown role for blood-derived non-classical monocytes as contributors to alternatively activated macrophages, highlighting them as key regulators of inflammatory response and regenerative outcome.

3.2 Introduction

The mononuclear phagocyte system plays a multi-faceted role in maintaining tissue homeostasis and responding to pathological processes such as autoimmune diseases, cancer, and aberrant wound healing. Monocytes circulate in the bloodstream during steady state and are robustly recruited to sites of inflammation, where they exert functions that include clearance of cellular debris, promotion of angiogenesis, and restoration of tissue integrity [95]. Circulating blood monocytes are considered a highly plastic and dynamic system of innate immune cells that initiate processes of organ and tissue remodeling [2, 95, 147]. Immunologically smart interventions that exploit the division of labor between different monocyte and macrophage populations require an understanding of the roles that these cells play in promoting repair, as unchecked activity of innate immune cells can perpetuate tissue damage through chronic inflammation and fibrosis.

Two distinct subpopulations of monocytes have been identified in mouse and human blood, which can be distinguished by well-characterized surface protein expression profiles. Classical inflammatory monocytes are identified by $Ly6C^{hi}CX3CR1^{lo}CD43^{lo}$ expression in mice ($CD14^{hi}CD16^{-}$ in human), whereas non-classical alternative monocytes are $Ly6C^{lo}CX3CR1^{hi}CD43^{hi}$ in mice ($CD14^{+}CD16^{+}$ in human) [148]. A third population of intermediate monocytes characterized by intermediate expression of Ly6C in mice

($CD14^{hi}CD16^{+}$ in humans) are thought to complement the functions of non-classical monocytes and may preferentially differentiate into dendritic cells within inflamed tissues [149, 150]. Under homeostasis, classical monocytes in blood decrease Ly6C expression and become non-classical $Ly6C^{lo}$ monocytes [14, 37], which patrol the luminal side of resting endothelium [49]. Classical monocytes also survey steady-state tissues and can traffic to lymph nodes without differentiating into macrophages [151]. During inflammation, monocytes exit peripheral blood and extravasate into tissue, where they may transiently persist as monocytes without differentiation and exert a host of functions within the damaged tissue [19, 56, 58, 151, 152]. Classical inflammatory monocytes present in the acute phases of injury secrete pro-inflammatory cytokines such as IL-6, iNOS, and TNF-α [152] and exhibit high levels of matrix metalloproteinase (MMP) and cathepsin production [8]. Conversely, $Ly6C^{lo}$ monocytes present later during inflammation secrete high levels of vascular endothelial growth factor (VEGF) and IL-10 and can induce endothelial cell proliferation to promote arteriogenesis [4, 8, 56]. We have previously shown that strategies that enhance the early recruitment of $Ly6C^{lo}$ monocytes correlate with later increases in arteriolar expansion and angiogenic activity [9, 54]. Recruited monocytes primarily differentiate into macrophages or dendritic cells, serving as an alternative source of wound macrophages to those derived from *in situ* proliferation of tissue resident populations [27].

Macrophages are highly responsive to cues within the injury niche, enabling them to dynamically modify their behavior in response to changes in the microenvironment and display extremely varied phenotypes. Classically activated ("M1") macrophages are primary players in pathogen destruction, secretion of inflammatory cytokines, and driving

T_H1-type responses [10]. Conversely, alternatively activated wound healing ("M2") macrophages (of which a number of subtypes have been described [10]) are associated with pro-regenerative activities such as angiogenesis [153, 154], extracellular matrix remodeling [70], secretion of anti-inflammatory cytokines [10], and resolution of inflammation [155]. The highly complex and heterogeneous nature of inflamed tissue microenvironments has rendered a general description of macrophage origin and function challenging. Within toxin-induced muscle injury [4], liver fibrosis [156], infection [157], and autoimmune disease [158], classical $Ly6C^{hi}$ monocytes are recruited from circulation and undergo *in situ* differentiation to be the primary contributors of injury $Ly6C^{lo}$ monocytes/macrophages. In contrast, sequential recruitment of classical $Ly6C^{hi}$ followed by non-classical $Ly6C^{lo}$ monocyte subsets after myocardial infarction [8], and direct recruitment of adoptively transferred $Ly6C^{lo}$ monocytes within excisional skin injury [9] and during the development of inflammatory arthritis [59] have been reported.

Harnessing myeloid cell functions for regenerative medicine applications requires an understanding of the cues that direct the localization and fate of these cells. Immunoregenerative materials seek to leverage the function of endogenous immune cells to guide the progression of inflammation and repair damaged tissue [86]. For example, local delivery of stromal-derived factor-1 (SDF-1) from desulfated heparin-containing poly(ethylene glycol) (PEG) hydrogels increases the frequency of $CXCR4^{hi}Ly6C^{lo}$ monocytes, which promotes capillary network expansion [54]. Moreover, co-delivery of macrophage colony-stimulating factor (M-CSF) with VEGF from PEG hydrogels increases the density of macrophages and the maturity of corneal blood vessels compared to VEGF alone [143]. However, whether specific populations of blood monocytes give rise to

defined macrophage phenotypes surrounding implanted materials remains unknown. In the present study, we utilized fate mapping strategies including bead-based *in situ* labeling and adoptive transfer of monocyte subsets to demonstrate that non-classical monocytes preferentially give rise to CD206+ M2-like macrophages in response to biomaterial implantation within cutaneous wounds. These results shed light on the fate of specific monocyte populations following biomaterial implantation after injury and indicate that non-classical monocytes are a promising therapeutic target for harnessing pro-regenerative inflammation to promote repair.

3.3 Results

3.3.1 Systemic inflammatory response induced by skin wounding and biomaterial implantation

The dorsal skinfold window chamber (DWC) model (**Figure 3a**) is a partial thickness excisional skin injury model that involves removing the epidermis and dermis to reveal the underlying sub-reticular vasculature (**Figure 3b**). We have previously used this model to investigate the recruitment of distinct monocyte subsets to inflamed tissue surrounding biomaterial implants [9, 54, 159]. In this study, the fate of monocytes that are recruited in response to cutaneous wounding and material implantation was tracked. Monocytes can be identified both in blood circulation and extravascular tissue space by gating out neutrophils (Ly6G+), and subsequently gating on CD11b+SSC^{lo} cells. Ly6C is differentially expressed by monocyte subsets within this population (**Figure 3c**).

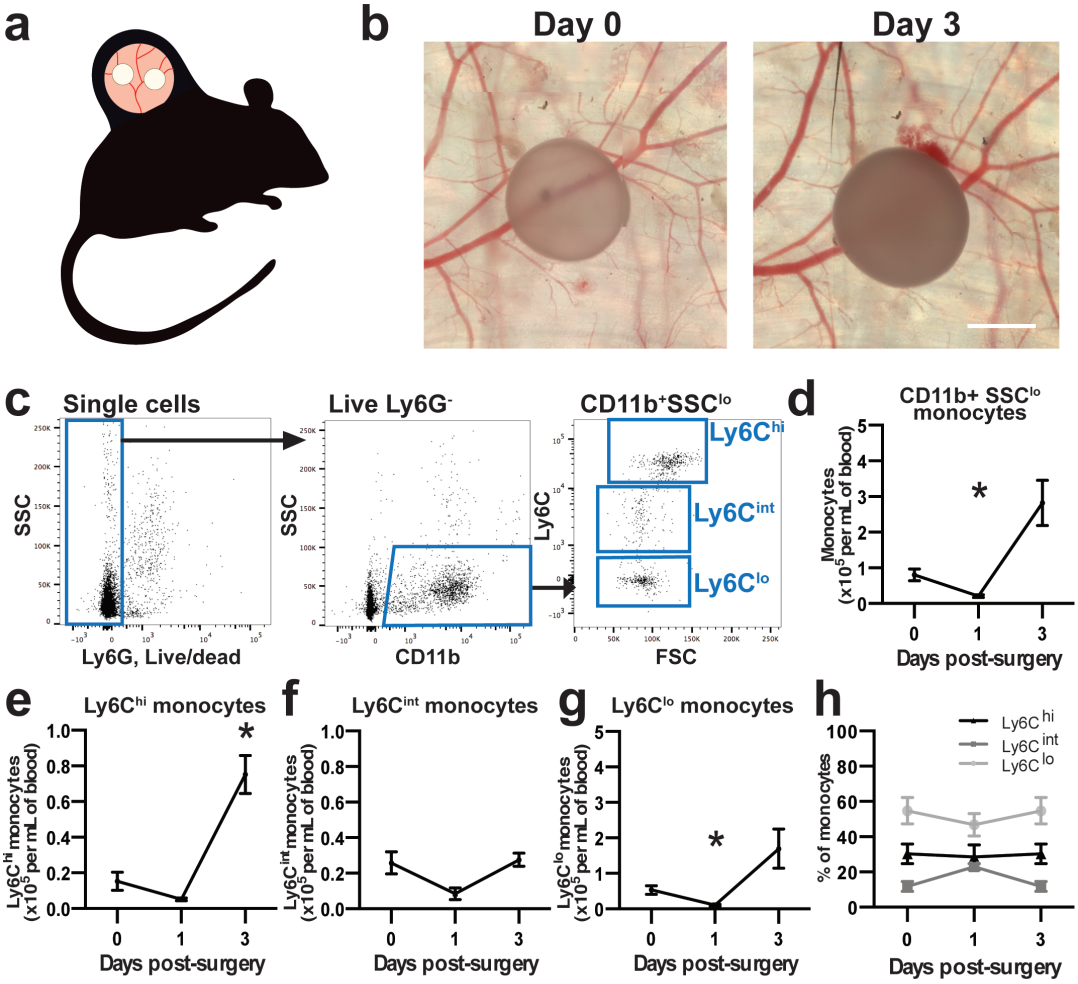

Figure 3. Wounding and biomaterial implantation induces acute changes in circulating monocytes. (a) Dorsal skinfold window chambers were implanted on C57/Bl6 mice and excisional wounding was induced by removing the outer layers of the dermis. (b) PLGA polymer films were placed on the exposed subcutaneous layer. Scale bar, 500µm. (c) Blood was collected for flow cytometry analysis. White blood cells were gated on CD11b+SSC^{lo} expression and categorized as Ly6C^{hi}, Ly6C^{int}, and Ly6C^{lo} monocytes based on Ly6C expression. Ly6G+, dead blood cells were excluded from analysis. (d) CD11b+SSC^{lo} monocytes and (e) Ly6C^{hi}, (f) Ly6C^{int}, and (g) Ly6C^{lo} monocytes per milliliter of blood 1 and 3 days post-injury. (h) Proportion of each monocyte subset expressed out of total CD11b+SSC^{lo} monocytes. Data presented as mean ± S.E.M. *$p<0.05$ relative to Day 0 blood by one-way ANOVA. n=5 animals per group.

DWC surgery and implantation of a polymeric poly(lactic-*co*-glycolic acid) (PLGA) thin film 1mm in diameter decreased the frequency of blood monocytes by nearly

four-fold 1 day post-injury, followed by a three-fold elevation by 3 days post-injury compared to blood taken at day 0 prior to surgery (**Figure 3d**). A three-fold decrease in the frequency of circulating classical Ly6C^{hi} monocytes was observed in the first day post-injury, followed by a five-fold increase by day 3 (**Figure 3e**). Ly6C^{int} monocytes were similarly decreased at day 1 by three-fold fold following injury but returned to baseline levels by day 3 (**Figure 3f**). Non-classical Ly6C^{lo} monocytes also initially decreased (by five-fold), but then increased by five-fold relative to day 0 (**Figure 3g**) and were the most abundant type of monocyte in blood for the duration of the study (**Figure 3h**).

These changes in circulating myeloid cell populations were accompanied by corresponding relative changes in bone marrow cell populations. At 3 days post-injury, higher frequencies of total, Ly6C^{hi}, and Ly6C^{int} monocytes were detected in bone marrow, while the frequency of Ly6C^{lo} monocytes decreased (**Figure 4a-d**). These results indicate that DWC surgery and biomaterial implantation induces systemic inflammation that involves alteration of blood monocyte composition and concomitant changes in bone marrow monocyte composition.

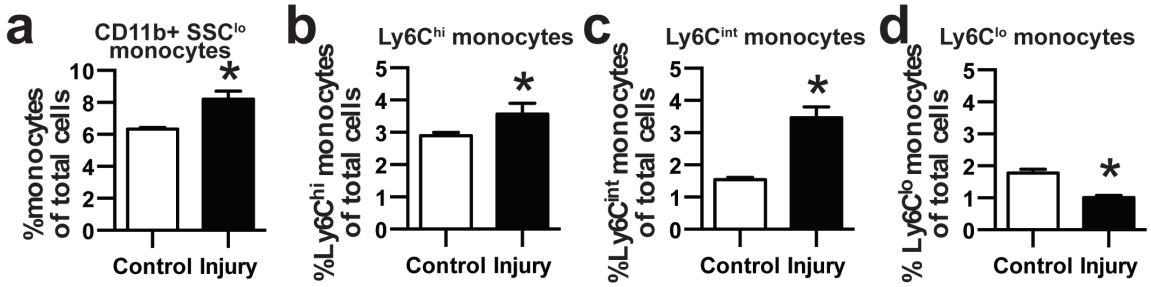

Figure 4. Bone marrow monocyte composition after wounding. Frequency of (a) CD11b+SSC^{lo} monocytes and (b) Ly6C^{hi}, (c) Ly6C^{int}, and (d) Ly6C^{lo} monocytes within bone marrow 3 days post-injury. Data presented as mean ± S.E.M. *$p<0.05$ by two-tailed t-test. n=4-10 animals per group.

3.3.2 Recruitment of labeled Ly6C^{lo} monocytes to injured skin

To further probe the fate of blood myeloid populations that were altered after injury, *in situ* labeling techniques to track blood monocytes were used. Circulating monocyte subsets were labeled *in vivo* prior to DWC surgery to facilitate cell tracking of each monocyte population as they entered inflamed dorsal tissue surrounding polymer implants. Non-classical Ly6C^{lo} monocyte labeling was performed by intravenous administration of fluorescent latex beads [160, 161] (**Figure 5a**). Within two hours of intravascular administration, latex beads are phagocytosed and equally distribute within Ly6C^{lo} and Ly6C^{hi} blood monocyte populations. However, by 24 hours after injection, latex beads primarily label Ly6C^{lo} monocytes due to physiological conversion of labeled Ly6C^{hi} monocytes and this labeling is sustained for up to 1 week [160]. Utilizing this strategy, blood Ly6C^{lo} monocytes were selectively labeled compared to classical Ly6C^{hi} monocytes after DWC (83.4 ± 9.7% Ly6C^{lo} monocytes vs. 14.5 ± 9.3% Ly6C^{int} monocytes and 0.0 ± 0.0% Ly6C^{hi} monocytes, day 1 post-injury) and the label was retained at similar proportions during the study (**Figure 5b,c**). Analysis of digested explanted dorsal skin tissue showed labeled cells originating from Ly6C^{lo} monocytes primarily remained Ly6C^{lo} within tissue (**Figure 5d**). The lower frequency of Ly6C^{hi} monocytes carrying the label in the tissue (9.6 ± 2.6% of LX+CD11b+SSC^{lo} cells) compared to the frequency of labeled Ly6C^{lo} cells (44.3 ± 8.2% of LX+CD11b+SSC^{lo} cells) indicates that circulating Ly6C^{lo} monocytes do not become Ly6C^{hi} post-extravasation (**Figure 5e**).

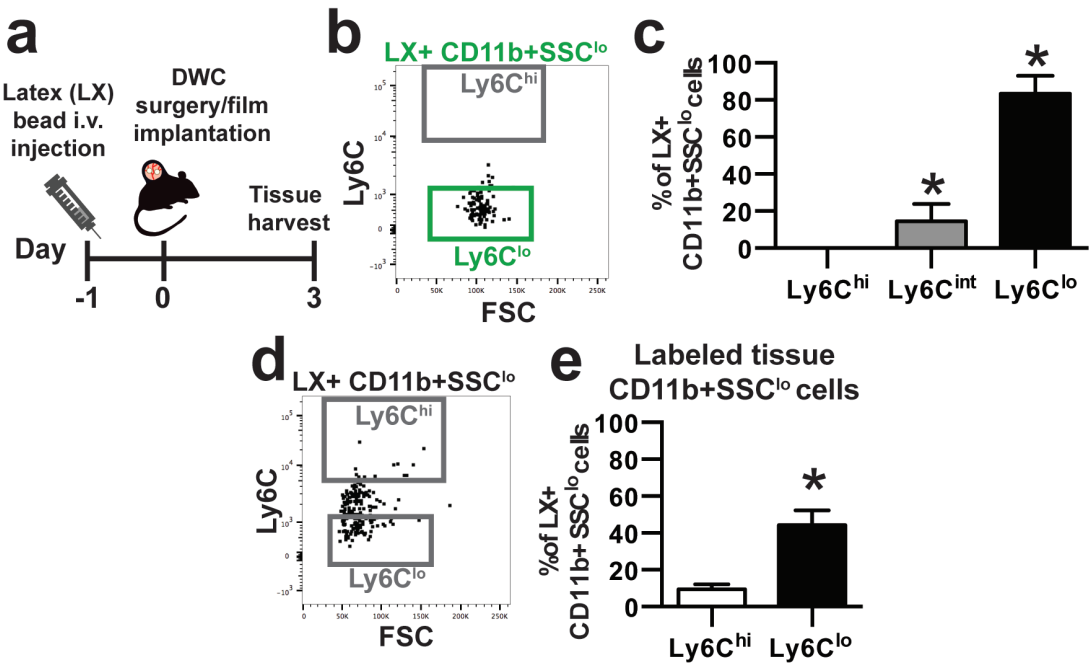

Figure 5. Latex bead-labeled Ly6C^{lo} monocytes recruited from blood circulation remain Ly6C^{lo} in inflamed dorsal tissue. (a) Latex (LX) beads were injected 1 day prior to DWC surgery to selectively label blood Ly6C^{lo} monocytes. (b) Representative flow cytometry dot plot and (c) quantification of labeled blood LX+CD11b+SSC^{lo} cells shows selective Ly6C^{lo} monocyte labeling 1 day post-injury. (d) Representative flow cytometry dot plot of labeled monocytes collected from digested dorsal tissue 3 days post-injury and (e) quantification of labeled Ly6C^{hi} and Ly6C^{lo} monocytes. Data presented as mean ± S.E.M. *p<0.05 by one-way ANOVA or two-tailed t-test. n=4-11 animals per group.

To explore whether non-classical monocytes differentiate into macrophages, expression of markers associated with macrophage differentiation and polarization on bead-labeled cells was measured (**Figure 6a**). Approximately half of labeled cells expressed F4/80, indicating that around half of recruited Ly6C^{lo} monocytes convert into macrophages or are phagocytosed by macrophages by 3 days post-injury (**Figure 6b**). About half of total F4/80+CD11b+ cells expressed CD206 (**Figure 6c**), whereas labeled cells were more likely to be immunophenotyped as CD206+ macrophages (91.0±3.4% of LX+F4/80+CD11b+ cells) than CD206- macrophages (**Figure 6d**). These data suggest that

blood-derived Ly6C^{lo} monocytes preferentially give rise to CD206+ wound macrophages in inflamed tissue surrounding material implants.

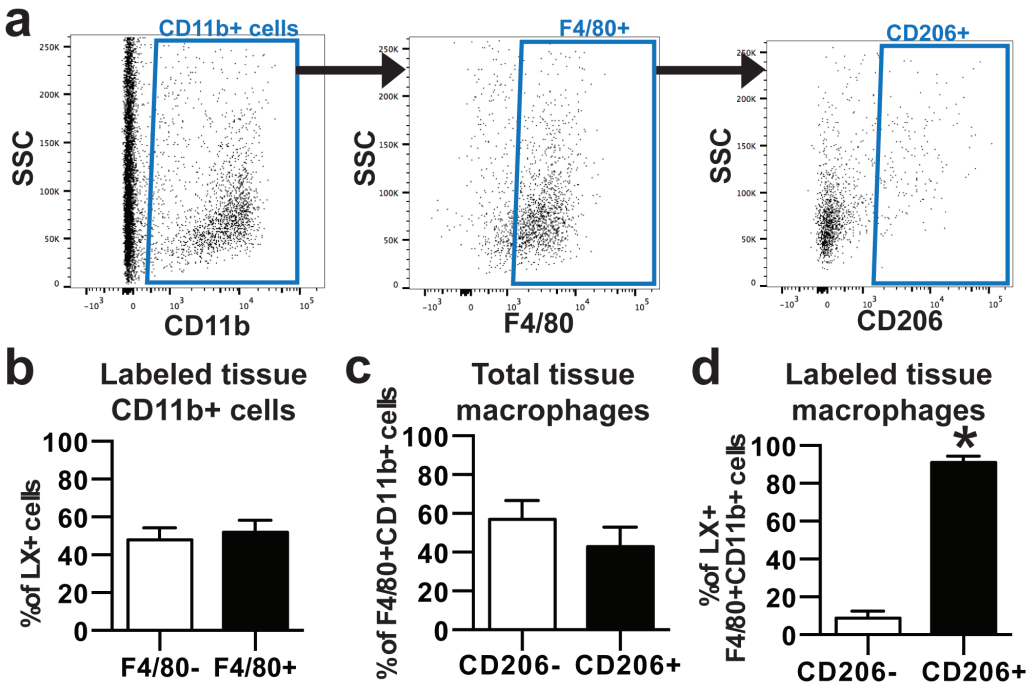

Figure 6. Latex bead-labeled Ly6C^{lo} monocytes recruited from blood circulation selectively give rise to CD206+ alternatively activated macrophages. (a) Gating strategy for tissue macrophages at 3 days post-injury. Tissue cells were gated on CD11b+F4/80+ cells to identify macrophages and subsequently assessed for CD206 expression for macrophage subpopulation analysis. (b) Frequency of bead-labeled F4/80+ cells in animals with labeled blood Ly6C^{lo} monocytes. (c) Frequency of CD206+ and CD206- cells out of total F4/80+CD11b+ cells. (d) Frequency of bead-labeled CD206+ cells out of total F4/80+CD11b+ cells. Data presented as mean ± S.E.M. *p<0.05 by two-tailed t-test. n=4-11 animals per group.

3.3.3 Recruitment of labeled Ly6C^{hi} monocytes to injured skin

Circulating Ly6C^{hi} blood monocytes were tracked in complementary bead-based labeling studies to explore whether these cells adopted similar fates during inflammation. Ly6C^{hi} monocytes were labeled by sequential administration of clodronate-loaded

liposomes 2 days prior to injury followed by latex beads 16 hours later (**Figure 7a**), as previously described [160, 161]. Clodronate liposomes administered intravascularly transiently deplete all blood monocytes, resulting in accumulation of latex beads in bone marrow cells that reappear in circulating Ly6C^{hi} monocytes 2 days later [160]. Pre-administration of clodronate liposomes before latex bead injection preferentially labeled Ly6C^{hi} monocytes (70.8 ± 13.3% Ly6C^{hi} monocytes vs. 26.9 ± 12.9% Ly6C^{int} monocytes and 2.7 ± 0.9% Ly6C^{lo} monocytes, day 1 post-surgery) during the study (**Figure 7b,c**).

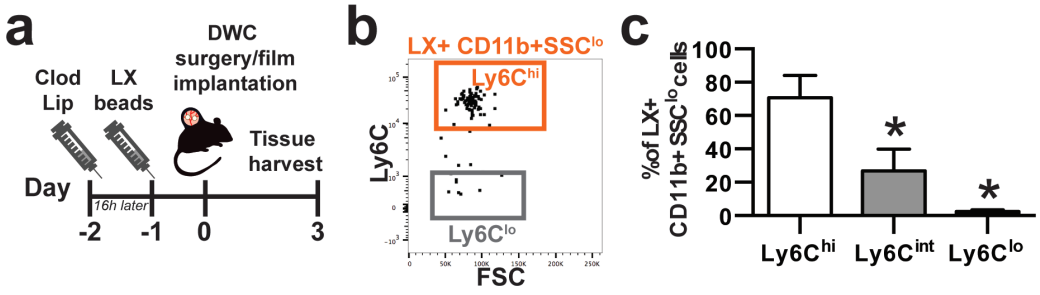

Figure 7. Selective labeling of blood Ly6C^{hi} monocytes. (a) Blood Ly6C^{hi} monocytes were selectively labeled by first depleting blood monocytes with intravascular clodronate liposome (Clod Lip) administration 2 days prior to injury, followed by LX bead-based labeling 16h later. (b) Representative flow cytometry dot plot and (c) quantification of labeled blood LX+CD11b+SSC^{lo} cells shows selective Ly6C^{hi} monocyte labeling 1 day post-injury. Data presented as mean ± S.E.M. *$p<0.05$ by one-way ANOVA. n=4 animals per group.

A relatively low frequency of labeled Ly6C^{hi} monocytes was detected in digested tissue (**Figure 8a**), confirming previous reports [4, 56, 58] that recruited Ly6C^{hi} monocytes do not persist as Ly6C^{hi} monocytes post-extravasation. Ly6C^{hi} monocytes likely rapidly convert *in situ* into Ly6C^{lo} monocytes, as a significantly greater frequency of labeled Ly6C^{lo} monocytes than Ly6C^{hi} monocytes were detected (**Figure 8b**). The frequency of F4/80+ cells within the latex bead-positive (LX+) population was not different between

Ly6C^{hi} monocyte and Ly6C^{lo} monocyte labeling (47.5± 17.3% vs. 48.0 ± 6.2% of LX+ cells), suggesting that both monocyte populations are equally capable of acquiring a macrophage phenotype after extravasation (**Figure 8c**). Labeled Ly6C^{hi} monocytes showed no preference for acquiring CD206 expression within 3 days of injury (**Figure 8d**), indicating that although blood-derived Ly6C^{hi} monocytes can contribute to CD206+ macrophages, they do so at a lower frequency than Ly6C^{lo} monocytes after clodronate liposome administration.

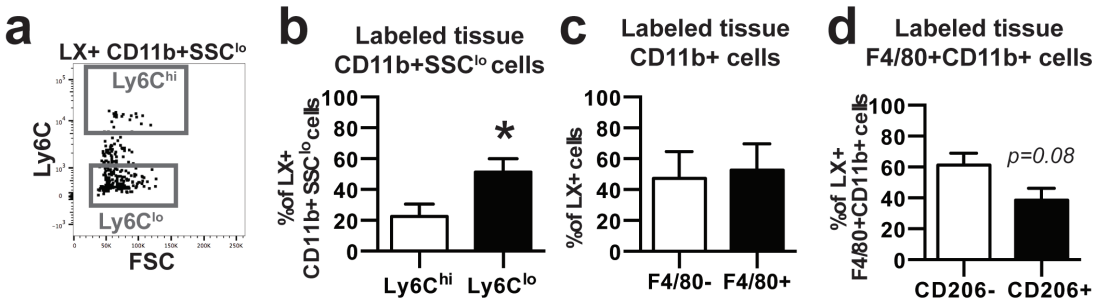

Figure 8. Tracking of latex bead-labeled Ly6C^{hi} monocytes recruited from blood circulation. (a) Representative flow cytometry dot plot of labeled monocytes collected from digested dorsal tissue 3 days post-injury and (b) quantification of labeled Ly6C^{hi} and Ly6C^{lo} monocytes. (c) Frequency of bead-labeled F4/80+ cells in animals with labeled blood Ly6C^{hi} monocytes. (d) Frequency of bead-labeled CD206+ cells out of total F4/80+CD11b+ cells. Data presented as mean ± S.E.M. *p<0.05 by two-tailed t-test. n=4 animals per group.

3.3.4 Reduction of circulating Ly6C^{lo} monocytes impairs CD206+ macrophage generation

Intravascular administration of clodronate liposomes transiently depletes all circulating monocytes; however, because blood Ly6C^{lo} monocytes are primarily derived from the conversion of Ly6C^{hi} monocytes, there is a delay in the repopulation of circulating

Ly6C^{lo} monocytes [14, 37]. This tool was employed to examine how decreasing the quantity of circulating non-classical monocytes impacts the generation of CD206+ macrophages during wound healing. As expected, a deficit in blood Ly6C^{lo} monocytes, but not Ly6C^{hi} monocytes, was observed 5 days after clodronate administration (**Figure 9a**). No differences in either monocyte subtype (**Figure 9b**), total F4/80+ macrophages (**Figure 9c**), or CD206- macrophages (**Figure 9d**) were observed in digested tissue 3 days post-injury; however, a lower frequency of CD206+ macrophages was observed (**Figure 9e**). These findings suggest that circulating Ly6C^{lo} monocytes are likely major contributors to the population of CD206+ wound macrophages.

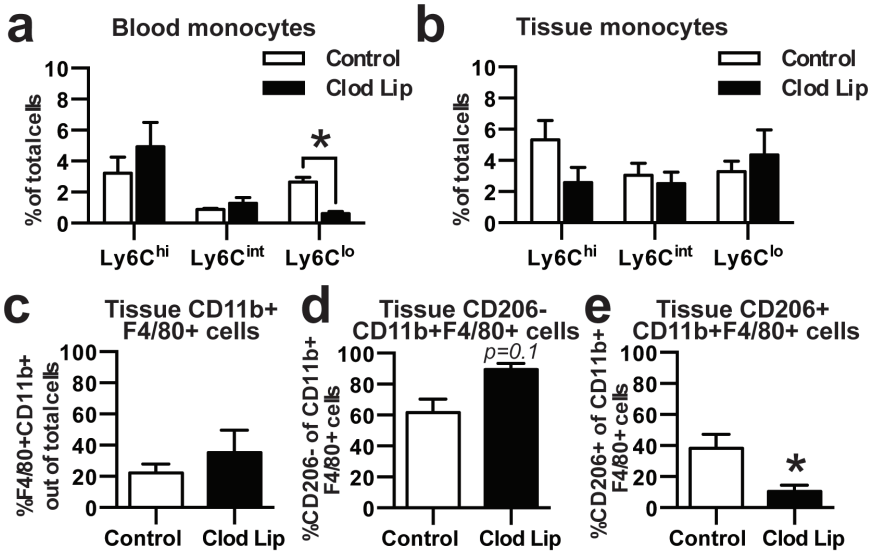

Figure 9. Loss of Ly6C^{lo} monocytes impairs generation of CD206+ alternatively activated macrophages. (a) Clodronate liposome (Clod Lip) administration two days before DWC surgery reduced the frequency in blood of Ly6C^{lo} monocytes, but not Ly6C^{hi} or Ly6C^{int} monocytes. (b) Frequency of Ly6C^{lo}, Ly6C^{int}, Ly6C^{hi} monocytes after Clod Lip administration in digested dorsal tissue 3 days post-injury. (c) Total CD11b+F4/80+ macrophages, (d) CD206- macrophages, and (e) CD206+ alternatively activated macrophages 3 days post-injury. Data presented as mean ± S.E.M. *$p<0.05$ by two-tailed t-test. n=4-11 animals per group.

3.3.5 Adoptively transferred Ly6C^{lo} monocytes preferentially differentiate into CD301b+CD206+ macrophages

To complement *in vivo* bead-based labeling strategies and further investigate the role that blood monocytes play in macrophage generation during inflammation, CD45.1+ Ly6C^{hi}CD43^{lo} or Ly6C^{lo}CD43^{hi} monocytes were sorted and adoptively transferred into CD45.2 mice at the time of DWC surgery (**Figure 10a**). While Ly6C^{lo}CD43^{hi} are a slightly more restricted population of Ly6C^{lo} monocytes, these two populations primarily overlap and the same is true for Ly6C^{hi}CD43^{lo} monocytes (**Figure 10b**). At 3 days post-injury, a very low frequency of CD45.1+CD45.2- cells were detected in digested dorsal (**Figure 10c**), indicating that few donor cells are present 3 days post-injury. A modest, but insignificant increase in the average number of total donor cells (normalized to tissue mass) originating as Ly6C^{lo}CD43^{hi} relative to those adoptively transferred as Ly6C^{hi}CD43^{lo} was detected (**Figure 10d**).

Donor cells collected from dorsal tissue 3 days post-injury were assayed for expression of monocyte and macrophage markers by flow cytometry (**Figure 11a**). CD301b marks a population of macrophages that appear in the midphase of skin wound healing and are required for effective cutaneous repair [162]. While F4/80 is present on all macrophages, co-expression of CD64 and MerTK exclusively distinguishes macrophages from monocytes [21]. These two populations significantly overlap, as 25.3 ± 2.1% of total F4/80+CD11b+ cells are also CD64+MerTK+, but nearly all CD64+MerTK+ cells are F4/80+ (**Figure 11a)** and all F4/80+ donor-derived cells also expressed CD64 and MerTK (**Figure 11b)**. We detected no difference in the overall number of CD64+MerTK+ macrophages in animal receiving adoptively transferred Ly6C^{hi}CD43^{lo} or Ly6C^{lo}CD43^{hi}

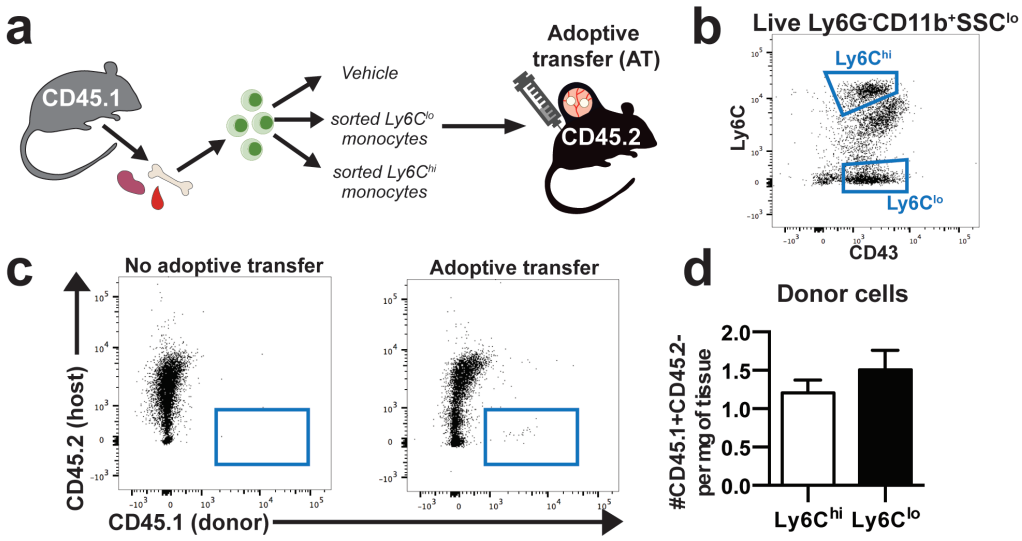

Figure 10. Adoptive transfer of Ly6C^{hi} and Ly6C^{lo} monocytes for fate tracking. (a) CD45.1+ Ly6C^{hi} or Ly6C^{lo} monocytes sorted from pooled bone marrow, blood, and spleen were adoptively transferred by i.v. injection to CD45.2+ mice at the time of DWC surgery. (b) Monocytes were sorted based on CD11b+SSC^{lo}Ly6G-Zombie- expression and Ly6C^{hi}CD43^{lo} expression or Ly6C^{lo}CD43^{hi} expression. (c) Donor-derived cells were identified in dorsal tissue 3 days post-injury as CD45.1+CD45.2-. (d) Total donor cells per milligram of tissue in mice receiving Ly6C^{hi} or Ly6C^{lo} monocytes. Data presented as mean ± S.E.M. n=5-6 animals per group.

monocytes (**Figure 11c**). However, a greater frequency of donor-derived wound healing CD301b+CD206+ macrophages was detected in animals receiving adoptively transferred Ly6C^{lo}CD43^{hi} monocytes compared to those that received Ly6C^{hi}CD43^{lo} monocytes (**Figure 11d**). No differences in the frequency of CD301b-CD206+CD64+MerTK+ (**Figure 11e**) or CD301b-CD206+F4/80+ macrophages (*data not shown*) were detected between the two grafts. These results further support the hypothesis that circulating non-classical monocytes differentiate into wound repair macrophages.

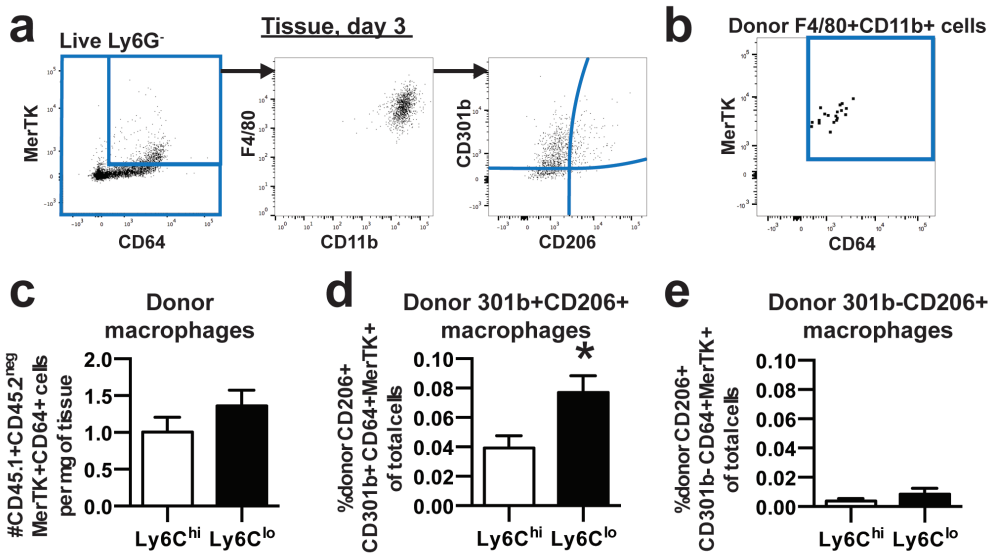

Figure 11. Adoptively transferred non-classical Ly6C^{lo} monocytes differentiate into CD206+ macrophages within inflamed peri-implant tissue 3 days post-injury. (a) Expression of F4/80, CD301b, and CD206 in MerTK+CD64+ macrophages. (b) Donor-derived F4/80+CD11b+ cells are also primarily MerTK+CD64+ (representative dot plot taken from animal receiving Ly6C^{lo} monocyte graft). (c) Number of donor-derived macrophages (MerTK+CD64+) 3 days post-injury in mice receiving adoptive transfer Ly6C^{hi} monocytes compared to mice receiving Ly6C^{lo} monocytes. (d) Frequency of donor-derived CD301b+CD206+ macrophages and (e) donor-derived CD301b-CD206+ macrophages. Data presented as mean ± S.E.M. *$p<0.05$ by two-tailed t-test. n=5-6 animals per group.

3.3.6 Characterization of chemokine receptors on mononuclear phagocytes

Our findings indicate that non-classical monocytes selectively give rise to alternatively activated macrophages, which play key roles in tissue repair [97, 144, 163]. In order to inform therapeutic targets for regulating recruitment of non-classical monocytes, we assessed the expression of the chemokine receptors sphingosine-1-phosphate receptor 3 (S1PR3) and VEGF receptors 1 and 2 (VEGFR1 and VEGFR2). Peripheral blood was collected from mice expressing green fluorescent protein (GFP) under the CX3CR1 promoter (CX3CR1$^{GFP/+}$ mice). CX3CR1^{hi} monocytes primarily

overlap with the Ly6C^{lo} monocyte population, and conversely, CX3CR1^{lo} monocytes are primarily Ly6C^{hi} (**Figure 12a**). Use of CX3CR1$^{GFP/+}$ as a readout for monocyte subset substantially minimizes the use of antibodies, which is particular useful for detection of S1PR3, which does not have available fluorophore-conjugated antibodies. S1PR3 surface expression is selectively higher on CX3CR1^{hi} blood monocytes (**Figure 12b,c**). While a modest shift in VEGFR1 expression occurred in CX3CR1^{hi} monocytes, we did not detect a significant difference in VEGFR1 expression between monocyte subsets (**Figure 12d,e**). VEGFR2 surface staining was higher on CX3CR1^{hi} monocytes compared to CX3CR1^{lo} monocytes (**Figure 12f,g**). These measurements indicate that elevated S1PR3 and VEGFR2 surface expression is a signature of non-classical monocytes.

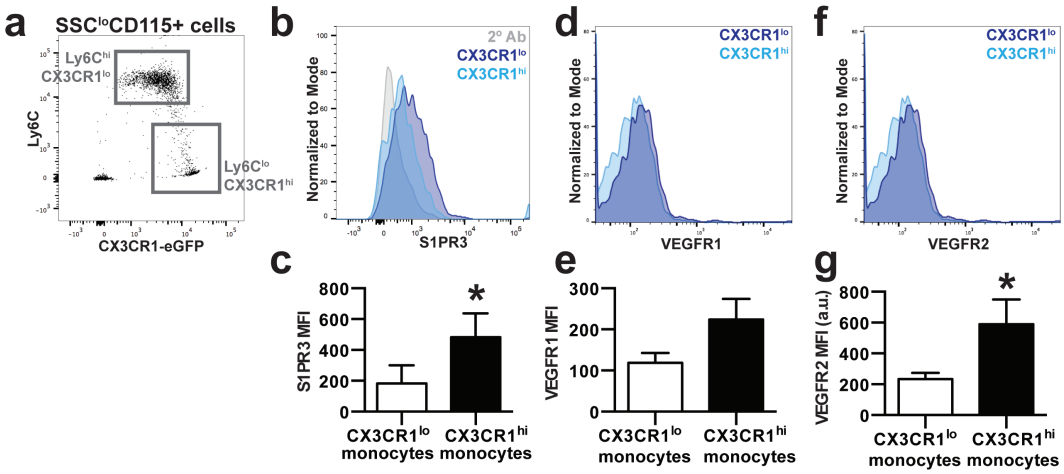

Figure 12. Expression of chemokine receptors in classical and non-classical monocytes. (a) Ly6C expression in CX3CR1^{hi} monocytes and CX3CR1^{lo} monocytes obtained from the blood of CX3CR1$^{GFP/+}$ mice, which identify Ly6C^{lo} monocytes and Ly6C^{hi} monocytes, respectively. (b,c) S1PR3 surface staining in blood CX3CR1^{hi} cells and CX3CR1^{lo} cells. (d,e) VEGFR1 surface staining in blood CX3CR1^{hi} cells and CX3CR1^{lo} cells. (f,g) VEGFR2 surface staining in blood CX3CR1^{hi} cells and CX3CR1^{lo} cells. Data presented as mean ± S.E.M. *$p<0.05$ by two-tailed t-test. n=3-6 animals per group.

3.4 Discussion

Monocytes are blood-borne mononuclear phagocytes that support tissue homeostasis and exit the vasculature at increased rates to differentiate into macrophages during inflammation. The precise relationship of circulating classical and non-classical monocyte subsets to defined macrophage populations remains unknown. We have shown that after skin wounding and biomaterial implantation, circulating non-classical monocytes extravasate into inflamed tissue and serve as biased progenitors of CD206+CD301b+ wound healing macrophages. Previous work has demonstrated that classical monocytes directly convert to non-classical monocytes and macrophages within inflamed tissue [4, 19]. Therefore, these studies elucidate a complementary role for non-classical monocytes and argue that these cells primarily differentiate into alternatively activated macrophages.

Non-classical Ly6C^{lo} monocytes patrol resting endothelium during homeostasis [49], and are present in circulation at a slightly higher frequency than classical Ly6C^{hi} monocytes (**Figure 3h**, 54.8±7.5% Ly6C^{lo} monocytes vs. 30.4±5.6% Ly6C^{hi} monocytes out of CD11b+SSC^{lo} cells). Interestingly, there was a transient reduction of circulating monocyte populations 1 day post-surgery, which could be due to acute cell recruitment from the blood to injured tissue, as monocytopoiesis occurs over several days [164]. As previously reported [8], circulating myeloid cells were elevated 3 days post-injury, including total CD11b+Ly6G-SSC^{lo} cells and Ly6C^{hi} and Ly6C^{lo} subpopulations (**Figure 3e-g**). Though a decrease in Ly6C^{int} monocytes was detected 1 day post-injury, there was no elevation at 3 days post-injury, indicating that the size of this population may not be altered by inflammatory stimuli. The observed changes in circulating cell populations during inflammation are likely due in part to alterations in myeloid cell trafficking from

the bone marrow, which displayed parallel changes in myeloid composition (**Figure 4**). These systemic changes in blood myeloid populations are likely a result of DWC surgery and not material implantation, as we have previously demonstrated that the number of rolling and adherent CX3CR1+ cells within dorsal skin vasculature is not significantly different between animals undergoing only DWC surgery and those that also received a PLGA implant [9].

Intravascular non-classical Ly6C^{lo} monocytes orchestrate the disposal of necrotic endothelial cells after activation with TLR7-targeted danger signals during inflammation [18, 49], whereas extravascular Ly6C^{lo} monocytes can promote angiogenesis and matrix remodeling via secretion of VEGF and matrix metalloproteinases [8]. The unique protein signature of non-classical monocytes, characterized by higher VEGF, TGF-β, and IL-10, and lower TNF-α and IL-1β expression compared to classical monocytes has resulted in the suggestion that these cells may constitute a class of "anti-inflammatory" monocytes [4, 8]. Previous studies have indicated that Ly6C^{lo} monocytes in inflamed tissues such as skeletal muscle and focal hepatic injury are derived from cells recruited as Ly6C^{hi} monocytes from the blood and are converted *in situ* to Ly6C^{lo} monocytes to promote wound healing and tissue repair [4, 19]. Other reports suggest that Ly6C^{lo} monocytes are directly and robustly recruited from the blood, leading to extravascular accumulation during inflammation [8, 49, 59]. While we observed that blood-derived Ly6C^{hi} monocytes enter inflamed tissue, reduce Ly6C expression (**Figure 8b**), and differentiate into macrophages (**Figure 8c, Figure 11c**), our studies indicate that Ly6C^{lo} monocytes are also directly recruited from circulation to injured tissues and able to give rise to macrophages (**Figure 11c-e**). Previous studies have indicated that adoptively transferred Ly6C^{lo}MHCII^{-}

monocytes do not infiltrate the skin [151], but this may be a result of differences in the grafted cell population ($Ly6C^{lo}MHCII^{-}$ monocytes vs. $Ly6C^{lo}CD43^{hi}$ monocytes in the current studies) or inflammatory stimuli (LPS injection vs. excisional skin injury in the current studies). Though $Ly6C^{lo}$ blood monocytes were decreased after clodronate liposome administration, no difference in the frequency of $Ly6C^{lo}$ monocytes was detected within injured skin (**Figure 9b**). Many studies have shown that $Ly6C^{hi}$ monocytes can convert to $Ly6C^{lo}$ monocytes in the blood or tissue [4, 37, 157]. Similarly, the presented data may reflect that, in the absence of $Ly6C^{lo}$ monocytes, circulation-derived $Ly6C^{hi}$ monocytes compensate and increase their rate of conversion into $Ly6C^{lo}$ monocytes in inflamed tissue.

An important finding of this work is that circulating $Ly6C^{lo}$ monocytes preferentially contribute to the CD206+ wound macrophage pool within skin injury compared to $Ly6C^{hi}$ monocytes. Analysis of peri-implant tissue for recruited latex bead-labeled $Ly6C^{lo}$ monocytes shows that this subset is predisposed to acquire a CD206+ alternatively activated M2-like [165] macrophage phenotype (**Figure 5e, Figure 11d**). Administration of clodronate liposomes enables selective labeling of $Ly6C^{hi}$ monocytes, while simultaneously reducing the frequency of $Ly6C^{lo}$ monocytes for 2-7 days after administration [37, 160]. Clodronate liposome-treated animals displayed no change in the frequency of overall macrophages within the skin injury after 3 days, but exhibited a decrease in the proportion of CD206+ macrophages (**Figure 9e**). Because tissue monocyte composition was unaffected by clodronate liposomes, these results may reflect a delay in generation of CD206+ macrophages. Additionally, the possibility that transient monocyte

depletion alters myeloid cell responses during inflammation cannot be excluded, as monocyte subsets are known to communicate with each other [14].

Latex bead-based labeling strategies are useful because they overcome many of the limitations of adoptive transfer, including *ex vivo* cell manipulation, pooling of donor cells, and low sensitivity due to poor cell recovery [50]. Importantly, there is no evidence that these labeling techniques alter monocyte recruitment or systemic inflammation [50]. However, interpretation of these studies relies on retention of latex beads within the cell that was originally labeled and no transfer to other cells. Therefore, cell tracking is best performed by use of complimentary tracking methods, including adoptive transfer, selective labeling techniques, and transgenic or knockout mice. Adoptive transfer of $5.55x10^5$ CD45.1+ $Ly6C^{hi}$ or $Ly6C^{lo}$ monocytes was performed by intravascular injection into CD45.2 mice at the time of DWC surgery (**Figure 10**). No differences were detected in the total number of CD45.1+ donor-derived cells per milligram of dorsal tissue between the two monocytes grafts, and further probed for markers of macrophage differentiation and polarization within donor cells. CD301b+CD206+ macrophages drive midstage skin regeneration by promoting fibroblast repopulation, cellular proliferation, and re-epithelialization [162]. In these adoptive transfer studies, a higher frequency of donor $Ly6C^{lo}$ monocytes acquired a CD301b+CD206+ macrophage phenotype compared to donor $Ly6C^{hi}$ monocytes (**Figure 11d**), indicating that circulation-derived $Ly6C^{lo}$ monocytes may be intrinsically predisposed to convert to dermal wound healing macrophages. Conversely, there was no difference in the frequency of donor-derived CD301b-CD206+ or number of total macrophages between mice receiving $Ly6C^{hi}$ or

Ly6C^{lo} monocytes. Taken together, these data support the hypothesis that non-classical monocytes undergo local conversion into alternatively activated macrophages.

Monocytes utilize chemokine receptors to migrate towards chemokine gradients produced during inflammation. Both VEGF and S1P are elevated after injury and are chemotactic for leukocytes [53, 166-168]. Blood-derived non-classical monocytes express higher levels of S1PR3 and VEGF2 on their surface compared to classical monocytes (**Figure 12**). We have previously demonstrated that non-classical monocytes also express higher levels of CXCR4 and are selectively recruited by heparin-PEG hydrogels delivering CXCR4's chemokine ligand, SDF-1 [54]. Consequently, biomaterial-mediated strategies that increase recruitment of non-classical monocytes through S1PR or VEGF signaling may be a promising strategy to increase accumulation of pro-regenerative subsets of mononuclear phagocytes within injured tissue.

3.5 Materials and Methods

3.5.1 Material fabrication

Films were fabricated as previously described[9]. Briefly, 350 mg PLGA (50:50 DLG 5E – Evonik Industries) was dissolved in 2ml dichloromethane in a glass scintillation vial via high-speed vortexing. Polymer solutions were poured into Teflon-coated petri dishes and allowed to dry at -20°C for 7 days. Before use, films were lyophilized overnight to remove any traces of solvent.

3.5.2 Dorsal skinfold window chamber surgery

All animal procedures were conducted according to protocols approved by the Georgia Institute of Technology or University of Virginia Institutional Animal Care and Use Committee. Male C57BL/6J mice (8-12 weeks) were fitted with sterile dorsal skinfold window chambers (APJ Trading Co) as previously described [9]. Briefly, mice were anesthetized with an intraperitoneal (i.p.) injection of ketamine/xylanzine (100/10 mg/kg) in sterile saline. Dorsal skin was shaved, depilated, and sterilized with three alternating washes of 70% ethanol and chlorhexidine. A double-layered skin fold was elevated off the back of the mouse and fitted with the titanium frame of the window chamber on the underside. The epidermis and dermis were removed from the top side of the skinfold in a ~12mm diameter circular area via surgical microscissors to reveal underlying vasculature. Exposed tissue was superfused with sterile saline to prevent desiccation. The titanium frame was then mounted on the top side of the skinfold, attached to the underlying frame counterpart, and sutured to the surrounding tissue. Two films were placed on top of the exposed subreticular dermis layer immediately after surgery (day 0) and exposed tissue

was sealed with a sterile glass window. Mice were euthanized 72 hours after surgery via CO_2 asphyxiation. The vasculature was immediately flushed with intracardiac infusion of saline follow by an intracardiac infusion of 4% paraformaldehdyde, prior to whole mounting of tissue and immunohistochemistry.

3.5.3 Flow cytometry

Peripheral blood was collected via cardiac puncture and bone marrow was collected via centrifugation (1000g for 5 mins) of isolated tibiae. The dorsal tissue circumscribing films was punched out with 6mm biopsy punches and pooled from both films within one animal for most studies. For adoptive transfer studies, all inflamed dorsal tissue was collected for analysis. Tissue was digested with collagenase (1mg/ml) at 37°C for 30 minutes and further disaggregated with a cell strainer to create a single cell suspension. Single cell suspensions of tissues were stained for flow cytometry analysis according to standard procedures and analyzed on a FACS-AriaIIIu flow cytometer (BD Biosciences). The following antibodies were used for cell phenotyping: APC-Cy7- or BV421-conjugated anti-CD11b (BioLegend), APC- or BV510-conjugated anti-Ly6C (BioLegend), PerCP-Cy5.5-conjugated CD43 (Biolegend), PE-Cy7-conjugated anti-GR-1 (BioLegend), APC-Cy7-conjugated anti-Ly6G (Biolegend), APC-conjugated anti-F4/80 (BioLegend), PE-Cy7- or FITC-conjugated anti-CD206 BioLegend), PE-Cy7-conjugated anti-CD301b, BV711-conjugated anti-CD64 (BioLegend), PE-conjugated anti-MerTK (Biolegend), BV605-conjugated anti-CD45.1, BV785-conjugated anti-CD45.2, PerCP-eFluor710 conjugated anti-CD115 (eBioscience), APC-conjugated anti-VEGFR1 (Biolegend), or APC-conjugated VEGF2 (Biolegend). Dead cells were excluded by staining with Zombie NIR™ (Biolegend) in protein-free buffer prior to antibody staining. Staining using BV

dyes was performed in the presence of Brilliant Stain Buffer (BD Biosciences). Positivity was determined by gating on fluorescence minus one controls. Absolute quantification of cell numbers in blood and tissue was performed by adding 25µL of AccuCheck counting beads to flow cytometry samples (Thermo Fisher Scientific). S1PR3 flow cytometry was performed by first performing Fc block (Biolegend), followed by staining cells with primary unconjugated anti-S1PR3 antibody (Alomone Labs) and secondary staining with DyLight 650 anti-rabbit IgG (Abcam). Positivity was determined by staining CX3CR1$^{GFP/+}$ cells with the secondary body only (no primary S1PR3 antibody).

3.5.4 Cell tracking of Ly6C^{lo} and Ly6C^{hi} monocytes

For selective labeling of Ly6C^{lo} monocytes, mice were administered 250µL of Fluoresbrite® Polychromatic Red latex beads intravenously one day prior to surgery (0.5µm, Polysciences - diluted 1:25 in sterile saline) via jugular vein injection. For selective labeling of Ly6C^{hi} monocytes, mice were administered 100µL of clodronate liposomes per 10g of mouse body weight (Dr. Nico van Rooijen, clodronateliposomes.com) intravenously two days prior to surgery, followed by administration of latex beads 16 hours later (one day prior to surgery). Labeling was confirmed by retro-orbital blood draw days 1 and 3 post-surgery. For adoptive transfer studies, white blood cells from bone marrow, spleen, and blood were collected from mice expressing the CD45.1 allelic variant and enriched for monocytes using an EasySep Mouse Monocyte Isolation Kit (Stem Cell Technologies). Cells were further purified by fluorescence activated cell sorting on a BD FACS AriaII cell sorter using the following markers: Ly6C^{hi} monocytes (SSC^{lo}CD11b^{+}Ly6C^{hi}CD43^{lo}) or Ly6C^{lo} monocytes

($SSC^{lo}CD11b^{+}Ly6C^{lo}CD43^{hi}$). Mice received 555,000 $Ly6C^{hi}$ or $Ly6C^{lo}$ monocytes via jugular vein injection on the day of surgery.

3.5.5 Statistical analysis

Data are presented as mean ± standard error of the mean (S.E.M.). All statistical analysis was performed in GraphPad Prism software. Comparisons of two groups were made using a two-tailed unpaired t-test, with Welch's correction if standard deviations were not equal. For studies with two independent variables, two-way ANOVA with Sidak's test for multiple comparisons was performed. $p<0.05$ was considered statistically significant.

4. LOCAL DELIVERY OF FTY720 PROMOTES RECRUITMENT OF ALTERNATIVELY ACTIVATED MACROPHAGES AND MUSCLE REPAIR[3, 4]

4.1 Abstract

Regeneration of soft tissue injuries requires the synchronized behavior of multiple cells that participate in repair. Deposition of a vascular network is one of the first steps during new tissue formation, both developmentally and after injury. We examined the role that myeloid cells play during revascularization and healing of skin and skeletal muscle injuries. We explored the effect of biomaterial-delivered FTY720, a sphingosine-1-phosphate receptor agonist, on myeloid cell infiltration and tissue repair. Local delivery of FTY720 promoted perivascular accumulation of non-classical monocytes and CD206+ alternatively activated macrophages in non-healing cutaneous wounds during the acute phase of inflammation. Treatment of ischemic or volumetric muscle injuries with FTY720-loaded materials enhanced accumulation of alternatively activated macrophages and promoted revascularization. In the later stages of repair, FTY720 improved muscle fiber regeneration and reduced fibrotic collagen deposition. These results indicate that biomaterials delivering factors such as FTY720 to enhance accumulation of pro-

[3] Portions of this chapter adapted from: Olingy CE, San Emeterio CL, Ogle ME, Krieger JR, Bruce AC, Pfau DD, et al. Non-classical monocytes are biased progenitors of wound healing macrophages during soft tissue injury. Sci Rep. 2017;7:447. Published under Creative Commons license.

[4] Portions of this chapter adapted from: San Emeterio CL, Olingy CE, Chu Y, Botchwey EA. Selective recruitment of non-classical monocytes promotes skeletal muscle repair. Biomaterials. 2017;117:32-43. License No. 4098910025385

regenerative myeloid subsets are a promising approach to improve repair of soft tissue injuries.

4.2 Introduction

Insufficient vascularization is a primary obstacle to recovery of tissues after traumatic injury, with regenerative therapies often seeking to enhance post-injury angiogenic and arteriogenic processes [169]. Deposition of a vascular network is one of the first steps during new tissue formation, both developmentally and after injury [170]. Consequently, successful biomaterial-based regenerative therapies must ensure proper oxygen and nutrient supply to recruited or transplanted cells through expansion of existing vascular networks [169]. Adult vascular remodeling is governed by a complex series of molecular and cellular events, with the recruitment and participation of leukocytes being necessary for successful angiogenesis [23]. Monocyte recruitment kinetics in particular have been implicated in a broad spectrum of therapeutic applications, including skeletal and myocardial muscle regeneration [4, 8], as well as the inflammatory response to biomedical implants [58].

Monocytes and macrophages play key roles in post-injury microvascular remodeling, as they are the predominant source of VEGF during the early phases of wound healing [69]. Classical and non-classical monocytes are sequentially recruited to ischemic injury through coordinated chemokine expression, exploiting the phagocytic and proteolytic activities of classical monocytes in early stages and the anti-inflammatory and pro-angiogenic properties of non-classical monocytes in the later phase of inflammation [8, 164, 171]. Non-classical monocytes promote microvascular remodeling through

secretion of soluble growth factors [58], extracellular matrix production, and mural support for newly developed vasculature [172]. Following extravasation from blood, recruited monocytes may transiently remain monocytes [56] or differentiate into macrophages or dendritic cells that persist through the resolution of inflammation [4, 58, 73]. Macrophages designated as classical inflammatory "M1" macrophages predominate early after injury, while alternatively activated "M2" macrophages orchestrate the later phases of tissue repair. Inflammatory macrophages respond to tissue damage signals and upregulate genes associated with alarmins and acute inflammatory-phase proteins [173], while alternatively activated macrophages begin the processes of inflammation resolution and wound healing [147]. Alternatively activated macrophages support angiogenesis [41, 174] and arteriogenesis [175], distinct processes that regulate post-injury vascular remodeling.

Mononuclear phagocytes also coordinate other processes of repair, including directing the activities of progenitor and parenchymal cells and regulating extracellular matrix deposition. For example, multiple studies have shown that depletion of circulating monocytes before toxin-induced muscle injury results in incompletely healed, fibrotic muscle [4, 176, 177]. Macrophages can regulate the response of progenitor cell populations after injury, promoting muscle satellite cell proliferation [73], osteogenesis of mesenchymal stem cells [178], and survival of irradiation-exposed hematopoietic stem cells [179]. Later during the inflammatory response, alternatively activated macrophages express genes encoding extracellular matrix (ECM) and ECM-remodeling proteins [173], control collagen fibril formation [45], and promote ECM deposition by fibroblasts [180]. However, unchecked activity of alternatively activated macrophages during chronic

inflammation can perpetuate fibrosis [181], which can impair restoration of a tissue's native structural and mechanical properties [182].

Sphingosine-1-phosphate (S1P) is a pleiotropic bioactive signaling lipid that is produced endogenously by red blood cells, platelets, and endothelial cells [183]. S1P activates signaling through five known G protein-coupled receptors, S1PR1-5, which are differentially expressed in almost every cell type. Local delivery of FTY720, a small molecule agonist of S1P1 and S1PR3-5, selectively recruits non-classical Ly6C^{lo} monocytes upon local delivery to inflamed skin injuries and promotes arteriogenic microvascular growth in an S1PR3-dependent manner [9]. Release of FTY720 from polymer nanofibers to mandibular bone defects increases the frequency of alternatively activated macrophages, promotes defect site revascularization, and facilitates mineralization [184]. Thus, S1PR signaling is a promising therapeutic target to modulate the inflammatory response and subsequent healing of soft tissue injuries.

In this work, we explored the immunomodulatory effects of FTY720 delivered from a biomaterial implant on monocyte and macrophage subsets associated with vascularization and tissue repair. Delivery of FTY720 induced homing of extravasated non-classical monocytes to peri-implant vasculature and accumulation of wound healing macrophages 3 days post-injury in the murine dorsal skinfold window chamber model. FTY720 promoted perivascular accumulation of alternatively activated macrophages within ischemic skeletal muscle and expansion of vascular networks. To explore whether FTY720-mediated immunomodulation improves muscle repair after traumatic injury, a novel model of volumetric muscle injury within the murine spinotrapezius muscle was used. FTY720 increased the frequency of non-classical monocytes and alternatively

activated macrophages 3 days post-injury, which correlated with enhanced defect site vascularization and collagen deposition. FTY720 improved regrowth of muscle fibers and the overall collagen architecture within regenerated tissue 7 days post-injury. These results indicate that immunomodulatory biomaterials that target specific mononuclear phagocyte populations can improve both revascularization and overall tissue quality after injury.

4.3 Results

4.3.1 FTY720 promotes perivascular localization of non-classical monocytes.

We have previously demonstrated that localized delivery of the small molecule FTY720 from PLGA thin films enhances recruitment of $Ly6C^{lo}$ monocytes to inflamed peri-implant tissue and supports arteriogenesis [9, 159]. FTY720 is a synthetic analog of sphingosine that acts as an agonist at S1PR1 and S1PR3-5. To further investigate the function and spatial distribution of monocytes recruited to inflamed tissue through S1PR signaling, we performed mouse dorsal skinfold window chambers (DWC), which enable utilization of intravital imaging modalities. The DWC model involves partial thickness excisional skin injury that removes the epidermis and dermis, with a transparent window placed over the exposed subreticular vasculature. We have previously used this model to investigate the inflammatory response and vascular remodeling around biomaterial implants in real time [9, 54, 159]. We performed intravital confocal microscopy of tissue surrounding FTY720-loaded PLGA implants 1 day post-surgery in mice expressing green fluorescent protein (GFP) under the CX3CR1 promoter ($CX3CR1^{GFP/+}$ mice). CX3CR1 is primarily expressed in monocytes and monocyte-derived cells, with CX3CR1 being highly expressed in non-classical monocytes and lowly expressed in classical monocytes [16].

CX3CR1^{hi} and CX3CR1^{lo} cells were distinguished within intravital images based on maximum fluorescence intensity. Delivery of FTY720 from implanted films increased the frequency of non-classical CX3CR1^{hi} monocytes 1 day post-surgery and decreased the distance of CX3CR1^{hi} monocytes to the nearest blood vessel (**Figure 13a-c**). CX3CR1^{lo} cells were located farther from the nearest blood vessel in the presence of FTY720 (**Figure 13d**). Additionally, CD68+CD206+ macrophages visualized by immunofluorescence adopted an elongated morphology along the vasculature surrounding FTY720 implants 3 days post-injury (**Figure 13e**).

To investigate whether perivascular localization is a signature of non-classical monocytes, we compared the spatial positioning of monocyte subsets *in vitro*. CX3CR1^{hi} and CX3CR1^{lo} monocytes sorted from bone marrow of CX3CR1$^{GFP/+}$ mice were co-cultured with murine endothelial cell networks on Matrigel. A significantly higher frequency of CX3CR1^{hi} non-classical monocytes compared to CX3CR1^{lo} classical monocytes localized to *in vitro*-forming vessel networks (**Figure 14a,b**). To determine whether monocytes positioned themselves in proximity to the vessels, we compared the proportion of cells within 20μm from the vessel to the positions of a computer-generated random distribution of cells. Random distributions were generated by stochastically positioning the same quantity of CX3CR1^{hi} or CX3CR1^{lo} monocytes on images of *in vitro* endothelial networks. The randomly-generated distributions were indistinguishable from the experimental distribution of CX3CR1^{lo} monocytes with respect to the proportion of

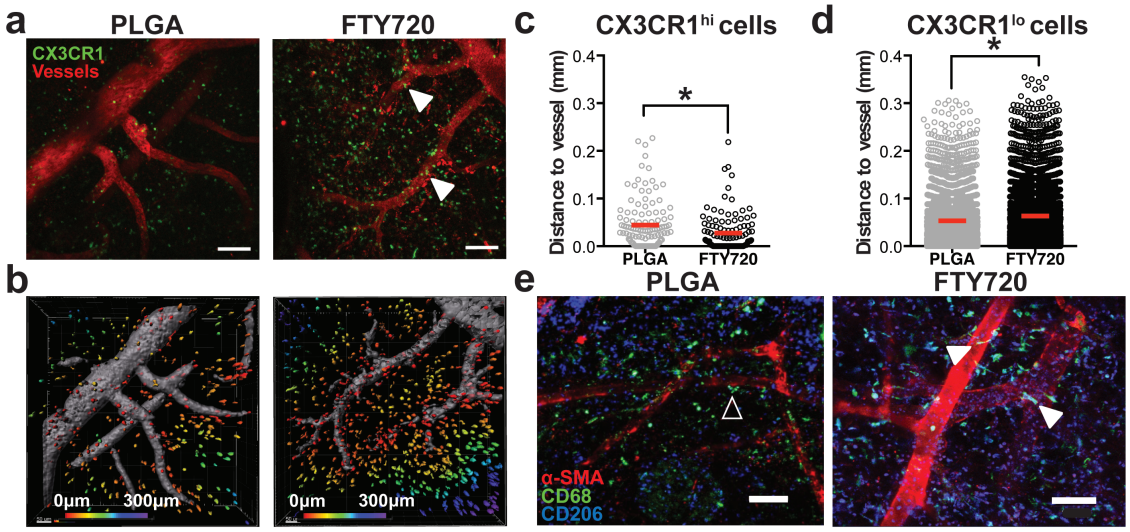

Figure 13. FTY720 recruits non-classical monocytes to the perivascular space. (a) Intravital imaging of DWCs in CX3CR1$^{GFP/+}$ transgenic mice 1 day post-injury. CX3CR1^{hi} cells preferentially accumulated around peri-implant arterioles (white arrows) (b) Representative surface renderings of CX3CR1+ cells, color-coded according to distance from the closest blood vessel with red cells being closest to blood vessels and purple cells being the farthest away. Vessels were labeled with i.v. injection of rhodamine-dextran. (c) Distance to the nearest blood vessels of CX3CR1^{hi} cells in animals treated with FTY720 compared to unloaded PLGA controls. (d) Distance to the nearest blood vessels of CX3CR1^{lo} cells. Statistical analyses were conducted using two-tailed Mann-Whitney test. *$p<0.05$, $n>100$ cells, across 3-4 animals per group. (e) Immunostaining of CD68+CD206+ macrophages and vasculature. In animals treated with unloaded PLGA, perivascular CD68+CD206+ macrophages were circular (open arrow), while in FTY720-treated animals, CD68+CD206+ macrophages associated closely with inflamed vasculature and adopted an elongated morphology (solid white arrows). Scale bars, 100µm.

cells in close proximity (less than 20µm) to the endothelial network (**Figure 14b**). Conversely, the frequency of CX3CR1^{hi} monocytes in close proximity to the endothelial network was significantly higher than the random position distributions (**Figure 14b**). These results indicate that non-classical monocytes preferentially localize near endothelial cells, which may prime them for differentiation into macrophages [185] or enable them to exert effects on the microvasculature [56, 154, 186].

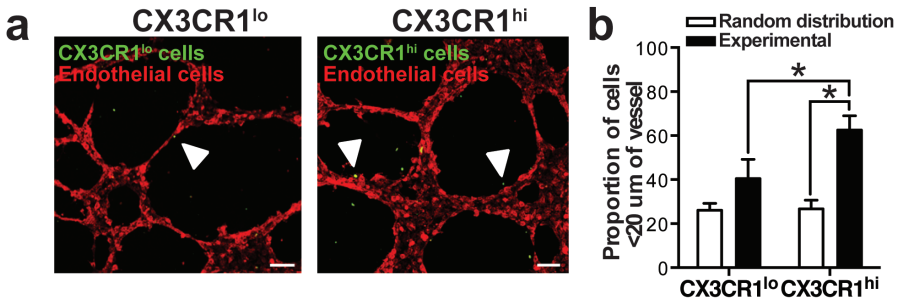

Figure 14. ***In vitro*** **association of monocytes and endothelial cells.** (a) Sorted CX3CR1^{lo} and CX3CR1^{hi} mouse monocytes associate with murine endothelial cell networks *in vitro* (solid white arrows) (b) The proportion of experimental CX3CR1^{hi} monocytes within 20μm of the vessel network compared to CX3CR1^{lo} monocytes and a model-simulated random distribution of cells. Data presented as mean ± S.E.M. *p<0.05 by two-way ANOVA. n=3 independent experiments.

4.3.2 Local delivery of FTY720 promotes accumulation of alternatively activated macrophages

We further explored the fate of specific blood monocyte populations in response to localized S1PR stimulation by selectively labeling Ly6C^{lo} and Ly6C^{hi} monocytes with latex beads (Chapter 3, **Figure 5**) followed by implantation of FTY720-loaded PLGA films in the DWC. No differences in the overall frequency of blood-derived Ly6C^{lo} monocytes was observed with FTY720 delivery compared to blank implant (**Figure 15a,c**). However, FTY720 increased the frequency of CD206+ macrophages within injured tissue 3 days post-surgery (**Figure 15b**). The conversion efficiency of labeled blood-derived Ly6C^{lo} monocytes into CD206+ macrophages was similar between groups, suggesting that FTY720 does not enhance the rate at which monocytes convert to CD206+ macrophages (**Figure 15d**).

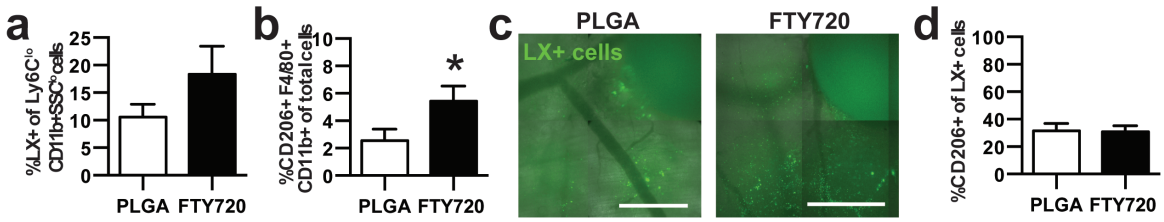

Figure 15. FTY720 promotes accumulation of alternatively activated macrophages. PLGA films loaded with FTY720 were implanted immediately after DWC surgery. (a) Proportion of latex bead-positive (LX+) Ly6C^{lo} monocytes derived from blood in tissue 3 days post-injury following labeling of Ly6C^{lo} monocytes. (b) Frequency of CD206+ macrophages in the presence of FTY720. (c) LX+ cells in tissue surrounding unloaded or FTY720-loaded implants. (d) Conversion efficiency of circulation-derived Ly6C^{lo} monocytes into CD206+F4/80+CD11b+ cells. Scale bars, 500µm. Data presented as mean ± S.E.M. *p<0.05 by two-tailed t-test. n=10-12 animals per group.

Selective labeling of Ly6C^{hi} monocytes (Chapter 3, **Figure 7**) demonstrates that FTY720 does not recruit circulation-derived Ly6C^{hi} monocytes to tissue when Ly6C^{lo} blood monocytes are reduced with clodronate liposomes (**Figure 16a,c**). We observed no changes in the frequency of total CD206+F4/80+CD11b+ cells (**Figure 16b**), suggesting that FTY720 is unable to increase the number of alternatively activated macrophages after reduction of circulating Ly6C^{lo} monocytes.

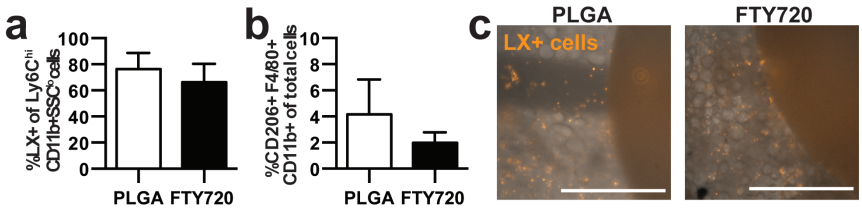

Figure 16. FTY720-induced accumulation of alternatively activated macrophages requires circulating Ly6C^{lo} monocytes. (a) Proportion of LX+ Ly6C^{hi} monocytes that were derived from blood following labeling of Ly6C^{hi} monocytes with Clod Lip. (b) Overall frequency of CD206+ macrophages in the presence of FTY720 after Clod Lip administration. (c) LX+ cells in tissue surrounding unloaded or FTY720-loaded PLGA implants. Scale bars, 500µm. Data presented as mean ± S.E.M. n=4 animals per group.

4.3.3 FTY720 increases perivascular accumulation of alternatively activated macrophages and promotes vascular network expansion after arteriole ligation

The recruitment kinetics, fate, and function of myeloid cells during inflammation is heavily dependent on the specific type of tissue injury [8, 156]. Consequently, we sought to determine whether application of FTY720-loaded materials to ischemic muscle injury produces similar patterns of immunomodulation. Feeder arteriolar vessels within the murine spinotrapezius muscle were ligated in CX3CR1$^{GFP/+}$ mice. The spinotrapezius muscle is a stabilizing muscle in the mouse dorsum that is extremely thin (60-200μm) [187, 188], enabling the use of three-dimensional (3D) confocal microscopy to examine tissue microstructures. Unloaded or FTY720-loaded PLGA films were implanted over the muscle immediately after injury and whole mount immunohistochemistry and confocal microscopy were performed. We observed a decrease in the overall area of CX3CR1^{hi} cells in FTY720-treated animals 3 days post-injury (**Figure 17a, b**). We observed no difference in the total number of CD206+ cells (**Figure 17c**), but an overall increase in the area ratio of CD206+ cells to CX3CR1^{hi} cells in FTY720-treated animals (**Figure 17d**).

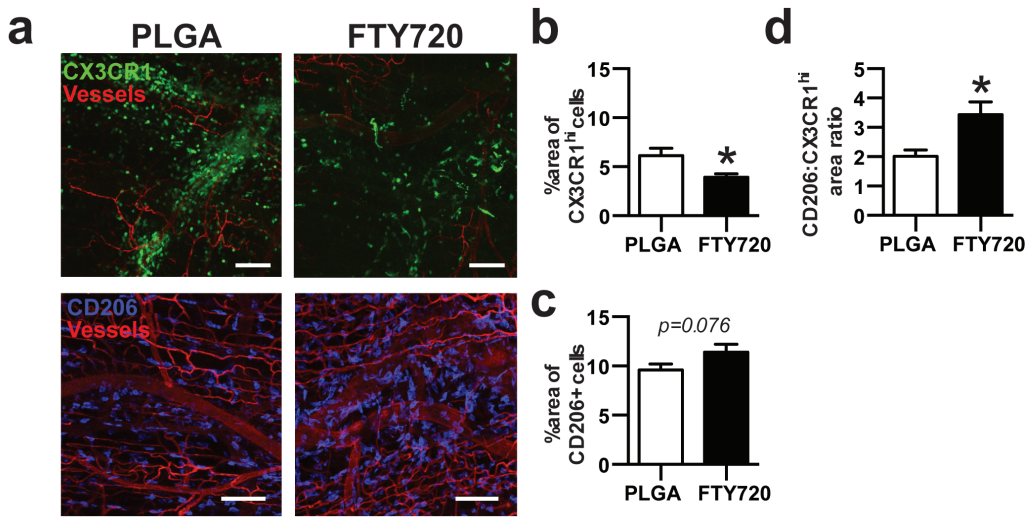

Figure 17. FTY720 alters monocyte/macrophage accumulation after arteriole ligation in the spinotrapezius muscle. (a) Immunofluorescence of muscle tissue 3 days after ligation of spinotrapezius muscle arterioles in CX3CR1$^{GFP/+}$ mice shows accumulation of CX3CR1^{hi} monocytes (top) and CD206+ macrophages (bottom) to lectin-stained vasculature 3 days post-ligation. (b) Area of CX3CR1^{hi} cells and (c) CD206+ cells in muscle tissue treated with unloaded FTY720-loaded PLGA 3 days post-ligation. (d) Area ratio of CD206+ to CX3CR1^{hi} cells. Data presented as mean ± S.E.M. *p<0.05 by two-tailed t-test. n=25-27 FOVs from 5 animals per group. Scale bars, 100µm.

Previous work has demonstrated that monocytes differentiate into alternatively activated macrophages in vascular niches [185]. We investigated the localization of CX3CR1^{hi} and CD206+ cells with respect to lectin-stained vasculature. No significant difference in CX3CR1^{hi} cells (**Figure 18a**), but more CD206+ cells (**Figure 18b**) were found within 50µm of blood vessels in FTY720-treated animals. Additionally, FTY720-treated animals had a greater vessel density and total length of arterioles 3 days after ligation, indicating that FTY720 promotes revascularization after ischemic muscle injury (**Figure 18d-e**).

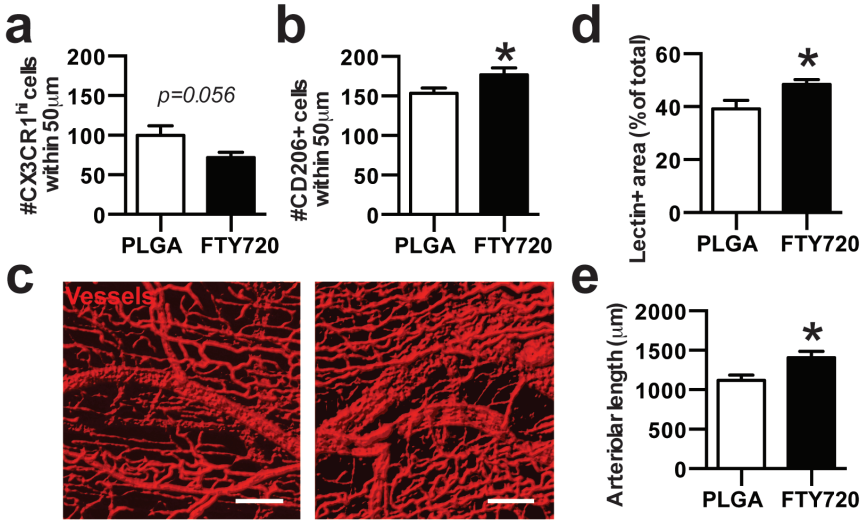

Figure 18. FTY720 promotes microvascular network expansion after muscle arteriole ligation. (a) Number of CX3CR1^{hi} cells and (b) CD206+ cells within 50μm of blood vessels. (c, d) Total density of lectin+ blood vessels and (e) the length of arterioles in the spinotrapezius muscle treated with FTY720 3 days post-ligation. Data presented as mean ± S.E.M. Statistical analyses performed using two-tailed t-tests. *p<0.05, n=25-27 FOVs from 5 animals per group. Scale bars, 100μm.

4.3.4 Characterization of myeloid cell response to full-thickness defect in the murine spinotrapezius muscle

In order to better study repair of traumatic tissue injuries and model clinical muscle loss, we developed a novel model of volumetric muscle loss (VML) in the murine spinotrapezius (**Figure 19a**). A 1mm circular defect in the spinotrapezius muscle heals over the course of 7 days, as quantified from desmin immunostaining of muscle fibers (**Figure 19b**). Consequently, removal of a 1mm diameter muscle defect is not critical-sized, but enables investigations into the mechanisms, rate, and quality of muscle repair. We then investigated the kinetics of myeloid cell trafficking in response to spinotrapezius VML injury. Within injured spinotrapezius muscle tissue, neutrophils peaked at 3 days post-injury (0.7±0.2% of all cells) and quickly decreased to baseline levels by 7 days post-

injury (**Figure 19c**). Ly6C^{hi} monocytes decreased from days 1 (0.7±1.2%) to 7 (0.3±0.5%), while Ly6C^{lo} monocytes peaked at day 3 (1.5±0.9%) post-injury and were retained at a similar frequency at day 7 (**Figure 19d**). MerTK and CD64 exclusively identify macrophages (MerTK+CD64+) [21], which steadily increase from day 1 (0.5±0.6%) to day 7 (3.0±1.0%) (**Figure 19e**). CD206+ macrophages also increase over time (0.4±0.6% at day 1 to 2.8±1.0% at day 7) (**Figure 19f**). These measurements indicate that neutrophils and Ly6C^{hi} monocytes accumulate in the acute inflammatory phase of VML injury, while macrophages, particularly CD206+ macrophages, predominate in the later phases of muscle injury and healing.

4.3.5 Local delivery of FTY720 increases the frequency of non-classical monocytes in injured muscle.

Given the immunomodulatory effects of FTY720 observed in wounded skin (**Figure 15)** and ischemic muscle (**Figure 17**), we sought to determine whether this strategy could be leveraged after VML injury to enhance accumulation of pro-regenerative myeloid cells. Implantation of a FTY720-loaded PLGA thin film over the muscle defect increased the frequency of Ly6C^{lo}, but not Ly6C^{hi}, monocytes compared to PLGA only or no implant controls, as determined by flow cytometry (**Figure 20a**). VML injury was induced in CX3CR1$^{GFP/+}$ mice to visualize recruitment of monocyte subsets distinguished by CX3CR1 expression. Very few CX3CR1-GFP+ cells were detected in the uninjured contralateral spinotrapezius muscle, and most of these cells were CX3CR1^{hi} (**Figure 20b**).

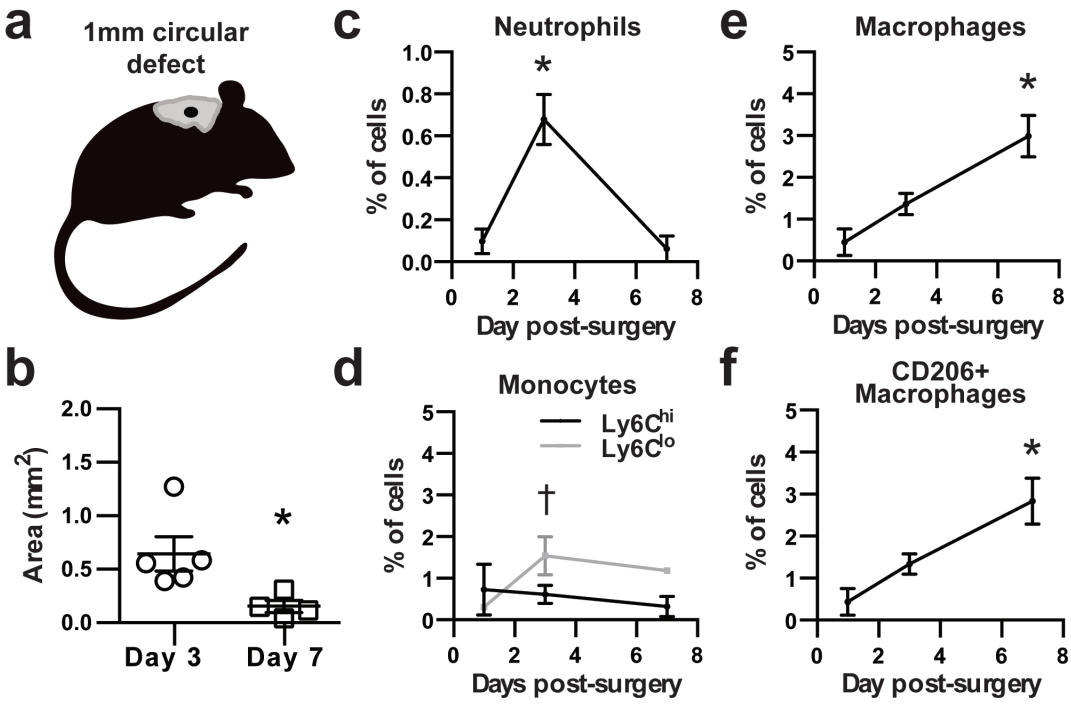

Figure 19. Mouse model of volumetric muscle loss in the murine spinotrapezius muscle. (a) A 1mm circular volumetric defect made in the spinotrapezius of wildtype mice heals over 7 days, as (b) quantified by desmin immunostaining. Statistical analyses were performed using two-tailed t-tests. *$p<0.05$, n=4-5 animals per group. (c) Neutrophils in injured muscle tissue peak at day 3 and decrease by day 7 post-injury (tissue neutrophils gated on MerTK-CD64-CD11c-CD11b+SSC^{hi}Ly6G^{hi}). (d) Ly6C^{hi} monocytes in injured muscle tissue decrease from day 1 to day 7 post-injury, while Ly6C^{lo} monocytes increase from day 1 to 3 and decrease by day 7 (tissue monocytes gated on CD11b+SSC^{lo}MerTK-CD64-CD11c-). (e) MerTK+CD64+ macrophages increase from day 1 to 7 post-injury. (f) CD206+ macrophages increase from day 1 to 7 post-injury. Data presented as mean ± S.E.M. $^{\dagger}p<0.05$ compared to Day 0 for Ly6C^{lo} monocytes or *$p<0.05$ compared to Day 0 for all other cell types by one-way ANOVA. n=4 animals per group.

Qualitative assessment of whole mount tissues shows that delivery of FTY720 increased accumulation of CX3CR1^{hi} cells in the peri-defect muscle tissue (**Figure 20c**), which is consistent with the flow cytometry data that shows increased Ly6C^{lo} monocyte frequency following FTY720 treatment. Previous studies have indicated that Ly6C^{lo} monocytes present during toxin-induced muscle inflammation are derived from Ly6C^{hi} monocytes rather than direct recruitment of circulating Ly6C^{lo} monocytes [4]. Using *in situ*

LX bead-based labeling (Chapter 3, **Figure 5**), Ly6C^{lo} blood monocytes were labeled in CX3CR1$^{GFP/+}$ mice 1 day prior to VML surgery to track the fate of Ly6C^{lo} monocytes during FTY720-mediated immunomodulation. Inspection of whole mount confocal images revealed a high frequency of LX+ cells in the muscle tissue (**Figure 20d**), demonstrating that labeled Ly6C^{lo} monocytes were directly recruited from circulation to the injured tissue. Interestingly, LX+ cells were primarily negative for CX3CR1 expression, indicating that these cells may have differentiated into a cell type that is lower in CX3CR1 expression (such as macrophages) or been cleared by phagocytosis. More LX+ cells were observed around the defect in the muscle tissue of FTY720-treated animals (**Figure 20d**).

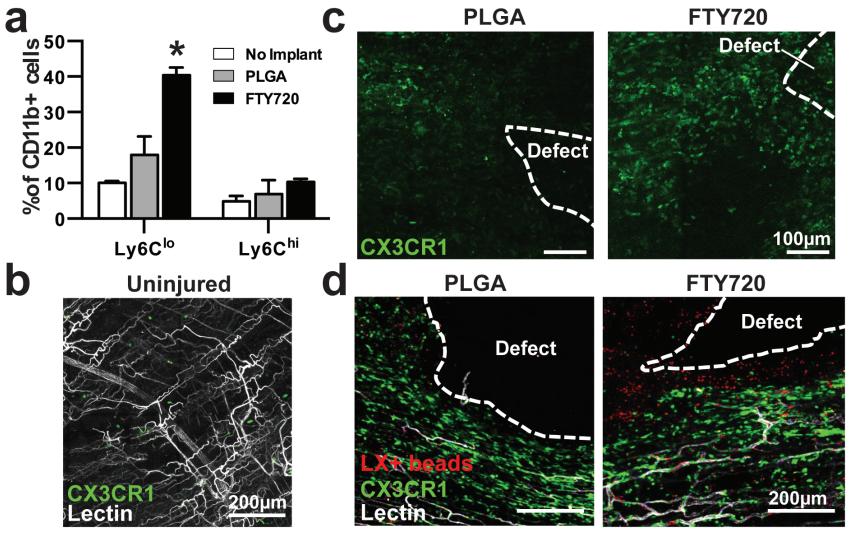

Figure 20. Delivery of FTY720 increases Ly6C^{lo}, CX3CR1^{hi} monocytes in volumetric muscle injury. (a) Frequency of Ly6C^{lo} and Ly6C^{hi} monocyte subsets 3 days post-injury during delivery of FTY720 from PLGA thin films to VML injury in wildtype mice (monocytes gated on CD11b+SSC^{lo}). (b) Uninjured, contralateral spinotrapezius muscle from CX3CR1$^{GFP/+}$ mice. (c) CX3CR1^{hi} cells within peri-defect tissue at day 3 in mice treated with an FTY720-loaded or unloaded implant. (d) Distribution of LX+ cells around VML defects 3 days post-injury. Data presented as mean ± S.E.M. *$p<0.05$ compared to Ly6C^{lo} monocytes in PLGA and no implant controls by two-way ANOVA. n=3-4 animals per group.

4.3.6 Local delivery of FTY720 increases accumulation of CD206+ alternatively activated macrophages in injured muscle

To quantify cellular infiltration into the defect, we measured the relative size of the avascular region with high myeloid cellularity (CX3CR1+ cells). FTY720-treated animals had a larger percentage of the defect filled with CX3CR1+ cells (**Figure 21a,b**). We observed a similar, but insignificant, trend following quantification of the proportion of the defect filled with CD68+ and CD206+ cells (*data not shown*). Interestingly, we noticed cellular regions that were sparse in CX3CR1+ cells but contained numerous CD68+ CD206+ cells. Since we previously observed conversion of non-classical monocytes into alternatively activated macrophages (Chapter 3, **Figure 10**), we investigated whether FTY720 also increases the frequency of CD206+ macrophages in injured muscle. Animals treated with FTY720 had more CD68+CD206+ alternatively activated macrophages in peri-defect tissue 3 days post-injury (**Figure 21c,d**). Close interactions of macrophages and endothelial cells have been associated with enhanced vascular remodeling and arteriogenesis [189, 190]. Quantification of the distance between CD68+CD206+ macrophages and the nearest CD31+ blood vessel within damaged spinotrapezius muscles revealed that CD206+ macrophages were located closer to vasculature with FTY720 treatment (**Figure 21e**).

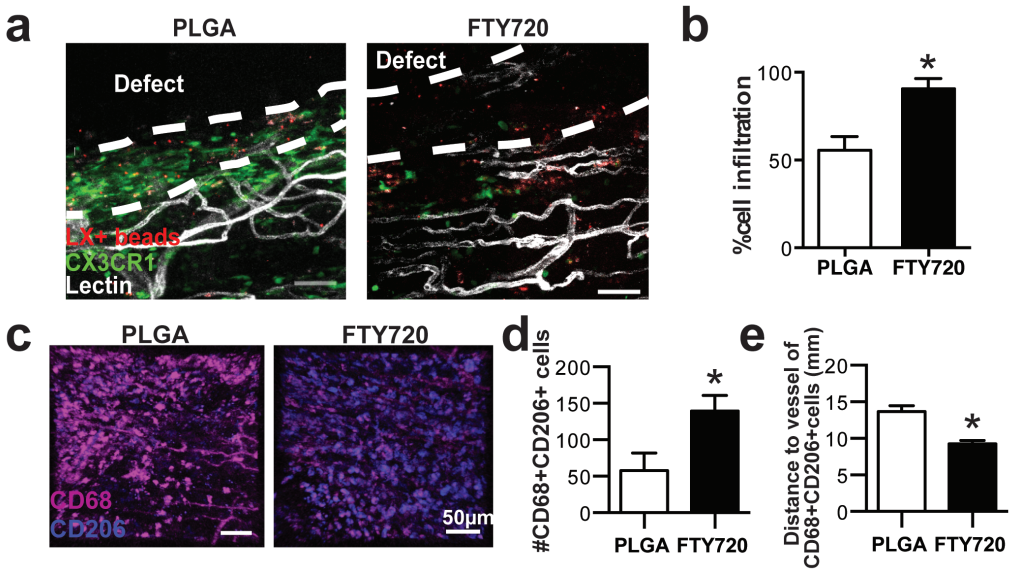

Figure 21. FTY720 increases the frequency of CD68+CD206+ cells in injured muscle of CX3CR1$^{GFP/+}$ mice. (a) Infiltration of CX3CR1+ and LX+ cells into the defect region in PLGA- and FTY720-treated mice 3 days post-injury. (b) Quantification of cellular infiltration in CX3CR1/LX bead/lectin-labeled muscles defects. (c, d) Density of CD68+CD206+ cells 3 days post-injury near muscle defects. (e) Quantification of the distance of CD68+CD206+ cells to the nearest CD31+ blood vessel 3 days post-injury. Data presented as mean ± S.E.M. *p<0.05 by two-tailed t-test. n=3-4 animals per group. Scale bars, 50μm.

4.3.7 FTY720 immunomodulation promotes early wound healing and improved regenerated muscle quality

To investigate whether FTY720-induced perivascular accumulation of CD206+ macrophages was associated with repair of injured skeletal muscle, we assessed wound healing parameters. By 3 days post-injury, local delivery of FTY720 was able to induce increased revascularization of the defect region (**Figure 22a,b**), as quantified by the density of area positive for CD31 immunostaining. Interestingly, the amount of revascularization in FTY720-treated animals was similar to animals with no implant (*data not shown*), indicating that PLGA may impair revascularization. Increased collagen deposition within

the defect area, as measured by imaging the second harmonic generation (SHG) signal, was observed in FTY720-treated animals (**Figure 22c**), coinciding with a significantly decreased non-collagenous void area (**Figure 22d**).

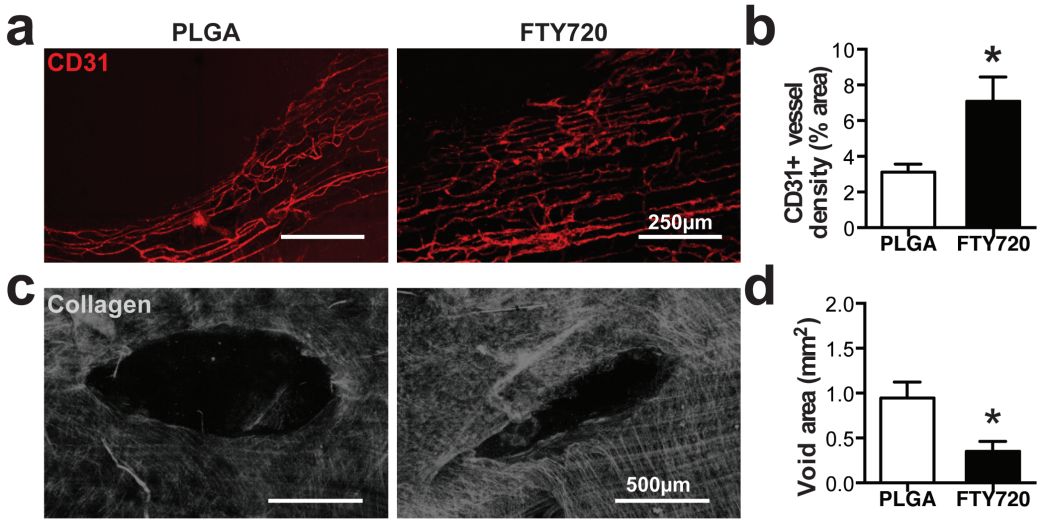

Figure 22. Delivery of FTY720 promotes muscle healing 3 days post-injury in CX3CR1$^{GFP/+}$ mice. (a) CD31 immunostaining to visualize defect area vascularization in PLGA- and FTY720-treated mice 3 days post-injury and (b) quantification of CD31+ vessel density. (c) Collagen deposition within the defect region visualized by two-photon microscopy and (d) quantification of the non-collagenous void area.

At day 7 post-injury, injured muscles were imaged with two-photon confocal microscopy for immunostained desmin and SHG collagen signal. Images were rendered using 3D imaging processing software to generate quantitative volumes of desmin and collagen signal. FTY720-treated animals displayed a lower volume ratio of collagen to desmin compared to PLGA animals (**Figure 23a,b**), indicating less interstitial fibrosis. Furthermore, control animals displayed highly aligned collagen fibrils compared to uninjured muscle, which is a hallmark of fibrotic scarring [191]. Regenerated fiber diameter was significantly higher in animals treated with FTY720 compared to PLGA only

(**Figure 23c,d**), and comparable to that observed in uninjured spinotrapezius muscle. Taken together, these findings demonstrate that immunomodulatory biomaterial strategies that coordinate inflammatory, angiogenic, and fibrotic processes can improve skeletal muscle repair.

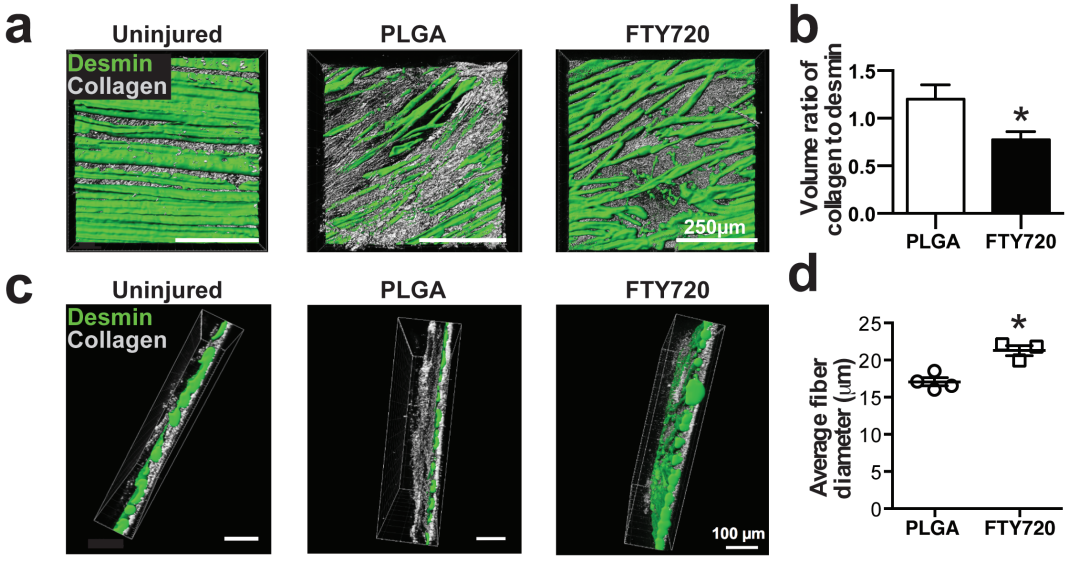

Figure 23. Local immunomodulation with FTY720 improves muscle repair 7 days post-injury in wildtype mice. (a) FTY720-treated mice have larger and more desmin+ muscle fibers (detected by immunostaining) that more closely recapitulates the structure of an uninjured contralateral control, as well as less dense and aligned collagen (detected by two-photon microscopy) compared to PLGA controls. (b) FTY720-treated mice have a reduced volume ratio of collagen to desmin. (c-d) FTY720-treated mice have regenerated muscle fibers with a larger diameter. Data presented as mean ± S.E.M. Statistical analyses were performed using two-tailed t-tests. *$p<0.05$, n=3-4 animals per group.

4.4 Discussion

In the present work, we have demonstrated that local delivery of the S1PR agonist FTY720 from PLGA thin films enhances accumulation of CD206+ alternatively activated macrophages and promotes vascularization of ischemic or traumatically injured skeletal muscle. The immunomodulatory effects of FTY720 are likely mediated in part through recruitment of non-classical monocytes, as their removal from circulation with clodronate liposomes impaired generation of alternatively activated macrophages. Perivascular localization of CX3CR1^{hi} monocytes in response to FTY720 delivery during the acute inflammatory phase after skin injury, and perivascular accumulation of CD206+ macrophages in injured muscle suggests that pro-regenerative myeloid cells may position themselves near the vasculature. FTY720 promoted multimodal tissue repair of traumatically injured muscle, including early collagen deposition, enhanced re-vascularization and muscle fiber regeneration, and reduced fibrotic deposition.

While macrophages are key mediators of the host response to implanted materials and govern the integration of implants into host tissue [101, 192], the role that their monocytic precursors play in regulating implant outcome has been largely unexplored. In our studies, around 45% of monocytes surrounding PLGA implants were Ly6C$^{lo/int}$. In previous work [54], we demonstrated that around 40% of monocytes around heparin-containing PEG hydrogels were Ly6C$^{lo/int}$. While lymphocyte, granulocyte, and macrophage accumulation are impacted by the type of material implanted [193], future studies are needed to determine how different classes of materials impact infiltration of monocyte and macrophage subsets. Delivery of FTY720 from a PLGA material increased the frequency of Ly6C^{lo} non-classical monocytes 3 days after volumetric muscle loss in

the spinotrapezius muscle (**Figure 20**a). Interestingly, we observed model-specific differences in the effect of FTY720 on monocyte recruitment, as we detected a decrease in CX3CR1^{hi} non-classical monocytes 3 days after arteriole ligation (**Figure 17b**). While this merits further investigation, one possibility is that the progression of inflammation is expedited during ischemic injury because of the need to rapidly restore blood supply and oxygen transport. CX3CR1 may also mark a slightly different myeloid population than those distinguished by Ly6C expression, as extravasated CX3CR1+ cells may also include dendritic cells and natural killer cells [194].

Macrophages are the primary source of angiogenic growth factors such as VEGF [69] and robust vascularization is associated with increased macrophage presence in and around biomaterial implants [143, 184]. M2-polarized macrophages (IL-4- or IL-10-stimulated) are considered pro-angiogenic both *in vitro* and *in vivo* [174, 195, 196], though recent studies have demonstrated that M1-polarized macrophages may also play key roles in angiogenesis [41, 57]. Hydrogel vascularization in response to growth factor delivery (platelet-derived growth factor and fibroblast growth factor) in the cornea was accompanied by accumulation of macrophages that produce both M1- and M2-associated mRNA transcripts, such as *Tnfa* and *Arg1*, respectively [143]. CD206 is expressed on bone marrow-derived macrophages that have been alternatively activated through exposure to IL-4 *in vitro* (also called M2a macrophages) [41]. The present work provides additional evidence that alternatively activated macrophages are associated with expansion of vascular networks, as muscles treated with FTY720 displayed increased vessel density (**Figure 18d, Figure 22b**), which coincided with increased numbers of M2-like CD206+ cells (**Figure 21d**). FTY720 likely acts on both immune cells and the endothelium, as loss

of S1PR3 in hematopoietic or parenchymal cells impairs FTY720-induced arteriogenic remodeling [9].

Adoptively-transferred non-classical monocytes selectively differentiate into CD206+ macrophages in injured skin (Chapter 3, [197]); therefore, we also explored whether FTY720 affects accumulation of alternatively activated macrophages. FTY720 increased the frequency of both F4/80+CD206+ macrophages in wounded skin (**Figure 15b**) and the number of perivascular CD68+CD206+ macrophages in injured muscle (**Figure 18b, Figure 21e**). Previously, we have also detected more M2-like macrophages within mandibular bone defects 3 weeks after implantation of FTY720-loaded polymer nanofibers [184]. Monocytes and macrophages can position themselves strategically by remodeling blood vessels within inflamed tissue [23, 189, 190]. Crosstalk between the vasculature and immune cells may provide instructional cues for alternative activation of macrophages [185]. *In vitro,* $CX3CR1^{hi}$ monocytes preferentially associated with endothelial cell networks (**Figure 14**), and *in vivo,* exhibit closer homing to inflamed vasculature in the presence of FTY720 (**Figure 13c**). While further studies are needed, it is possible that the vasculature provides microenvironmental cues that educate non-classical monocytes to convert into alternatively activated macrophages via signaling with the endothelium [185]. Increased perivascular positioning of alternatively activated macrophages in FTY720-treated animals coincided with increased density of vasculature in injured muscle (**Figure 18d, Figure 22b**) compared to PLGA control animals. Similarly, during chronic arterial occlusion, CD163+ macrophages are clustered in the perivascular space at sites of collateral growth in remodeling vasculature [198].

Consequently, both the phenotype of monocytes and macrophages, as well as their spatial distribution is likely an important feature when assessing their function.

In addition to promoting vascularization, FTY720 also supported overall healing of traumatically injured skeletal muscle (**Figure 22d, Figure 23**). Alternatively activated macrophages can promote muscle repair by providing a source of regenerative growth factors such as IGF-1 [199] and promoting satellite cell differentiation into mature myotubes [4, 73]. Macrophages control collagen deposition from fibroblasts in an IL-4rα-dependent manner [45], a process that is vital to wound healing within the skin. Assessment of the defect area via SHG imaging of collagen showed that FTY720 results in increased collagen content and a smaller defect area 3 days post-injury (**Figure 22c,d**). By 7 days post-injury, regenerated fiber diameter was significantly higher in FTY720-treated animals and the collagen architecture more closely mimicked that of native uninjured muscle (**Figure 23**). Future studies should focus on whether monocytes and macrophages are absolutely required for FTY720-mediated repair, and if so, which repair processes they primarily target. Taken together, these results indicate that incorporation of FTY720 into biomaterial implants can induce pro-regenerative immunomodulation and promote tissue revascularization and repair.

4.5 Materials and Methods

4.5.1 Material fabrication

Films were fabricated as previously described [9]. Briefly, 350 mg PLGA (50:50 DLG 5E – Evonik Industries) was dissolved in 2ml dichloromethane in a glass scintillation vial via high-speed vortexing. For drug-loaded films, 1.75 mg of FTY720 (Cayman Chemical) was added at a 1:200 drug:polymer weight ratio, and mixed until completely incorporated. Polymer solutions were poured into Teflon-coated petri dishes and allowed to dry at -20°C for 7 days. Before use, films were lyophilized overnight to remove any traces of solvent.

4.5.2 Dorsal skinfold window chamber and tracking of monocyte subsets

All animal procedures were conducted according to protocols approved by the Georgia Institute of Technology or University of Virginia Institutional Animal Care and Use Committee. Male C57BL/6J or B6.129P-Cx3cr1tm1Litt/J mice ($CX3CR1^{GFP/+}$) mice (8-12 weeks) were fitted with sterile dorsal skinfold window chambers (APJ Trading Co) as previously described [9], and as described in Chapter 3 Materials and Methods. Two films were placed on top of the exposed subreticular dermis layer immediately after surgery (Day 0) and exposed tissue was sealed with a sterile glass window. Mice were euthanized 72 hours after surgery via CO_2 asphyxiation. The vasculature was immediately flushed with intracardiac infusion of saline follow by an intracardiac infusion of 4% paraformaldehdyde, prior to whole mounting of tissue and immunohistochemistry. For selective labeling of $Ly6C^{lo}$ monocytes, mice were administered 250μL of Fluoresbrite® Polychromatic Red latex beads intravenously one day prior to surgery (0.5μm, Polysciences - diluted 1:25 in

sterile saline) via jugular vein injection. For selective labeling of Ly6C^{hi} monocytes, mice were administered 100μL of clodronate liposomes per 10g of mouse body weight (Dr. Nico van Rooijen, clodronateliposomes.com) intravenously two days prior to surgery, followed by administration of latex beads 16 hours later (one day prior to surgery).

4.5.3 Flow cytometry

Prior to tissue collection, mice were euthanized via CO_2 asphyxiation. The dorsal tissue circumscribing films was punched out with 6mm biopsy punches and pooled from both films within one animal. For characterization of myeloid cell composition in spinotrapezius muscles without an implant, a 6mm biopsy punch of muscle tissue centered on the defect was taken. For studies with an implant (unloaded or FTY720-loaded), the entire spinotrapezius muscle was collected. Tissue was digested with collagenase (1mg/ml) at 37°C for 45 minutes and further disaggregated with a cell strainer to create a single cell suspension. Single cell suspensions of tissues were stained for flow cytometry analysis in 3% FBS according to standard procedures and analyzed on a FACS-AriaIIIu flow cytometer (BD Biosciences). The following antibodies were used for immunophenotyping of cells collected from dorsal tissue: APC-Cy7-conjugated anti-CD11b (BioLegend), APC-conjugated anti-Ly6C (BioLegend), PE-Cy7-conjugated anti-GR-1 (BioLegend), APC-conjugated anti-F4/80 (BioLegend), or PE-Cy7-conjugated anti-CD206 (BioLegend). Positivity was determined by gating on fluorescence minus one controls. Absolute quantification of cell numbers in blood and tissue was performed by adding 25μL of AccuCheck counting beads to flow cytometry samples (Thermo Fisher Scientific). The following antibodies were used for immunophenotyping of cells collected from muscle: BV510-conjugated anti-CD11b (BioLegend), PerCP eFluor-710-conjugated anti-CD115

(eBioscience), APC-Cy7 conjugated anti-CD11b (BioLegend), BV421-conjugated anti-CD11c (BioLegend), APC conjugated anti-Ly6C (BioLegend), PE-Cy7 conjugated anti-GR-1 (BioLegend), BV711-conjugated anti-CD64 (BioLegend), PE-conjugated anti-MerTK (R&D Systems), APC-Cy7-conjugated anti-Ly6G (BioLegend), PE-Cy7-conjugated anti-CD206 (BioLegend).

4.5.4 Intravital image acquisition

Mice were anesthetized with isofluorane, the glass window was removed, and dorsal tissue was superfused with saline to prevent desiccation. Up to two films were implanted into the window chambers on the day of surgery (day 0). To label perfused vasculature, mice were anesthetized with isoflurane and given a retro-orbital injection of high molecular weight TRITC-conjugated dextran (2 MDa; Life Technologies). For imaging, the anesthetized mouse was secured to the microscope stage in a custom adapter, the glass window was removed, and dorsal tissue was superfused with sterile saline. Intravital confocal microscopy was conducted with a 20X water immersion objective (NA=1.0) on a Zeiss LSM710 NLO microscope and z-stack images were acquired immediately proximal to the films. For 3D analysis in Imaris (Bitplane), images of 708x708μm regions were acquired adjacent to the implant to visualize immune cell distribution in the close surrounding tissue. Cells expressing CX3CR1-GFP were identified in Imaris using the surface tool. CX3CR1+ surfaces were identified by smoothing with a 2μm grain size and an automatic threshold on absolute intensity. Touching objects were split using a seed points diameter of 10μm. $CX3CR1^{hi}$ versus $CX3CR1^{lo}$ cells were discriminated by applying a filter to select surfaces with a high fluorescence intensity in the CX3CR1-GFP channel (above 150 max intensity). Vessels were identified in Imaris by

drawing a surface on the TRITC-dextran fluorescent channel with a 3μm grain size, manually-selected threshold value (determined based on each image), and manually-selected volume filter to remove small debris. To calculate the distance between CX3CR1+ cells and the nearest blood vessel, a distance transformation was applied to TRITC-dextran vessel surfaces and the median position of each CX3CR1+ cell within this space was recorded.

4.5.5 Angiogenesis assay with monocyte co-culture

C166 murine yolk-sac endothelial cells (ATCC) were propagated in flasks coated with 0.1% gelatin (Stem Cell Technologies) using endothelial growth medium (Angioproteomie) and incubated at 37˚C and 5% CO_2 atmosphere. Monocytes were isolated from bone marrow of male CX3CR1$^{GFP/+}$ mice and sorted using a FACS-AriaIIIu to discriminate CX3CR1^{hi} monocytes and CX3CR1^{lo} monocytes. Endothelial tube forming assays were performed in 15-well angiogenesis slides (Ibidi) as follows. Wells were coated with BD Matrigel^{TM} and seeded with C166 cells (7500 cells/ well) and CX3CR1^{hi} or CX3CR1^{lo} monocytes (2000 cells/well). After 20 hours, co-cultures were fixed and labeled with rhodamine-phalloidin. Images were captured using a Zeiss LSM 700 confocal (10x magnification) and Zen software (Zeiss). The centroid of each monocyte was identified and the distance to the nearest endothelial tube formation was calculated using a custom MATLAB code. For each vessel image, a random distribution of "cells" was overlaid on the image (equal to the number of monocytes in the original image) and the distance of the "random cells" to the nearest vessel was calculated. The experimental monocyte distance to vessel was then compared to the computer-generated randomized cell distance to vessel to determine whether the cells preferentially distribute themselves near vessel segments.

4.5.6 Spinotrapezius ischemia model

Mice were anesthetized with an i.p. injection of ketamine/xylazine/atropine (60/4/0.2 mg/kg). Ligation surgeries were performed as previously described [190]. Briefly, a small incision was made on the dorsum above the lateral edge of the right spinotrapezius at the edge of the fat pad. The fascia was separated from the top of the muscle and the fat pad moved before isolating an anatomically reproducible feeding arteriole entering the muscle from below. This feeding arteriole was ligated with 10-0 nonabsorbable suture in two places and cut. The fat pad and fascia were moved back into position and the skin was closed with 8-0 non-absorbable suture. To allow visualization of vascular endothelium of arterioles in $CX3CR1^{GFP/+}$ mice, anesthetized mice were administered an intra-jugular injection of labeled isolectin (IB4-Alexa Fluor 568; Life Technologies), which was allowed to circulate for 10 minutes. Anesthetized mice were euthanized via CO_2 asphyxiation 72 hours post-surgery. The vasculature was immediately flushed with an intracardiac infusion of adenosine (70 mg/L) in Ringer's solution followed by an intracardiac infusion of 4% paraformaldehyde.

4.5.7 Spinotrapezius volumetric muscle loss model and $Ly6C^{lo}$ monocyte labeling

All animal procedures were conducted according to protocols approved by the Georgia Institute of Technology Institutional Animal Care and Use Committee. Male C57BL/6J (The Jackson Laboratory) or B6.129P-Cx3cr1tm1Litt/J mice ($CX3CR1^{GFP/+}$) (The Jackson Laboratory) of age 8-12 weeks old were used for all animal studies. A 1mm full thickness defect in the spinotrapezius muscle was created as follows. The dorsum of the mouse was shaved and hair removal cream applied to completely remove hair. Skin

was sterilized with three washes of 70% ethanol and chlorhexidine. A longitudinal 1 inch incision (cranial to caudal) was made just after the bony prominence of the shoulder blade. The overlying fascia was dissected away and the spinotrapezius muscle identified. Using flat-tipped tweezers, the edge of the spinotrapezius was lifted up. The muscle was reflected and positioned against a sterile piece of wood. A 1mm biopsy punch was made through the muscle, using the wooden piece as support. The muscle was replaced and 1.5 mm implant placed over the punch defect. The incision was closed with mouse wound clips.

In order to visualize cells within injured muscle originating as circulating Ly6C^{lo} monocytes, CX3CR1^{GFP}/+ mice were administered Fluoresbrite® Polychromatic Red latex beads (0.5μm, Polysciences) intravenously 1 day prior to surgery via jugular vein injection. Prior to injection, latex beads were diluted 1:25 in sterile saline as previously described [50]. Labeling was confirmed by retro-orbital blood draw immediately prior to surgery (1 day after bead administration) and subsequent flow cytometry analysis.

4.5.8 Whole mount immunohistochemistry

For lectin-based labeling of the vasculature in CX3CR1$^{GFP/+}$ mice, Alexa Fluor 568 isolectin IB4 (1mg/mL, Life Technologies) was diluted (50μL of isolectin, 150μL saline) and administered by jugular vein injection 15 minutes prior to euthanasia. Post-euthanasia, mouse vasculature was perfused with warm saline followed by 4% PFA until tissues were fixed. Dorsal tissue and spinotrapezius muscles were explanted and permeabilized overnight with 0.1-0.2% saponin. The tissues were blocked overnight in 5-10% mouse serum. Tissues were incubated at 4˚C overnight in solution containing 0.1% saponin, 5% mouse serum, 0.5% bovine serum albumin, and the following conjugated fluorescent

antibodies: Alexa Fluor 594 or PE anti-CD31 antibody (BioLegend, eBioscience) or Alexa Fluor 568 isolectin IB4 (Life Technologies) for blood vessel visualization, Alexa Fluor 647 anti-CD68 (AbD Serotec) for monocyte/macrophage visualization, and Alexa Fluor 488 anti-CD206 (AbD Serotec) or Alexa Fluor 647 anti-CD206 (Biolegend). For desmin immunostaining in muscle, identical tissue processing procedures were followed and muscles were incubated overnight with Alexa Fluor 488 anti-desmin (1:200 dilution, Abcam) alone or in combination with PE anti-CD31 and Alexa Fluor 647 anti-CD206 (1:200 dilution, BioLegend). Following immunostaining, tissues were washed 4 times for 30 minutes each, mounted in 50/50 glycerol/phosphate buffered saline and imaged until fluorescence signal was lost (for dorsal tissue) or through the entire thickness of the muscle (~200 microns) on a Zeiss LSM 710 NLO confocal microscope or a Nikon confocal microscope. Acquisition parameters were kept identical across all animals.

4.5.9 Imaging and quantification of whole mount immunohistochemistry

For monocyte/macrophage quantification after arteriole ligation, 3-4 different fields of view (FOVs) per muscle containing a collateral arteriole with monocytes/macrophages evident were located manually. Full-thickness z-stack (2μm step size) volume renders of these FOVs were generated using a 20X oil immersion objective. Simultaneous visualization of CX3CR1-GFP cells with immunohistochemical markers is not possible due to leakage of GFP from the cells following permeabilization. Therefore, imaging of CX3CR1-GFP spinotrapezius muscles occurred immediately after perfusion fixation and further immunostaining was subsequently performed as described in the previous methods section. A threshold at which only the brightest $CX3CR1^{GFP/+}$ cells ($CX3CR1^{hi}$) were visible was applied to all images. Vessel-associated CD206+ and

CX3CR1^{hi} cells were defined as cells falling within the 2-dimensional area of the vessel in question and within 50μm of the vessel border. ImageJ (NIH) imaging software was used to quantify vessel length and density. Arterioles were distinguished from venules by degree of lectin binding, vessel size, and morphology. Cell counts and green channel thresholding to designate CX3CR1^{hi} cells were performed in Adobe Photoshop (Adobe Systems Incorporated).

For 3D monocyte/macrophage quantification after VML muscle injury, 1 crop per animal of 332x332μm was taken from the area adjacent to the defect. Crops were chosen based on matching anatomical vessel morphology from both CX3CR1$^{GFP/+}$ images and the subsequently stained CD206, CD68, and CD31 images. Cells co-expressing CD68 and CD206 were identified in Imaris using the surface tool. CD68+ surfaces were identified by smoothing with a 1.5μm grain size and an automatic threshold on absolute intensity. Touching objects were split using a seed points diameter of 13.8μm. Cells that co-expressed two markers were identified by applying an additional filter to select surfaces with a high fluorescence intensity in the CD206 channel (above 17.7 mean intensity). Vessels were identified in Imaris by drawing a surface on the CD31 fluorescent channel with a 1.66μm grain size, manually-selected threshold value (determined based on each image), and manually-selected volume filter to remove small debris. To calculate the distance between CD68+CD206+ cells and the nearest blood vessel, a distance transformation was applied to CD31+ vessel surfaces and the median position of each CD68+CD206+ cell within this plane was recorded.

For collagen imaging after VML injury, a two-photon chameleon laser (tuned to λ=810nm) and collection range of 380-420nm was utilized with acquisition parameters

kept identical across animals. Z-stacks were collected from the beginning to end of collagen signal visible across the entire x-y plane analyzed. Max intensity projections were generated from 3D confocal images for 2D analysis in Zen software (Zeiss). Quantification of vascularization and collagen deposition was performed in ImageJ software (NIH). An elliptical region of interest (1.370mm high by 1.778mm wide) was centered over each defect and the image was thresholded to display only areas of positive fluorescence signal, with the same threshold applied to all images. The number of pixels positive for the fluorescence channel of interest was normalized to the total area of the region of interest. The percentage of cell infiltration was determined by tracing the border between lectin-positive regions and the avascular zone. The area of this region was measured. A secondary trace between the cellular (CX3CR1+) region and acellular zone was made. The area of this region was measured and subtracted from first measurement to measure the region of cell infiltration into the defect. This value was normalized to the first measurement. Void area was measured by tracing the edges of collagen-positive signal and identifying void area as the area that is collagen-negative. 2D fiber diameter was determined by measuring the widest portion of each regenerated muscle fiber (determined based on the morphology of desmin-positive regions) within the defect region from the day 7 maximum intensity projections.

4.5.10 Statistical analysis

Data are presented as mean ± standard error of the mean (S.E.M.), unless otherwise noted. All statistical analysis was performed in GraphPad Prism software. For pairwise comparisons, unpaired t-test (according to experimental design) with Welch's correction if variance was significantly different was used. For non-parametric test (performed for

intravital imaging analysis), a two-tailed Mann-Whitney test was used. For comparisons of more than two groups, one-way ANOVA with Dunnett's post-test was used for multiple comparisons. For grouped analyses, two-way ANOVA with Sidak's post-test was used for multiple comparisons. Unless otherwise noted, $p<0.05$ was considered statistically significant.

5. QUANTITATIVE ANALYSIS OF THE TEMPORAL PROGRESSION OF INFLAMMATION AROUND ENGINEERED HYDROGELS

5.1 Abstract

Significant advances have been made in the development of materials that better mimic native tissues; however how these materials interact with the host immune system after implantation remains incompletely understood. In the current work, we explored the progression of inflammation around protease-degradable PEG hydrogels functionalized with bioadhesive RGD (Arg-Gly-Asp) peptides by using high-dimensional flow cytometry data paired with intravital image acquisition. Incorporation of RGD into PEG hydrogels did not impact the overall composition of innate immune cells adherent to the material surface after 1, 3, 7, and 14 days of subcutaneous implantation in mice. Hydrogel implantation significantly altered myeloid cell composition compared to uninjured tissue: during the acute inflammatory phase, monocytes and neutrophils were the primary cell type recruited to subcutaneously implanted hydrogels, while macrophages and dendritic cells predominated the later stages. Using intravital confocal microscopy, we visualized real-time myeloid cell interactions with hydrogels implanted in dorsal skinfold window chambers. Myeloid cells moved at greater velocities around hydrogels compared to distal tissue, and velocity was further increased by RGD functionalization. These results shed light on the progression of inflammation in response to implantation of engineered hydrogels.

5.2 Introduction

Significant advances have been made in the development of materials that better mimic native tissues through incorporation of biofunctionality [200-202], transplantation of exogenous cells [140, 203], and matching host tissue mechanical and structural properties [204, 205]. Hydrogel materials are particularly appealing because of their crosslinked matrix that resembles native tissues and their high water content, enabling cell and growth factor delivery [200]. Hydrogels derived from synthetic polymers such as poly(ethylene glycol) (PEG) serve as a building block for engineering desired biological responses by providing a matrix whose mechanical properties, structural composition, and bioactivity can be finely controlled [206]. While these advances have generated promising pre-clinical results [207-209], how biofunctional hydrogels interact with the host immune system after implantation remains incompletely understood.

Implantation of a foreign material induces a physiological response that is both spatially and temporally regulated, and varies widely depending on the material properties [86]. Within 5 seconds of contact with whole blood, protein adsorption and platelet activation occurs on titanium oxide surfaces [87]. The composition and bioactivity of adsorbed proteins evolves over time and depends on the concentration of proteins in the surrounding microenvironment, their affinity for the material surface, and their conformation on the surface [88]. Immune cells recruited to the material interact with the surface through integrin ligation to adsorbed proteins such as complement proteins, fibrinogen, and fibronectin [100, 101]. Neutrophils are recruited within 16 hours after material implantation during the acute inflammatory phase [90], but may persist for as long as two weeks, as is the case for polymer microparticles implanted in the mouse peritoneum

[91]. Neutrophil activation and degranulation results in the release of proteolytic enzymes and reactive oxygen species that may contribute to material degradation [93], as well as initiate subsequent phases of inflammation [92].

Monocytes are recruited from circulation in response to mediators released from neutrophil granules that alter local chemokine production by endothelial cells and resident macrophages, as well as induce expression of intercellular adhesion molecules [94]. Extravasated monocytes differentiate into macrophages or dendritic cells (DCs) in response to M-CSF or GM-CSF, respectively [95]. Mononuclear phagocytes exhibit significant heterogeneity *in vivo* [95], with their phenotype being correlated with outcomes such as wound healing, vascularization, and implant integration. Blood monocytes exist in two principle subsets in both humans and rodents, including classical monocytes that are early pro-inflammatory responders during infection or injury and non-classical monocytes that patrol the resting endothelium and participate in reparative processes after injury [86]. Macrophages can similarly display a wide spectrum of different gene and protein expression patterns, that have been primarily classified as classically activated or "M1" macrophages and alternatively activated "M2" macrophages, although macrophages are extremely diverse and this nomenclature is likely an oversimplification [210]. Crosstalk with other immune cells, including apoptotic neutrophils [96] and paracrine signals derived from T helper cells [97], regulate the phenotype of monocytes and macrophages. We have previously demonstrated that biomaterial-based strategies that enhance recruitment of non-classical monocytes and their subsequent differentiation into alternatively activated macrophages is associated with enhanced vascularization [197] and muscle repair after traumatic injury [72]. While immune cells are required for biomaterial-induced tissue

repair [97], persistent or dysfunctional inflammation has been associated with fibrosis [211], carcinogenesis [212], and implant failure [85, 213].

In the current work, we explored the progression of inflammation around degradable PEG hydrogels functionalized with the bioadhesive ligand RGD (Arg-Gly-Asp) by using high-dimensional flow cytometry data paired with intravital image acquisition. Cell-adhesive peptides such as RGD have been broadly used throughout the biomaterials field to enhance host cell interactions with materials that typically resist protein fouling [214]. Previous work has indicated that functionalization of hydrogels with RGD increases cell infiltration into the material and promotes vascularization [61, 215]. In the current work, we demonstrate that incorporation of RGD into PEG hydrogels does not impact the overall composition of innate immune cells adherent to the material surface at 1, 3, 7, and 14 days post-implantation. We found that, compared to uninjured tissue, implantation of PEG hydrogels substantially increased infiltration of CD11b+ myeloid cells. During the acute inflammatory phase, monocytes and neutrophils were the primary cell type recruited to subcutaneously implanted hydrogels, while macrophages and dendritic cells predominated the later stages. Over the course of 14 days, monocyte and macrophage populations transitioned from a pro-inflammatory phenotype to an alternatively activated phenotype. Using intravital confocal microscopy in transgenic mice heterozygously expressing GFP under the CX3CR1 promoter, we visualized myeloid cell interactions with implanted hydrogels in real-time. The presence of a hydrogel increased the distance travelled and velocity of myeloid cells moving through interstitial tissue. RGD functionalization further increased the velocity of CX3CR1+ cells compared to control

hydrogels, and this effect was localized to the material surface. These results shed light on the progression of inflammation in response to implantation of engineered hydrogels.

5.3 Results

5.3.1 Temporal profile of the myeloid response to degradable PEG hydrogels

We engineered degradable poly(ethylene glycol) (PEG) hydrogels using 20 kDa 4-arm PEG macromers containing terminal maleimide groups (PEG-MAL) that can react with free cysteines on peptides or full-length proteins. PEG-MAL macromers were crosslinked with the cysteine-flanked peptide GCRDVPMSMRGGDRCG (VPM) that contains a protease cleavage site (**Figure 24a**). In order to explore how adhesive peptide functionalization impacts myeloid cell recruitment, PEG-MAL macromers were functionalized with cysteine-terminated RGD or scrambled peptide control (RDG) prior to crosslinking. Combination of functionalized PEG-MAL with VPM rapidly forms a hydrogel (**Figure 24b**).

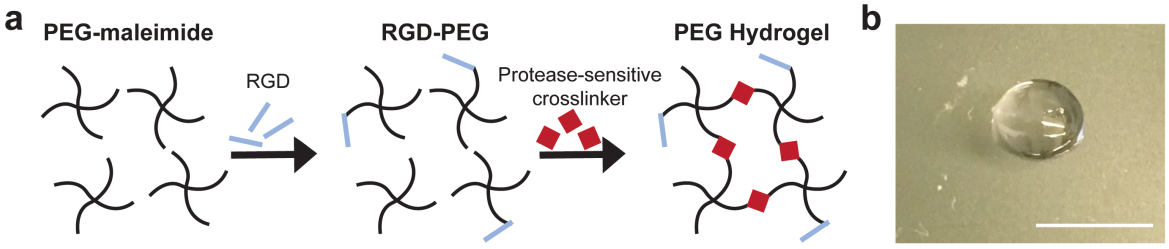

Figure 24. Protease-degradable biofunctional PEG hydrogels. (a) 4-arm PEG-maleimide macromers (20 KDa) were functionalized with RGD peptides and crosslinked with a cysteine-flanked protease sensitive crosslinker (VPM), forming a hydrogel. (b) Macroscopic photo of a PEG hydrogel. Scale bar, 5mm.

To investigate the kinetics of myeloid cell accumulation around PEG hydrogels, we injected hydrogel precursors (functionalized PEG-MAL and VPM crosslinker) into the subcutaneous space of mice, where the hydrogels polymerized *in situ*. Each mouse received two hydrogel implants: a control hydrogel containing RDG on the left side and a RGD-functionalized hydrogel on the right side. At 1, 3, 7, or 14 days after implantation, the hydrogels were explanted and digested with collagenase to extract adherent cells for immunophenotyping by flow cytometry (**Figure 25a**). Macrophages were identified based on expression of both CD64 (FcγR1) and Mer tyrosine kinase (MerTK) (**Figure 25b**), which distinguishes macrophages from monocytes that express CD64, but not MerTK [151]. DCs were identified based on high expression of CD11c, which also corresponded to a population of cells that express high levels of major histocompatibility complex class II (MHCII) (*data not shown*). The remaining CD11b+ cells were composed of Ly6G+ neutrophils and CD64+ monocytes that were low in side scatter (SSC) (**Figure 25b**).

After 1 day of implantation, CD11b+ myeloid cells were 39.5% of adherent cells collected from RGD hydrogels, and about 49.6% for RDG hydrogels (**Figure 25c**). This frequency varied over Days 3 through 14 from 61.8% to 72.9%, and was not sensitive to the presence of active adhesive ligand. Ly6G+ neutrophils were present at the highest frequency 1 day post-implantation (11.7% for RDG hydrogels, 4.1% for RGD hydrogels), and decreased to less than 1% of all cells by 7 days post-implantation (**Figure 25d**). CD64+SSC^{lo} monocytes decreased over the course of 14 days, with the highest frequency measured occurring at 1 day post-implantation (19.7% for RDG hydrogels, 18.6% for RGD hydrogels) (**Figure 25e**). By 14 days post-implantation, less than 3% of cells were monocytes. Conversely, MerTK+CD64+ macrophages increased over the time course

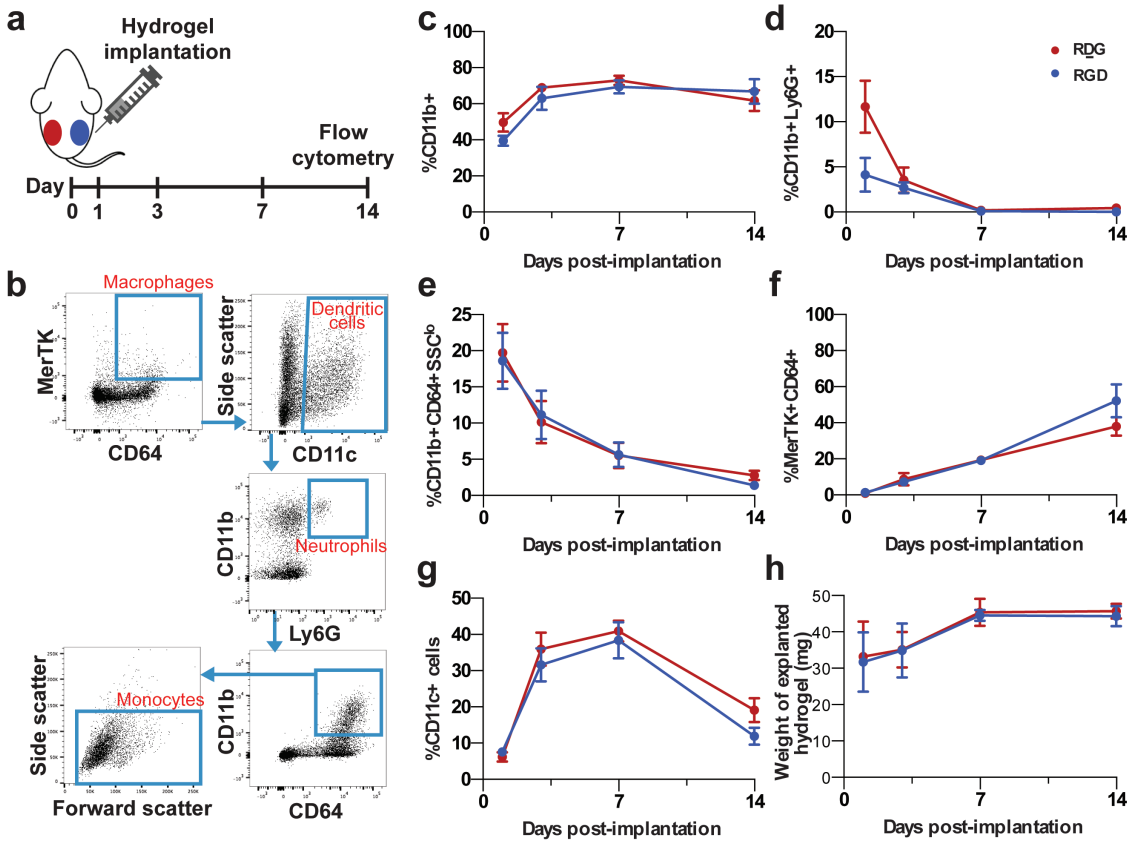

Figure 25. *In vivo* assessment of inflammatory response to PEG hydrogels implanted subcutaneously in mice. (a) One RGD hydrogel and one RDG (scrambled peptide control) hydrogel were injected within the subcutaneous space in mice. Hydrogels were explanted at 1, 3, 7, or 14 days after implantation for flow cytometry. (b) Adherent cells were collected from digested hydrogels and immunophenotyped by flow cytometry. Single cells were plotted as MerTK versus CD64. Macrophages were identified as MerTK+CD64. Among the remaining cells, dendritic cells were identified as CD11c+, neutrophils were identified as Ly6G+CD11b+, and monocytes were identified as CD64+CD11b+SSC^{lo}. Total frequency of (c) CD11b+ myeloid cells, (d) neutrophils, (e) monocytes, (f) macrophages, and (g) dendritic cells. (h) Explanted hydrogel weight over time. Data expressed as mean ± S.E.M. n=3-7 animals per group.

measured (**Figure 25f**). While macrophages were less than 1% of total cells 1 day post-implantation, macrophages were the most abundant cell population 14 days post-implantation (38.1% for RDG hydrogels, 52.2% for RGD hydrogels). CD11c+ DCs were initially less than 7% of all cells 1 day post-implantation, but were the most abundant cell

type measured at days 3 and 7 post-implantation (**Figure 25g**). At 14 days post-implantation, the frequency of DCs dropped, (19.2% for RDG hydrogels, 11.9% for RGD hydrogels), perhaps due to increase in macrophages. No differences in the weight of hydrogels explanted at different time points was detected (**Figure 25h**). While the hydrogels are expected to degrade *in vivo* in response to protease production and decrease in total mass over time, an increase in the number (and mass) of adherent cells could explain why no changes in hydrogel weight occurred.

5.3.2 Comparison of recruited cells and cells present in homeostatic subcutaneous tissue

In order to investigate how hydrogel implantation alters immune cell composition from resident populations present during homeostasis, we performed flow cytometry on resting tissue harvested from the subcutaneous space. The overall frequency of CD11b+ myeloid cells (9.6%) was significantly lower than cells collected from RGD-functionalized hydrogels at days 1-14 post-implantation (**Figure 26a**). The proportion of neutrophils was elevated compared to resting tissue 1 day after hydrogel implantation, but returned to baseline levels for the remainder of the study (**Figure 26b**). The proportion of monocytes was elevated above basal levels at days 1 and 3 post-implantation, but returned to baseline by 7 days (**Figure 26c**). The proportion of macrophages in resting subcutaneous tissue was greater than 1 day after hydrogel implantation (15.3% vs 0.9% out of CD11b+ cells), which was highest 14 days after implantation (77.2%) (**Figure 26d**). Although only a subset of CD11c+ DCs express CD11b, 42.6% of CD11b+ cells were also CD11c+ in uninjured tissue, which decreased to 15.8% 1 day after hydrogel implantation (**Figure 26e**). Overall,

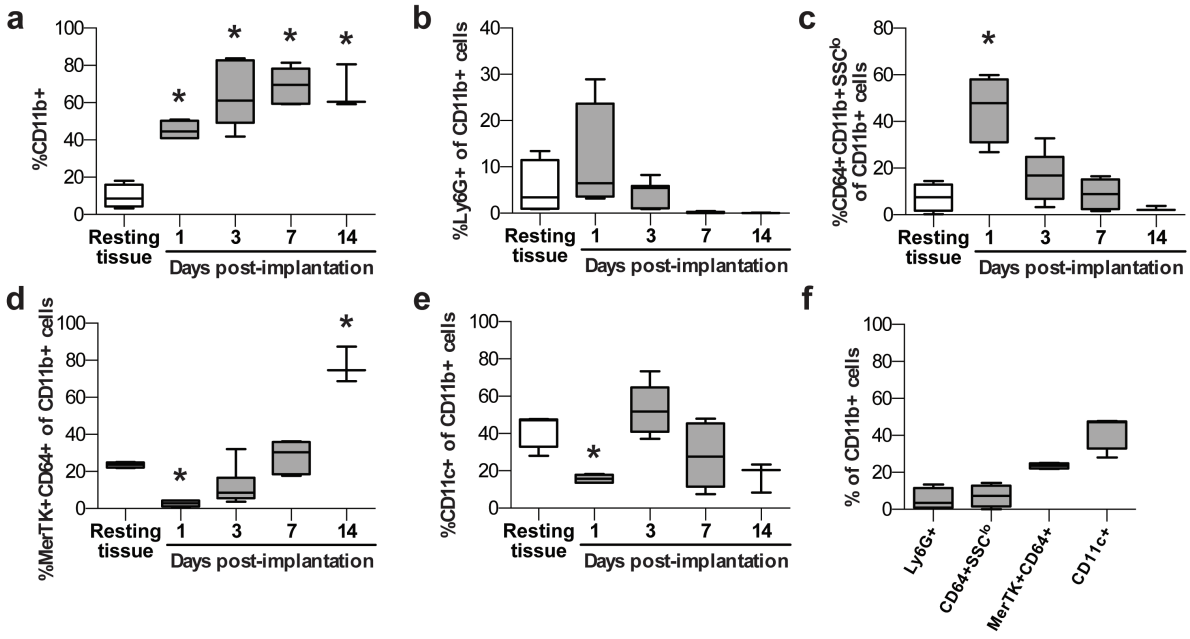

Figure 26. Myeloid cells recruited to implanted hydrogels are phenotypically different from those present in uninjured subcutaneous tissue. (a) Overall frequency of CD11b+ myeloid cells in uninjured subcutaneous tissue (resting tissue) compared to subcutaneously-implanted RGD hydrogels at different time points. (b) Frequency of Ly6G+ neutrophils, (c) CD64+SSC^{lo} monocytes, (d) MerTK+CD64+ macrophages, and (e) CD11c+ dendritic cells expressed out of total CD11b+ cells. (f) Overall composition of CD11b+ myeloid cells in resting subcutaneous tissue. Data expressed as minimum, 25th percentile, median, 75th percentile, maximum. *$p<0.05$ by one-way ANOVA. n=3-7 animals per group.

CD11c+ DCs that also express high levels of MHCII (*data not shown*) are the most abundant subset of CD11b+ cells in resting subcutaneous tissue (**Figure 26f**).

5.3.3 Pro-inflammatory monocyte and macrophage populations are replaced with anti-inflammatory populations over the course of 14 days

During inflammation, monocytes progressively lose Ly6C expression [8, 69]. While biomaterial implantation induces monocyte recruitment [85], the kinetics of recruited monocyte subsets remain unknown. Classical and non-classical monocyte subsets

were discriminated based on Ly6C expression (**Figure 27a**). At 1 day post-implantation, most monocytes were Ly6C^{hi} (87.4% for RDG hydrogels, 83.8% for RGD hydrogels) (**Figure 27a,b**). By 3 days post-implantation, around half of all monocytes had converted to Ly6C^{lo}, and over 90% of monocytes were Ly6C^{lo} at 7 and 14 days post-implantation (**Figure 27a,c**). Interestingly, the Ly6C^{int} population increased in size from day 1 to day 3, but decreased thereafter (**Figure 27d**).

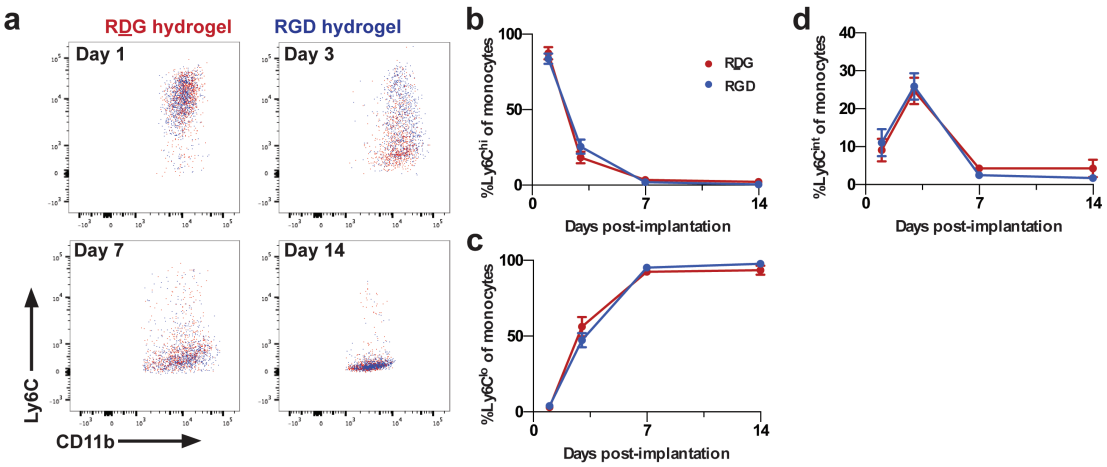

Figure 27. Temporal evolution of monocytes around PEG hydrogels. (a) Representative flow cytometry dot plots of CD64+SSC^{lo} monocytes collected from explanted RDG (red) or RGD (blue) hydrogels. Quantification of the frequency of (b) classical Ly6C^{hi}, (c) non-classical Ly6C^{lo}, or (d) Ly6C^{int} monocytes, expressed as a frequency of total monocytes. Data expressed as mean ± S.E.M. n=3-7 animals per group.

Recruited monocytes can differentiate into macrophages or dendritic cells. While IL-4 signaling induces M2a macrophage polarization *in vitro* [86], IL-4 signaling also plays key roles in the generation of foreign body giant cells and chronic inflammation in the context of non-degradable biomaterial implants [216]. To better understand the kinetics of different macrophage populations around degradable PEG hydrogels, we probed expression of the costimulatory molecule CD86 (expressed on M1-like macrophages [11])

and the C-type lectin receptor CD206 (expressed primarily on M2a macrophages [41]). At 1 day post-implantation, the total frequency of MerTK+CD64+ macrophages was very low and a majority of these macrophages were primarily $CD86^{neg}$ (**Figure 28a**). By 3 days post-implantation, around 6% of all macrophages were $CD86+CD206^{neg}$ (**Figure 28a, b**), while the majority of macrophages were negative for both CD86 and CD206 (75.6% for RDG hydrogels, 78.0% for RGD hydrogels). The proportion of $CD86+CD206^{neg}$ macrophages decreased over the course of 14 days, while the proportion of $CD86^{neg}CD206+$ macrophages continued to increase, with a majority of macrophages displaying this phenotype by 14 days post-implantation (**Figure 28a,c**). Interestingly, macrophages harvested from uninflamed subcutaneous tissue are primarily $CD86+CD206^{neg}$ (44.8% of total macrophages) (**Figure 28d**). These results indicate that macrophages progressively lose CD86 expression and gain CD206 expression during the course of inflammation induced by hydrogel implantation.

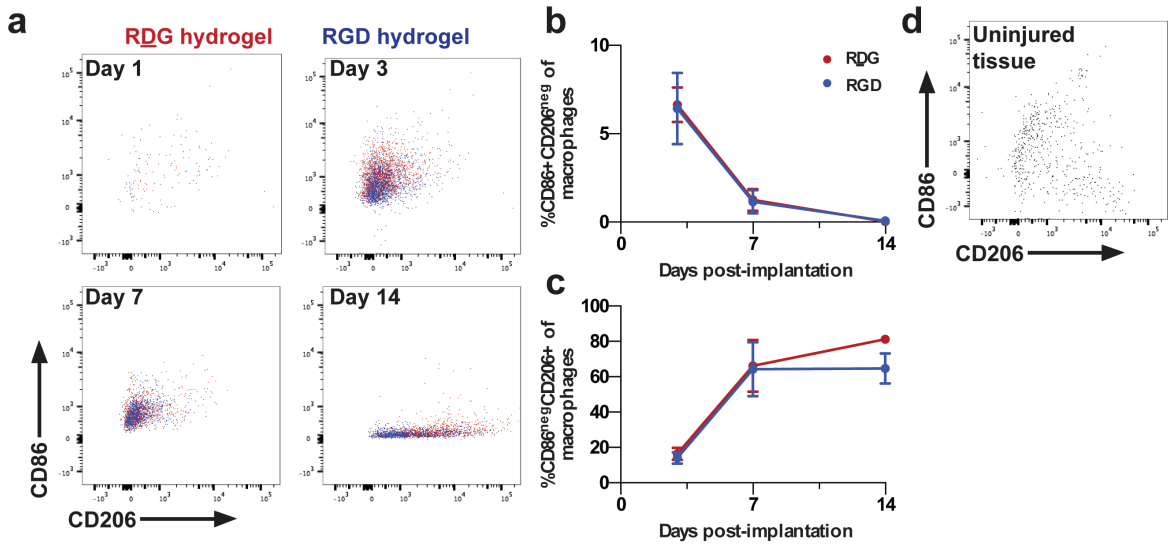

Figure 28. Temporal evolution of macrophages around PEG hydrogels. (a) Representative flow cytometry dot plots of MerTK+CD64+ macrophages collected from explanted RDG (red) or RGD (blue) hydrogels. Quantification of the frequency of (b) M1-like CD86+CD206^{neg} and (c) M2-like CD86^{neg}CD206+ macrophages, expressed as a frequency of total macrophages. (d) Representative dot plot of macrophages collected from uninjured subcutaneous tissue. Data expressed as mean ± S.E.M. n=3-7 animals per group.

5.3.4 Myeloid cell recruitment to hydrogels functionalized with cyclic RGD

We also explored whether hydrogel functionalization with a cyclic RGD peptide, for which the integrin $\alpha_v\beta_3$ has a 10-fold greater affinity than linear RGD [217], impacts bulk recruitment of myeloid cells. No differences in the overall frequency of neutrophils, monocytes, macrophages, or dendritic cells were detected between RDG- and cyclic RGD-functionalized hydrogels 3 days after subcutaneous implantation (**Figure 29a**). There were also no differences in the frequencies of monocyte and macrophage subsets (**Figure 29b,c**), further supporting the finding that functionalization with RGD adhesive ligands does not impact the composition of cells recruited to implanted hydrogels.

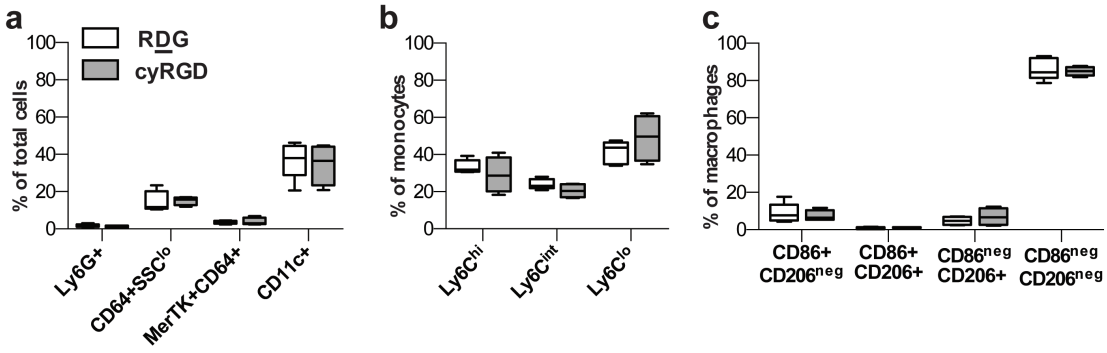

Figure 29. Impact of functionalization with cyclic RGD on myeloid cell recruitment to PEG hydrogels. (a) Overall frequency of Ly6G+ neutrophils, CD64+SSClo monocytes, MerTKCD64+ macrophages, and CD11c+ dendritic cells 3 days after implantation of RDG- or cyclic RGD (cyRGD)-functionalized hydrogels. Frequency of (b) monocyte and (c) macrophage subsets. Data expressed as minimum, 25th percentile, median, 75th percentile, maximum. n=4-5 animals per group.

5.3.5 High-dimensional analysis of temporal progression of inflammation around PEG hydrogels

To further explore myeloid cell heterogeneity within our data set, we performed t-distributed stochastic neighbor embedding (tSNE) analysis, which is a non-linear dimensional reduction technique that has been applied to flow and mass cytometry data [218]. Manual gating of flow cytometry data is often biased and is limited by the ability to visualize only two dimensions simultaneously. Samples collected from RGD hydrogels at 1 or 3 days post-implantation were downsampled, electronically barcoded, and combined into a single file for tSNE analysis. Each dot represents a single cell projected into low-dimensional tSNE space. Cells taken from Day 1 hydrogel samples primarily segregate from cells taken from Day 3 hydrogel samples (**Figure 30a**), emphasizing the phenotypic

differences of these two time points. We manually gated on cells that were CD11b+ or CD11c+ to investigate the distribution of myeloid cells in tSNE space (**Figure 30b**). We found that spatial separation of samples from different time points occurred for both myeloid and non-myeloid cells, which is interesting given that our panel was selected to focus on myeloid subset discrimination. tSNE was able to separate manually gated myeloid cell subsets of neutrophils, monocytes, DCs, and macrophages that were identified using Figure 25b gating (**Figure 30c**). Overlay of manual gates indicates that most of the phenotypic diversity between Day 1 and 3 samples is likely due to shifts in the frequency of each myeloid cell subset. For example, the appearance of clusters 1 and 2 at Day 3 (**Figure 30a**), is due to the absence of macrophages and DCs in Day 1 samples (**Figure 30c, Figure 25f,g**). Cluster 4 is Ly6G+ neutrophils, and Day 1 and Day 3 neutrophils are located near each other, but the slight separation may reflect subtle phenotypic differences. Additionally, this tSNE map indicates that monocytes and DCs are the most heterogeneous for expression of the markers including in our analysis. Mapping the global expression of Ly6C highlights the reduction of Ly6C expression in monocytes present 3 days post-implantation (**Figure 30d**). Conversely, tSNE regions associated with Day 3 samples displayed increased MHCII expression (**Figure 30e**).

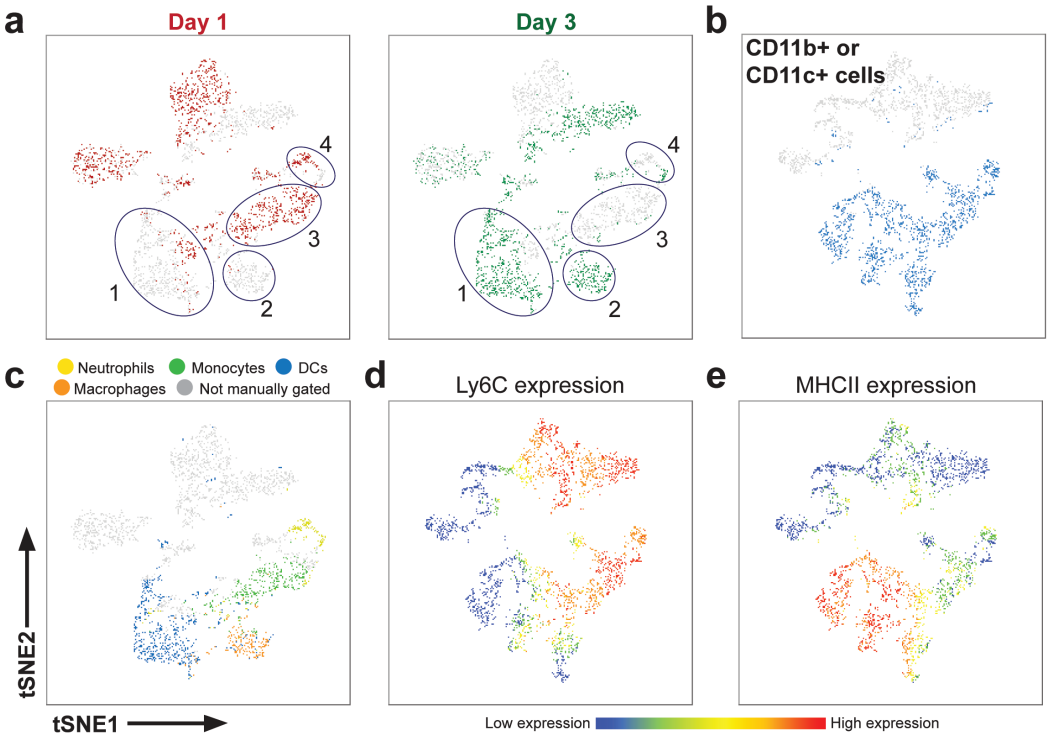

Figure 30. High-dimensional analysis of temporal progression of inflammation around PEG hydrogels. (a) Application of tSNE to cells collected from subcutaneously implanted hydrogels 1 day post-implantation (red) or 3 days (green). tSNE map represents 8 total samples (4 from each time point) and each dot represents a single cell projected from high-dimensional space onto the tSNE axes, which are in arbitrary units. Clusters were identified manually. (b) Manual gating of myeloid CD11c+ or CD11b+ cells and (c) Ly6G+CD11b+ neutrophils, CD64+CD11b+ monocytes (green), CD11c+MHCII+ dendritic cells (blue), and MerTK+CD64+ macrophages (orange). Cells not classified by manual gating are shown in gray. Expression of (d) Ly6C and (e) MHCII in tSNE space.

Consistent with manual gating, we observed no global shifts in the distribution of cells collected from RDG or RGD hydrogels (**Figure 31**). These results support the quantitative analysis performed using biased manual gating and reveal heterogeneity that evolves temporally in myeloid cell subsets during hydrogel-induced inflammation.

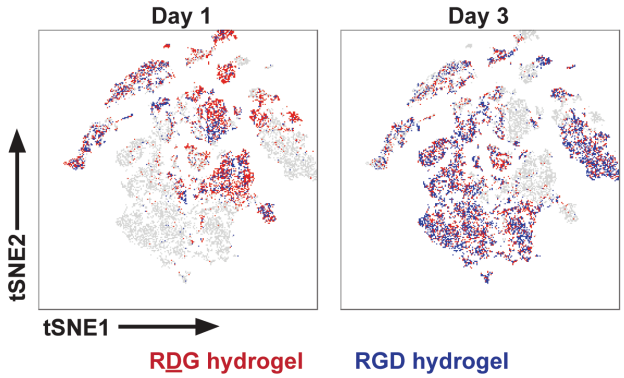

Figure 31. High-dimensional analysis of myeloid response to adhesive ligand functionalization of PEG hydrogels. Application of tSNE to cells collected from subcutaneously implanted RDG- (red) or RGD- (blue) functionalized PEG hydrogels 1 or 3 days post-implantation.

5.3.6 Implantation of PEG hydrogels in mouse cutaneous wounds

While subcutaneous implantation likely induces minor tissue damage during hydrogel injection, this model does not mimic larger scale soft tissue injuries. In order to explore the inflammatory response to engineered hydrogels in the context of non-healing dermal wounds, we performed dorsal skinfold window chamber surgeries, which involves excising the epidermis and outer layers of the dermis, inducing a robust systemic inflammatory response [197]. Immediately after surgery, we placed a pre-cast hydrogel functionalized with RDG or RGD on the exposed subcutaneous layer of the dermis (**Figure 32a**). At 3 days post-injury, we explanted the hydrogels from the dorsal tissue and immunophenotyped adherent cells by flow cytometry. Around 40% of total cells after 3 days were Gr-1^{hi}Ly6C^{int} neutrophils (41.9% for RDG hydrogels, 44.1% for RGD hydrogels) (**Figure 32b**), which was much higher than the frequency of neutrophils detected 3 days after hydrogel implantation in the subcutaneous space (**Figure 25d**).

Around 20% of total cells were F4/80+ (22.8% for RDG hydrogels, 22.0% for RGD hydrogels), which is expressed on monocytes/macrophages. Similarly, in the subcutaneous space, around 20% of total cells were immunophenotyped as monocytes or macrophages (**Figure 32b**). These results indicate that the inflammatory environment surrounding implanted hydrogels impact the composition of hydrogel-adherent leukocytes.

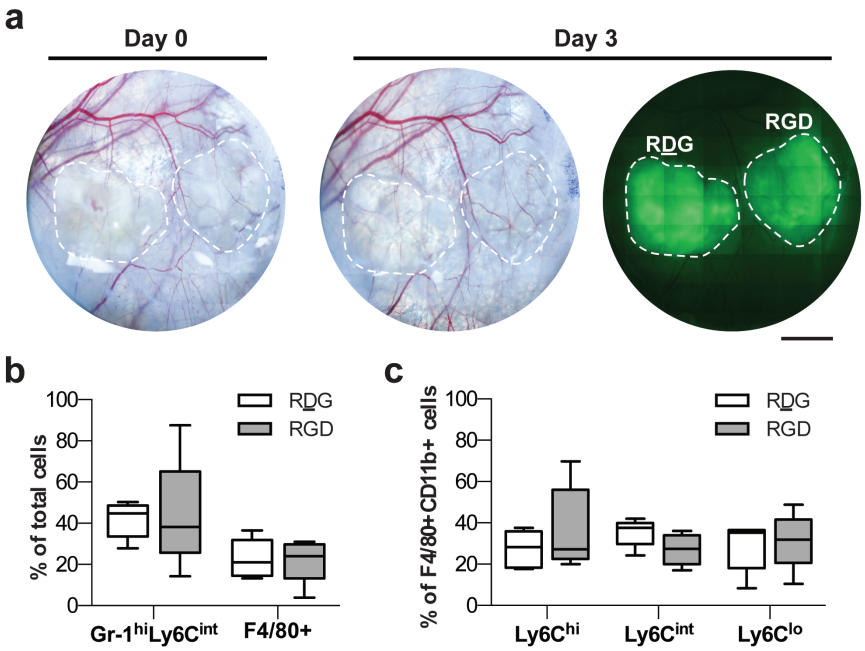

Figure 32. Implantation of PEG hydrogel is mouse dorsal skinfold window chambers. (a) One RDG- and one RGD-functionalized pre-formed hydrogel was placed on the exposed subcutaneous layer. Scale bar, 2.5mm. (b) Adherent cells were immunophenotyped by flow cytometry 3 days after implantation. CD11b+ cells were identified as neutrophils based on Gr-1^{hi}Ly6C^{int} expression and monocytes/macrophages based on F4/80+ expression. (c) Monocyte/macrophage subsets were further characterized based on Ly6C expression. Data expressed as minimum, 25th percentile, median, 75th percentile, maximum. n=5 animals per group.

5.3.7 Intravital imaging of myeloid cell migration around PEG hydrogels

While flow cytometry provides single cell information necessary for immunophenotyping, expression of selected surface markers do not necessarily reflect subtle changes in cell function. To explore the activity of myeloid cells around engineered hydrogels, we performed intravital confocal imaging in mice that heterozygously express GFP under the CX3CR1 promoter ($CX3CR1^{GFP/+}$ mice). CX3CR1 is expressed primarily on monocytes, but also expressed on macrophages and some dendritic cells [194]. One day after surgery, we placed RDG or RGD-functionalized PEG hydrogels on the exposed subcutaneous layer of the dermis (**Figure 33a**). At 3 days post-surgery, we performed intravital laser scanning confocal microscopy and acquired 25-30 minute videos at the edge of each hydrogel or in tissue distal to both gels (**Figure 33b**). A fluorescent tag was incorporated into the hydrogels during fabrication to enable visualization of the material surface and identification of the hydrogel edge (**Figure 33c**).

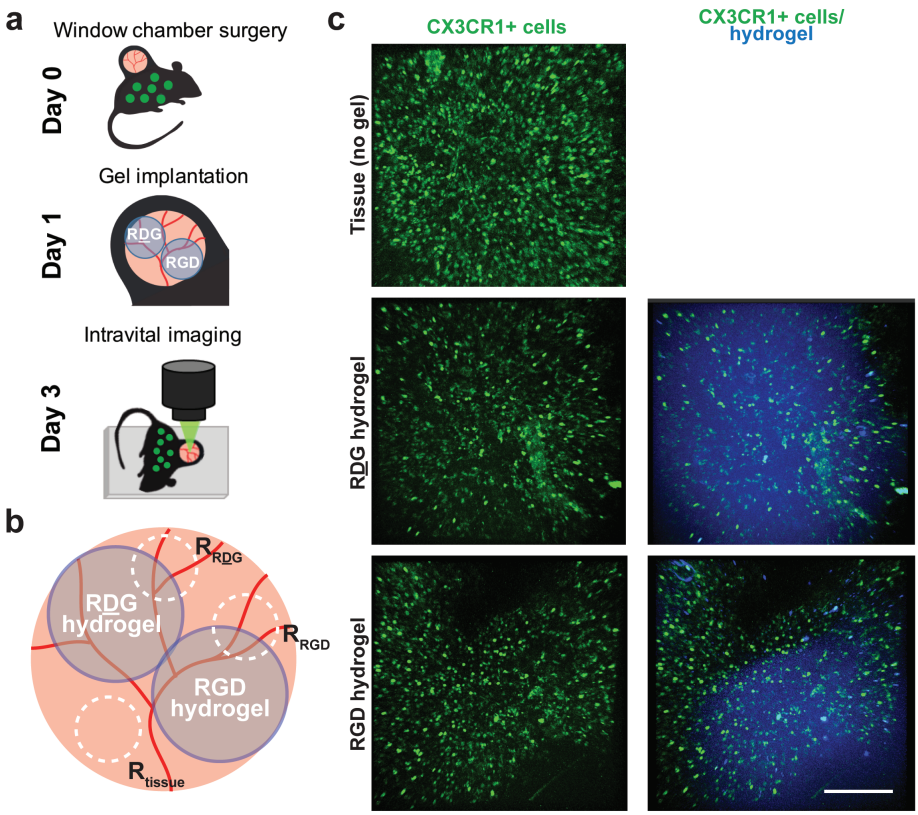

Figure 33. Intravital assessment of myeloid cell migration around PEG hydrogels. (a) Dorsal skinfold window chambers were performed in CX3CR1$^{GFP/+}$ mice. One RDG- and one RGD-functionalized hydrogel was placed on the exposed subcutaneous layer 1 day after surgery. At 3 days post-injury, intravital confocal microscopy was performed. (b) Time-lapse images were acquired near at the edge of each hydrogel and in tissue distal to both hydrogels that contained no gel. (c) Z-stacks acquired in each region; CX3CR1+ cells shown in green, fluorescently-tagged hydrogel shown in blue. Scale bar, 100μm.

Using 3D image processing software, we tracked the migration of CX3CR1+ cells in real time (**Figure 34a**). We detected an increase in the average track length around both RDG (55.7±32.9μm) and RGD (53.9±29.1μm) hydrogels compared to tissue far away from either hydrogel (33.9±16.4μm), but no differences between the two hydrogel formulations (**Figure 34b**). Interestingly, we detected an increase in the mean and maximum velocity of CX3CR1+ cells around RGD hydrogels compared to both RDG hydrogels and tissue

without a hydrogel (**Figure 34c,d**). The velocity of cells moving around RDG hydrogels was also greater compared to distal tissue containing no hydrogel. The path straightness, which is the track displacement normalized to the track length, was lower on both RDG and RGD hydrogels compared to distal tissue (**Figure 34e**). These results indicate that CX3CR1+ myeloid cells migrate differently through interstitial space in close proximity to a hydrogel implant than in tissue lacking a material, and that functionalization of PEG hydrogels with RGD enhances cell velocity.

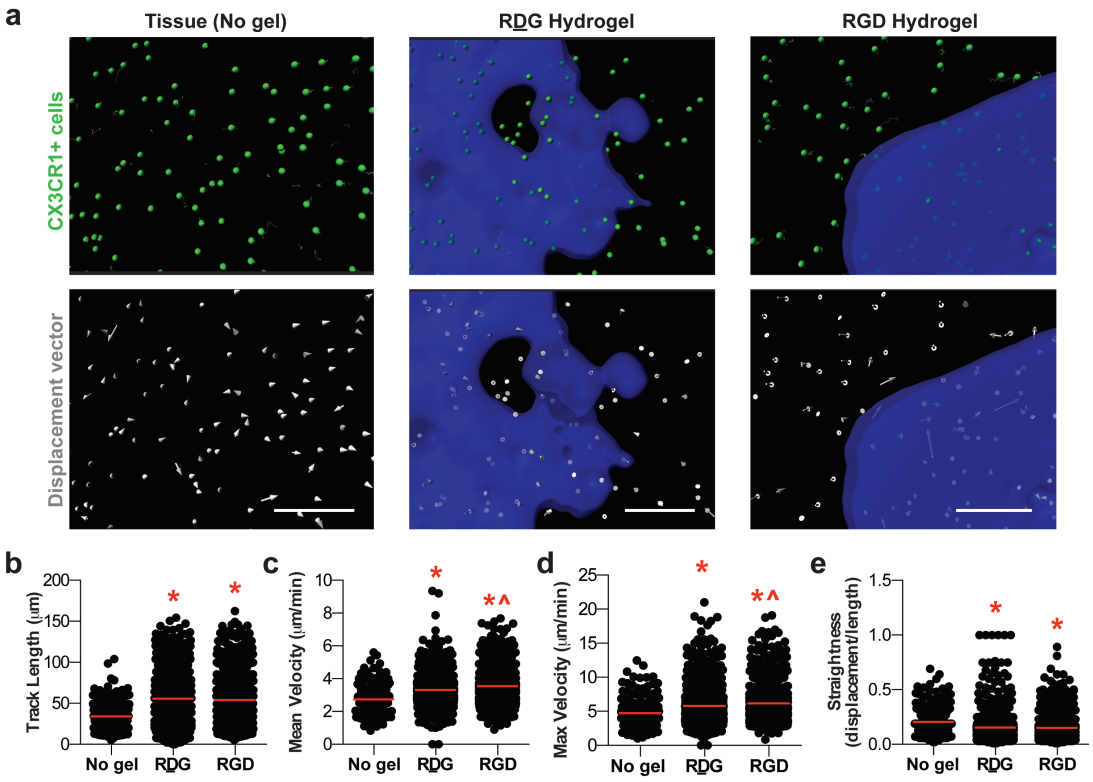

Figure 34. Migration of CX3CR1+ cells around PEG hydrogels. (a) Representative renderings of cell tracks (top row) and displacement vectors (bottom row) generated during image processing to track cell migration. Scale bars, 100μm. (b) Track length (in μm), (c) mean velocity (in μm/minute), (d) maximum velocity (in μm/minute), and (e) track straightness (displacement normalized to the path length) of CX3CR1+ cells moving in tissue without a hydrogel or around hydrogels functionalized with RDG or RGD. Red bar indicates the mean. *p<0.05 compared to no gel, ^p<0.05 compared to RDG hydrogel by Kruskal-Wallis. n>219 cells across 3 mice.

To further explore the how adhesive ligand functionalization impacts the migration of CX3CR1+ cells, we classified cells by their shortest 3D distance from the hydrogel surface. More CX3CR1+ cells were found within 10μm of RGD-functionalized hydrogel surfaces than RDG surfaces (**Figure 35a**). This measurement was normalized to the total volume of the hydrogel within the acquired image due to variability in the surface area imaged. Most tracks were within 30μm of the hydrogel surface (69.6% for RGD hydrogels) (**Figure 35b**), but this is likely due to the fact that we were unable to image the entire tissue depth with sufficient time resolution, and therefore focused primarily on acquiring data at the hydrogel-tissue interface. The mean and maximum velocity of CX3CR1+ cells were greater around RGD hydrogels compared to RDG hydrogels only if the cells were located within 30μm of the hydrogel surface (**Figure 35b,c**). At greater distances (30-50μm and >50μm), cells were insensitive to the presence of adhesive ligand on the hydrogel. The velocity of cells greater than 30μm from the hydrogels was also compared to the velocity of cells in distal tissue (**Figure 34b**). Despite the insensitivity to adhesive ligand at further distances, CX3CR1+ cells still displayed higher velocities than in distal tissue (2.8±0.8μm/min for distal tissue, 3.6±1.1μm/min for RDG hydrogels >50μm, and 3.9±0.9μm/min for RGD hydrogels >50μm). Taken together, these results suggest that RGD functionalization increases the velocity of myeloid cells that are within 30μm of the hydrogel surface, but the presence of a material has an effect on cell migration on longer length scales.

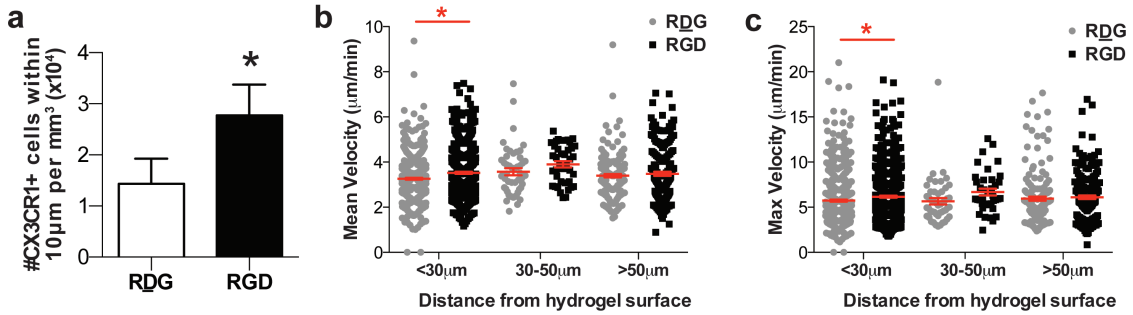

Figure 35. Migration of CX3CR1+ cells as a function of distance from hydrogel surface. (a) Number of CX3CR1+ cells with 10μm of RDG- and RGD-functionalized hydrogels, normalized to the hydrogel volume contained in each image. (b) Mean and (c) maximum velocity (expressed in μm/minute) of CX3CR1+ cells, classified according to their minimum distance from the hydrogel surface. Red bar indicates the mean. *$p<0.05$ compared to RDG hydrogel by Kruskal-Wallis. n>803 cells across 3 mice.

CX3CR1 is differentially expressed on monocyte subsets, with non-classical monocytes being CX3CR1^{hi} and classical monocytes being CX3CR1^{lo}. We have previously demonstrated that approximately half of monocytes are non-classical by 3 days after window chamber surgery [197]. In order to explore whether migration is different between CX3CR1^{hi} and CX3CR1^{lo} cells, we classified half of all tracks as CX3CR1^{hi} cells based on GFP fluorescence intensity. The remaining tracks were classified as CX3CR1^{lo} and compared across migration metrics. The mean velocity was not different between CX3CR1^{hi} and CX3CR1^{lo} cells in all regions imaged (**Figure 36a**). Conversely, CX3CR1^{hi} cells displayed an increase in total track length and a decrease in track straightness compared to CX3CR1^{lo} cells in all regions imaged (**Figure 36b,c**). These measurements indicate that CX3CR1^{hi} cells move greater distances than CX3CR1^{lo} cells in interstitial tissue, but this motion is less directed and does not involve a change in velocity. Interestingly, the metrics that were insensitive to adhesive ligand presence (path length and straightness) were significantly different between CX3CR1^{hi} and CX3CR1^{lo} cells, while

the metrics that were sensitive to adhesive ligand presence (mean and maximum velocity) were not.

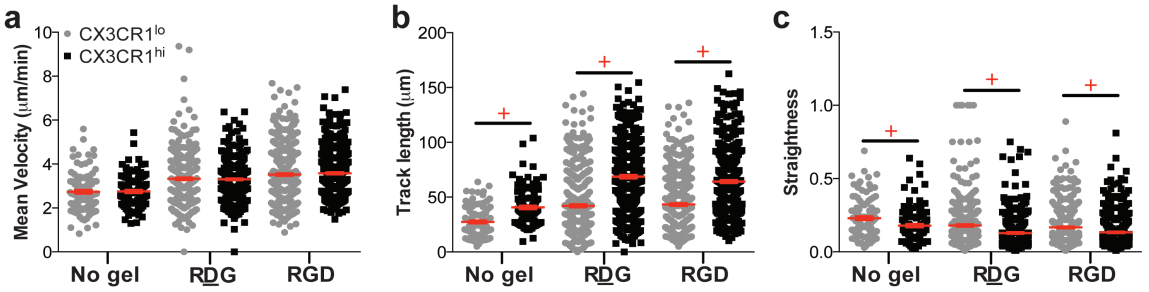

Figure 36. Migration of CX3CR1^{lo} and CX3CR1^{hi} cells around PEG hydrogels. (a) Mean velocity (expressed in μm/minute), (b) track length expressed in μm), and (c) path straightness (the displacement normalized to the path length) of CX3CR1^{hi} and CX3CR1^{lo} cells. *p<0.05 compared to RDG hydrogel by Kruskal-Wallis. n=219-876 cells across 3 mice.

5.4 Discussion

The inflammatory response to biomedical implants plays a critical role in the long-term success of the implant, including artificial hip replacements [219], pacemaker leads [213], and breast implants [220]. The global implantable medical devices market was estimated to be around 25 billion dollars in 2007, and is expected continue to rise [221]. While engineered hydrogels have been increasingly used for regenerative medicine applications [222], how these materials interface with the host immune system remains incompletely understood. Additionally, while adhesive ligand functionalization appears to alter the host response to non-degradable hydrogels [89], the host response to degradable hydrogels with or without adhesive ligands remains uncharacterized. In this study, we examined whether incorporation of integrin-targeted RGD peptides within protease-

degradable PEG hydrogels impacts bulk cell recruitment to the material, as well as microscale cellular interactions at the hydrogel-tissue interface.

The recruitment and activity of leukocytes plays key roles in biomaterial outcomes such as ability to promote tissue repair [97], vascularization [41], and fibrous encapsulation [223]. Myeloid cell recruitment to PEG hydrogels was characterized by early and robust monocyte recruitment, clearance of neutrophils by 3 days post-implantation, and sustained generation of macrophages and DCs (**Figure 25**). Scaffolds derived from cardiac extracellular matrix induced robust recruitment of monocytes/macrophages, dendritic cells, and T cells 1 week after volumetric muscle injury [97]. Loss of IL-4 signaling, T and B cells, or Rictor signaling (which drives polarization of T helper 2 cells), reduced generation of M2 macrophages and prevented scaffold-induced muscle regeneration [97]. While the current work focused on the myeloid response to PEG hydrogels, our data indicates that PEG hydrogels support generation of $CD86^{neg}CD206+$ without delivery of exogenous biomolecules (**Figure 28**). M2 macrophages have been associated with bone [184], skeletal muscle [72], nerve [144], and skin repair [162], indicating that PEG may be a desirable material to use for regenerative medicine applications. Alginate, a naturally occurring polysaccharide, induces sustained neutrophil recruitment (around 15% of cells at all time points) and a gradual increase in the frequency of macrophages (around 70% at day 14) over the course of 28 days of intraperitoneal implantation [223]. Loss of macrophages, but not neutrophils, completely abrogated fibrous encapsulation of alginate, with evidence that macrophages recruit fibrosis-potentiating B lymphocytes [223]. Consequently, future studies should investigate the interplay between innate and adaptive immune cells in response to implantation of PEG-based materials.

Immune cells recruited to a material interact with the surface through integrin ligation to adsorbed proteins such as complement components, fibrinogen, and fibronectin [100, 101]. Mass spectrometry analysis of adsorbed proteins collected from PEG hydrogels revealed that albumin is the most abundant protein after 30 minutes of subcutaneous implantation in mice, although complement component 3 (C3) and 8 (C8) were also detected [89]. Integrins are heterodimeric proteins composed of an alpha and a beta chain that pair in a cell type-specific manner to enable cell-matrix and cell-cell interactions [102]. Phagocytes (including neutrophils, monocytes, and macrophages) can express the β_1, β_2, and β_3 chains, which dimerize to form integrins that include $\alpha_L\beta_2$ (LFA-1), $\alpha_M\beta_2$ (Mac-1), $\alpha_5\beta_1$, and $\alpha_V\beta_3$ [102]. Functionalization of material surfaces with integrin ligands such as RGD and PHSRN (sequences derived from fibronectin and other ECM proteins) and GFOGER (derived from collagen) have been used to increase cell adhesion [224], but whether these ligands promote adhesion of specific immune cells remains unknown. Consistent with previous reports [61], we found that RGD functionalization of PEG hydrogels increases the overall number of myeloid cells at the material surface (**Figure 35a**). However, incorporation of either a linear or cyclic RGD peptide did not alter the overall composition of biomaterial-adherent cells compared to a scrambled peptide control (**Figure 25, Figure 29**), suggesting that RGD does not promote adhesion of specific immune cell populations. RGD primarily interacts with $\alpha_V\beta_3$, although at least 8 out of the 24 total can bind to RGD [225]. The affinity or expression of specific integrins on myeloid cells may be dependent on cell activation, as is the case is the case for Mac-1, whose expression increases in neutrophils and monocytes after local administration of TNF- α to the vasculature [104]. One interpretation of our results is that cells do not sense material-

bound adhesive ligands during extravasation from the vasculature, which represents the primary recruitment event. Subsequently, RGD functionalization and integrin activation does not change the phenotype of cells that have already been recruited to the material surface, although subtle shifts in cell phenotype that are not captured by our flow cytometry analysis remain possible.

Integrin signaling appears to play different roles in leukocyte migration, depending on the environment in which the cell is migrating. For example, monocytes utilize the integrin LFA-1) to crawl along the endothelium and extravasate into the tissue [49, 108]. Conversely, leukocyte migration through interstitial space is not integrin-dependent and instead involves amoeboid-like flowing and squeezing motions [108]. The critical parameter appears to be whether the cell comes in contact with a 2D barrier, such as the endothelium. Biomaterials provide a unique context to migrating cells, where the surface serves as a 2D barrier, but materials that are porous or have topographical features may be interpreted by cells as an analogous environment to interstitial space. In the current study, we demonstrate that CX3CR1+ myeloid cells move at greater speeds near hydrogels presenting integrin ligands (**Figure 34**). This effect appears to be primarily localized to the material surface, as there was no detectable difference in migration speed between RDG- and RGD-functionalized materials at distances greater than 30μm (**Figure 35**). Previous work has demonstrated that integrins (particularly Mac-1) are required for macrophage adhesion to complement proteins adsorbed to biomaterial surfaces [100]. Additionally, integrin signaling appears to play key roles in mediating the function of biomaterial-associated leukocytes, as blockade of Mac-1 in macrophages reduces pro-inflammatory cytokine production and reduces fibrous encapsulation [109]. Delayed exposure of RGD

using a caged peptide system reduced fibrous capsule thickness around non-degradable PEG hydrogels [61]. Fibrous encapsulation primarily occurs around non-degradable materials; however, previous work demonstrated that degradable materials can induce a transient and modest fibrotic response that disappears as the material degrades [226]. Future studies are required to better understand the role of adhesive ligand functionalization and myeloid cell adhesion in fibrous encapsulation of degradable PEG hydrogels.

5.5 Materials and Methods

5.5.1 Poly(ethylene glycol) hydrogel fabrication

Four-arm poly(ethylene glycol) (PEG, 20 kDA molecular weight) end-functionalized with maleimide (>95% purity, Laysan Bio) at 4.5% weight/volume was used for all hydrogel formulations. PEG macromers were functionalized with RGD peptide (GRGDSPC), cyclic RGD peptide (Arg-Gly-Asp-D-Phe-Cys, Peptides International), or RDG scrambled peptide control (GRDGSPC), and crosslinked with the cysteine-flanked peptide VPM (GCRDVPMSMRGGDRCG) (AAPPTec) in 0.5M MES buffer, pH 5.5. The final concentration of RGD or RDG was 1.0mM and the final concentration of VEGF was 10μg/mL. The crosslinker concentration was based on the concentration of non-reacted maleimide groups remaining on PEG macromers. To generate pre-formed hydrogels for intravital imaging, the hydrogel was cast in a 4mm diameter circular silicon mold. After crossslinking, hydrogels were incubated at 37˚C for 15 minutes and then swelled in PBS for at least 30 minutes. For studies where hydrogels were fluorescently tagged, RDG or RGD was dissolved in sodium bicarbonate and tagged with Alexa Fluor 405 NHS Ester (Life Technologies) according to the manufacturer's recommendation. Tagged RDG or RGD was combined with unlabeled peptide in a 1:3 ratio for conjugation to PEG-MAL.

5.5.2 Subcutaneous implant model

All animal procedures were conducted according to protocols approved by the Georgia Institute of Technology Animal Care and Use Committee. Male C57BL/6J mice (8-12 weeks) were used for subcutaneous implant studies. Mice were anesthetized with vaporized isoflurane at 5% concentration and maintained under anesthesia at 1-3%. The

animal's dorsal skin was shaved, depilated, and sterilized with chlorhexidine and 70% isopropanol. All animals received a single dose of sustained release buprenorphine (1.2mg/kg injected intraperitoneally) prior to implantation. A 23G needle was first inserted into the subcutaneous space where hydrogels were to be implanted. Hydrogel precursors were mixed in a tube and rapidly pulled into a 31G insulin syringe for subcutaneous injection. One hydrogel (25μL volume) was placed on each side of the spine (two total hydrogels per animal). Animals were euthanized by CO2 inhalation for flow cytometry analysis at 1, 3, 7, or 14 days post-implantation.

5.5.3 Dorsal skinfold window chamber model

Male C57BL/6J or B6.129P-Cx3cr1tm1Litt/J mice ($CX3CR1^{GFP/+}$) mice (8-12 weeks) were used for dorsal skinfold window chamber studies. A sterile dorsal skinfold window chambers (APJ Trading Co) was placed on the mouse dorsum as previously described [227]. Briefly, mice were anesthetized with vaporized isoflurane at 5% concentration and maintained under anesthesia at 1-3%. The dorsal skin was shaved, depilated, and sterilized with 70% ethanol and chlorhexidine. One of the window chamber titanium frames was fitted on the underside of a double-layered skin fold on the back of the mouse. A 12mm diameter circular area of epidermis and dermis was removed from the top of the skinfold using surgical microscissors, revealing the underlying vasculature. Sterile saline was superfused on the exposed tissue throughout surgery to prevent desiccation. The upper titanium frame was placed on the top side of the skinfold, secured to the underlying frame, and sutured to the surrounding tissue. The exposed subreticular dermis was flushed with sterile saline and sealed with a sterile glass window layer (a circular cover slip). For flow cytometry studies, two hydrogels (one R<u>D</u>G and one RGD,

15μL volume each) was placed on top of the exposed subcutaneous tissue immediately after surgery. For intravital imaging studies, one day after surgery (day 1), the cover slip was removed and two hydrogels were placed on top of the exposed tissue. The window chamber was resealed with a new sterile cover slip. Animals were euthanized by CO2 inhalation for flow cytometry analysis at 3 days post-implantation.

5.5.4 Immunophenotyping by flow cytometry

Hydrogels were explanted from the subcutaneous space or window chamber, weighed, and placed in cold PBS containing calcium and magnesium. Hydrogels were washed for 30 minutes on a shaker to remove non-adherent cells. Adherent cells were isolated by digesting hydrogels with collagenase type 1A (1mg/ml) at 37°C for 30 minutes and further disaggregated with a cell strainer to ensure a single cell suspension. Single cell suspensions were stained for flow cytometry analysis in 3% FBS/PBS according to standard procedures and analyzed on a FACS-AriaIIIu flow cytometer (BD Biosciences). The following antibodies were used for immunophenotyping: BV421- or BV510-conjugated anti-CD11b (BioLegend), APC- or BV510-conjugated anti-Ly6C (BioLegend), PerCP-Cy5.5-conjugated anti-CD11c (Biolegend), PE-Cy7-conjugated anti-GR-1 (BioLegend), APC-Cy7-conjugated anti-Ly6G (Biolegend), BV711-conjugated anti-CD64 (BioLegend), PE-conjugated anti-MerTK (Biolegend), APC-Cy7-conjugated anti-F4/80 (Biolegend), PE-Cy7- or BV605-conjugated anti-CD206 (Biolegend), FITC-conjugated anti-CD86 (Biolegend), PE-Cy7-conjugated anti-MHCII (Biolegend). Staining using BV dyes was performed in the presence of Brilliant Stain Buffer (BD Biosciences). Positivity was determined by gating on fluorescence minus one controls. Absolute quantification of

cell numbers was performed by adding 25μL of AccuCheck counting beads to flow cytometry samples (Thermo Fisher Scientific).

5.5.5 High-dimensional tSNE analysis

Prior to tSNE dimensional reduction, each flow cytometry sample was pre-gated to select single cells, and then downsampled to up to 1500 events in FlowJo Version 10.2. For samples that contained less than 1500 events, no downsampling was performed (the lowest number of single cells in a sample was 763). After downsampling, each sample was electronically barcoded so that all samples could be concatenated to into a single file for tSNE analysis. A composite tSNE map that utilized data points from all samples (8 total samples: 4 from Day 1 RGD hydrogels, 4 Day 3 RGD hydrogels). tSNE analysis was executed in FlowJo software using the following surface markers: CD11b, CD64, MerTK, CD11c, MHCII, Ly6C, Ly6G, CD86, and CD206. The following tSNE parameters were used: 1000 iterations, 30 perplexity, 200 Eta (learning rate), and 0.5 theta.

5.5.6 Intravital confocal microscopy

Mice were anesthetized with vaporized isoflurane at 5% concentration and maintained under anesthesia at 1-3%. The glass cover slip was removed and sterile saline was administered to the exposed dorsal tissue to prevent desiccation. The anesthetized mouse was secured to the microscope stage in a custom adapter placed on top of a heating block to maintain body temperature. Intravital confocal microscopy was performed using a 20X water immersion objective (NA=1.0) fixed to an inverter on a Zeiss LSM710 NLO microscope. Time-lapse z-stack images were acquired at each hydrogel edge. A step size of 5μm was used in the z-direction. Videos of 25-30 minutes were acquired at each

location, with a time step of 30 seconds and a total of 2-3 videos acquired for each hydrogel, and one video acquired in distal tissue without a hydrogel.

5.5.7 Intravital imaging analysis

For 3D analysis in Imaris (Bitplane), time-lapse imageswere acquired adjacent to the implant to visualize immune cell distribution in the close surrounding tissue. Cells expressing CX3CR1-GFP were identified in Imaris using the surface tool. CX3CR1+ surfaces were identified by smoothing with a 2.77μm grain size and a threshold value of 7.71 on absolute intensity. Touching objects were split using a seed points diameter of 10.4μm with a quality threshold above 3.53. $CX3CR1^{hi}$ versus $CX3CR1^{lo}$ cells were discriminated by assigning half of all cells to each group based on maximum fluorescence intensity in the CX3CR1-GFP channel. The hydrogel surface was identified using the surface tool with a 10μm grain size and a manually selected threshold value on absolute intensity. To calculate the distance between cells and the hydrogel surface, a distance transformation was applied to the hydrogel surface and the minimum distance of each cell was recorded. To track cell activity over time, cells were identified in Imaris using the spots tool. Estimated diameter was set to 8.00μm with background subtraction enabled and an automatic threshold on quality. Tracks were selected for analysis if they lasted at least 300 seconds. Tracks were set to a maximum distance of 10.0 μm and a max gap size of 3μm. Because statistical comparisons were made on a single-cell basis, an equal number of cells was used for analysis of each video. The minimum number of detected track was 73.

Therefore, for videos with more than 73 tracks, we randomly selected 73 tracks for analysis.

5.5.8 Statistical analysis

Data are presented as mean ± standard error of the mean (S.E.M.), unless otherwise noted. For box and whiskers plots, whiskers represent the minimum and maximum; box represents the 25^{th} to 75^{th} percentile, with a line denoting the median. All statistical analysis was performed in GraphPad Prism software. For comparisons of two groups, paired or unpaired t-test (according to experimental design) was used. For grouped analyses, two-way ANOVA with Sidak's post-test was used for multiple comparisons. For intravital imaging data, a non-parametric Mann-Whitney test (for comparing two groups) or a Kruskal-Wallis test with Dunn's test for multiple comparisons (for comparing more than two groups) was used. $p<0.05$ was considered statistically significant.

6. VASCULAR ENDOTHELIAL GROWTH FACTOR DELIVERY FROM DEGRADABLE HYDROGELS ALTERS MYELOID CELL RECRUITMENT

6.1 Abstract

Revascularization of biosynthetic matrices to support survival of endogenous or transplanted cells is a major challenge in tissue engineering and regenerative medicine. The innate immune system plays key roles in facilitating vascularization by providing physical and biochemical cues to endothelial cells. In the current work, we investigated myeloid cell recruitment to protease-degradable poly(ethyelene glycol) (PEG) hydrogels delivering vascular endothelial growth factor (VEGF) and functionalized with RGD adhesive peptides. VEGF delivery from degradable hydrogels alters bulk myeloid cell recruitment, particularly at later time points. Following subcutaneous hydrogel implantation in mice, we detected an increase in monocytes and dendritic cells, but a decrease in macrophages during VEGF delivery from PEG hydrogels, regardless of incorporation of RGD adhesive ligands. Monocyte phenotype was unaffected, but an increase in the proportion of $CD86^{neg}CD206+$ alternatively activated macrophages occurred in the presence of VEGF. In dorsal skinfold window chambers, we observed that myeloid cells move greater distances in tissue far from VEGF hydrogels compared to unloaded hydrogels. However, myeloid cells moved slower and shorter distances near the source of VEGF. These findings demonstrate the impact that VEGF incorporation and adhesive ligand functionalization have on the inflammatory response to hydrogel implantation, which will likely be important to the translation of angiogenic therapies.

6.2 Introduction

A major challenge in tissue engineering and regenerative medicine is re-vascularization of biosynthetic matrices and engineered vasculature is often limited in its capacity to support repair. Physiologically, most cells in the body are located within 100-200μm of a capillary, which enables proper oxygenation and nutrient delivery [228]. After traumatic or ischemic injury, remodeling or expansion of existing vasculature represents a key step in restoring tissue function [170]. Numerous approaches aiming to revascularize ischemic tissues and enhance recovery have been proposed, but pro-angiogenic drugs have not translated clinically and therapeutic angiogenesis remains a major challenge. For example, delivery of vascular endothelial growth factor (VEGF) has been investigated, but high concentrations of native VEGF can lead to enhanced vascular leakage and abnormal restructuring of blood vessels, similar to the vascular dysfunction observed in cancer [229]. Conversely, controlled delivery of VEGF from engineered matrices enables sustained delivery at physiological doses, and supports functional re-vascularization [140, 201, 230]. A better understanding of the physiological effects of angiogenic growth factor delivery from biomaterials will enable improved therapies for treatment of cardiovascular diseases and large-scale traumatic injuries.

The VEGF family of growth factors includes four isoforms, with VEGF-A playing the primary role in developmental, physiological, and pathological blood vessel growth [231]. VEGF-A (VEGF) is produced by many cell types, including activated platelets, fibroblasts, myeloid cells, and endothelial cells, in part in response to stabilization of the transcription factor hypoxia-inducible factor 1-alpha during low oxygen levels (HIF-1α) [166]. VEGF signals primarily through VEGFR2 on endothelial cells to induce cell

survival, migration, and proliferation [231], but also recruits accessory cells such as monocytes and macrophages through VEGFR1 [232]. Myeloid cells play multi-faceted roles in supporting vasculogenesis, angiogiogenesis, and arteriogenesis, both through direct interaction with the vasculature and through paracrine signaling. Genetic mutation of colony stimulating factor receptor 1 (CSFR1), which is essential for normal development of the mononuclear phagocyte system leads to the formation of aberrant and immature vascular networks [7, 23]. During development, macrophages position themselves near the endothelium to help bridge tip cells from different vessel segments and create nascent fusion sites within vascular networks [23]. Post-developmentally, macrophages play a reparative role by physically pulling endothelial cells together after vascular rupture and facilitating repair [233].

Monocytes and macrophages display significant heterogeneity *in vivo*, enabling them to perform extremely varied and tissue-specific functions [95]. During homeostasis, blood monocytes are composed of classical and non-classical subsets [16], while macrophage heterogeneity is primarily determined by the tissue of residence [21]. Following injury, classical monocytes are the first monocytic responders, followed by their conversion into or direct recruitment of non-classical monocytes that produce anti-inflammatory and wound healing mediators [8]. Macrophages derived from monocytes or locally-proliferating tissue resident populations display a wide spectrum of activation states that are primarily determined by paracrine signals from other leukocytes, endothelial cells, and stromal cells [147]. Macrophage phenotype has been described on a spectrum ranging from "M1" classically activated macrophages to "M2" alternatively activated macrophages, although this nomenclature is likely an oversimplification of macrophages

in vivo, where phenotype and function is extremely varied. Both non-classical monocytes and alternatively activated macrophages present during the later stages of inflammation have been associated with revascularization and tissue repair. Loss of NR4A1, a nuclear factor that is critical for development of non-classical monocytes, impairs revascularization after myocardial infarction [234]. Loss of IL-4 receptor α, which plays a major role in alternative activation of macrophages, prevents proper endothelial cell-matrix interactions during skin repair, leading to abnormal vascular morphology and hemorrhage [45]. Additionally, while most research has focus on the role of monocytes and macrophages in vascularization, neutrophils and dendritic cells may also provide important functions [235, 236].

Given the role of myeloid cells in supporting vascularization [55] and the role that VEGF signaling plays in their recruitment [56], the objective of this study was to investigate innate immune cell recruitment to synthetic hydrogels delivering VEGF. Previous work has indicated that incorporation of adhesive ligands such as Arg-Gly-Asp (RGD) into hydrogels enhances VEGF-induced vascularization [61]. Therefore, we also explored how RGD functionalization impacts cell recruitment during VEGF delivery. We fabricated protease-degradable poly(ethylene-glycol) (PEG) hydrogels with covalently-tethered VEGF and functionalized with RGD, which has been previously used to vascularize bone defects and transplanted islets [140, 237]. These matrices were implanted in the subcutaneous space of mice to assess the composition of adherent myeloid cells by high-dimensional flow cytometry. We also explored the migration of myeloid cells around VEGF hydrogels implanted in dorsal skinfold window chambers using real-time intravital confocal microscopy. We hypothesized that delivery of VEGF from PEG hydrogels would

enhance recruitment of myeloid cells that support vascularization, including monocytes and alternatively activated macrophages.

6.3 Results

6.3.1 VEGF-tethered PEG hydrogels for on demand angiogenic growth factor delivery

We engineered degradable poly(ethylene glycol) (PEG) hydrogels for on demand VEGF delivery by conjugating VEGF-A_{165} (VEGF) to 4-arm PEG macromers (20 kDa) containing terminal maleimide groups (PEG-MAL). VEGF has a thiol-containing free cysteine that can react with PEG-MAL, forming a PEG-VEGF conjugate. After VEGF conjugation, PEG-VEGF was reacted with a cysteine-terminated RGD adhesive peptide or a scrambled peptide control (RDG). Functionalized macromers were crosslinked with the cysteine-flanked peptide GCRDVPMSMRGGDRCG (VPM) that contains a cleavage site for proteases such as matrix metalloproteinases (**Figure 37**). Protease-mediated degradation of the hydrogel matrix enables VEGF delivery, which occurs gradually over two weeks when implanted subcutaneously [238]. Previous work has demonstrated that VEGF conjugated to PEG-MAL matrices remains bioactive, promoting endothelial cell proliferation *in vitro* and vascularization *in vivo* [140].

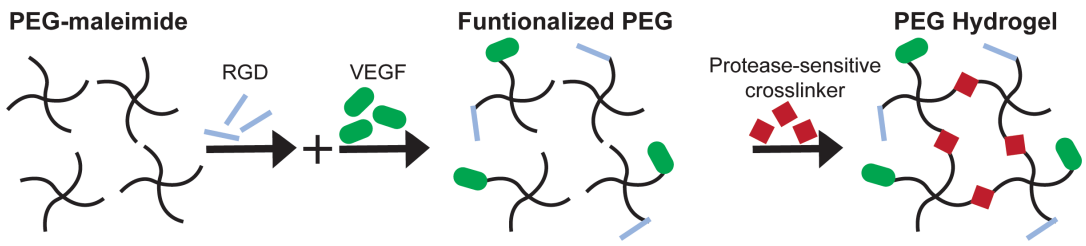

Figure 37. On demand VEGF delivery from protease-degradable PEG hydrogels. 4-arm PEG-maleimide macromers (20 KDa) were functionalized with cysteine-containing VEGF and RGD peptides. Functionalized macromers were crosslinked with a protease sensitive crosslinker (VPM), forming a hydrogel. Degradation of the hydrogel matrix results in VEGF delivery.

6.3.2 Effects of VEGF delivery and adhesive ligand presentation on myeloid cell recruitment

While VEGF is chemotactic for myeloid cells [56], the effects of biomaterial-delivered VEGF on the inflammatory response remains unknown. To investigate the kinetics of myeloid cell accumulation around degradable PEG hydrogels delivering VEGF, we mixed functionalized PEG-MAL and VPM crosslinker and immediately injected the pre-hydrogel solution into the subcutaneous space of mice, where hydrogels formed *in situ*. Each mouse received two hydrogels that were either unloaded or loaded with 250ng of VEGF: a control hydrogel containing RDG and a RGD-functionalized hydrogel on the opposite flank. After 3, 7, or 14 days of implantation, the hydrogels were explanted, digested with collagenase to extract adherent cells, and immunophenotyped by flow cytometry (**Figure 38a**). Macrophages were identified based on co-expression of MerTK and CD64, DCs were identified based on high expression of CD11c, neutrophils were

identified as Ly6G+CD11b+ cells, and monocytes were identified among the remaining cells as CD64+CD11b+SSC^{lo} (Chapter 6, **Figure 25b**).

We compared data collected from animals with VEGF-loaded hydrogel implants to data collected from animals receiving unloaded hydrogels (Chapter 6, **Figure 25**). The frequency of CD11b+ myeloid cells was similar across all groups, indicating that neither VEGF nor RGD adhesive ligand impact the overall recruitment of myeloid cells (**Figure 38b**). In all groups, Ly6G+ neutrophils were present at the highest frequency 1 day post-implantation, and decreased by 7 days post-implantation (**Figure 38c**). While the average percentage of neutrophils was higher in both VEGF hydrogel formulations (0.10±0.11% for unloaded RGD hydrogel vs. 5.30±7.85% for VEGF-loaded RGD hydrogel), we detected no significant differences by ANOVA. The frequency of CD64+SSC^{lo} monocytes was higher for RDG- and RGD-functionalized VEGF hydrogels compared to unloaded hydrogels at 14 days after implantation (**Figure 38c**). We also detected fewer MerTK+CD64+ macrophages around both VEGF hydrogel formulations compared to unloaded hydrogels at day 14, but not at earlier time points (**Figure 38e,g**). While the frequency of CD11c+ DCs decreased from day 7 to day 14 around unloaded hydrogels, no decrease was observed around VEGF hydrogels (**Figure 38f)**, and the frequency of DCs was higher around VEGF hydrogels at day 14 (**Figure 38h**). These results indicate the VEGF delivery from PEG hydrogels primarily impacts the composition of myeloid cells at later time points (day 14), and that RGD presentation does not impact bulk cell recruitment both in the absence and presence of VEGF.

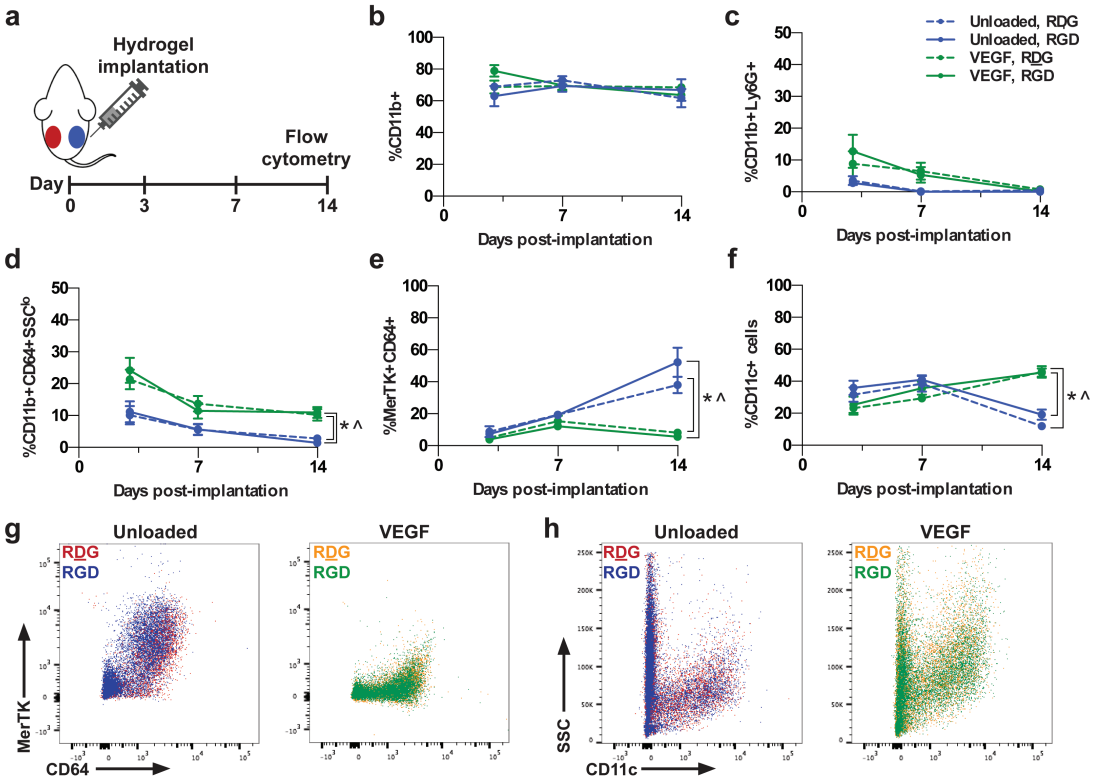

Figure 38. ***In vivo*** **effect of VEGF delivery from PEG hydrogels on inflammatory cell recruitment.** (a) Each mouse received unloaded or VEGF-loaded hydrogel subcutaneous implants. One RGD and one RDG (scrambled peptide control) hydrogel were injected in the subcutaneous space above each rear flank. Hydrogels were explanted at 3, 7, or 14 days after implantation. Adherent cells were collected from digested hydrogels and immunophenotyped by flow cytometry. Total frequency of (b) CD11b+ cells, (c) neutrophils, (d) monocytes, (e) macrophages, and (f) dendritic cells. Representative flow cytometry dot plots from day 14 from which (g) macrophages and (h) dendritic cells were identified. Data expressed as mean ± S.E.M. *$p<0.05$ compared to unloaded RDG hydrogel, ^$p<0.05$ compared to unloaded RGD hydrogel by one-way ANOVA at the indicated time point. n=3-11.

6.3.3 Effect of VEGF delivery and adhesive ligand presentation on accumulation of monocyte/macrophage subsets

Non-classical monocytes, characterized by low expression of Ly6C [16], and alternatively activated macrophages, characterized by high expression of CD206 [41], have

been associated with vascularization after ischemic injury [8, 154]. We explored the effect of PEG hydrogel-delivered VEGF on accumulation of pro-angiogenic monocyte and macrophage subsets *in vivo*. Consistent with previous findings in other inflammatory contexts [8, 69], we found that monocytes recruited to all hydrogel formulations progressively lost Ly6C expression from day 3 to day 7 post-implantation (**Figure 39a**). By day 14, more than 93% of all monocytes were $Ly6C^{lo}$ (**Figure 39b**), and there was no effect on monocyte composition in response to VEGF delivery or RGD presentation. The proportion of macrophages that were $CD86+CD206^{neg}$ (M1-like) was highest for all hydrogel formulations at 3 days post-implantation (between 2% and 7%), but was not significantly different between the groups (**Figure 39c**). The proportion of inflammatory $CD86+CD206^{neg}$ macrophages decreased over 14 days of implantation, while the proportion of $CD86^{neg}CD206+$ macrophages increased from day 3 to day 14 (**Figure 39d**). At 14 days post-implantation, we detected a greater proportion of $CD86^{neg}CD206+$ macrophages around RGD-functionalized VEGF hydrogels compared to unloaded RGD hydrogels (**Figure 39d,e**). Taken together, VEGF delivery from PEG hydrogels did not impact the composition of recruited monocytes at the tested time points, but increased accumulation of alternatively activated macrophages 14 days after implantation.

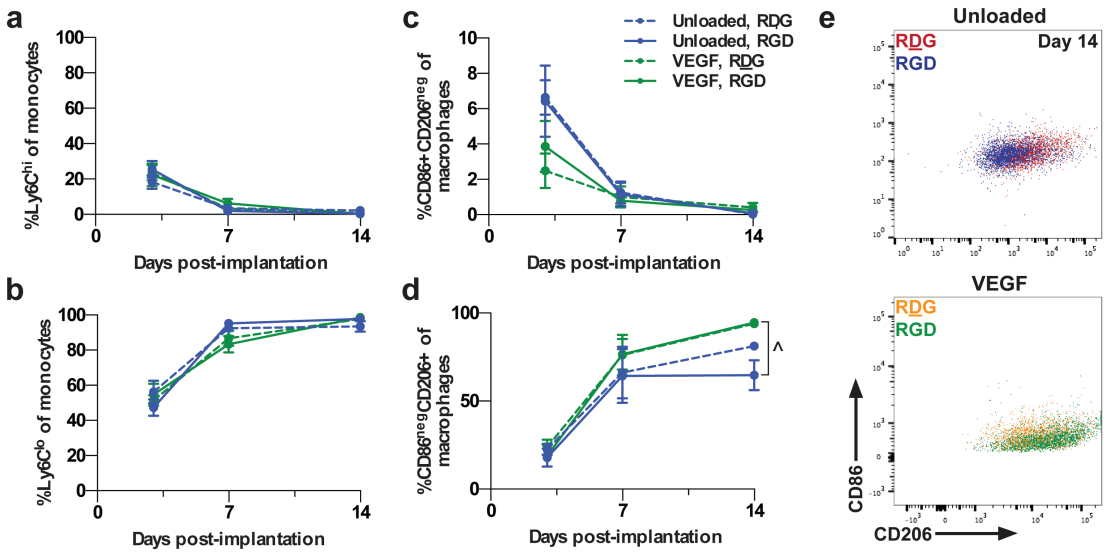

Figure 39. Temporal evolution of monocytes and macrophages around PEG hydrogels delivering VEGF. Quantification of the frequency of (a) classical Ly6C^{hi} and (b) non-classical Ly6C^{lo} monocytes, expressed as a frequency of total monocytes. Quantification of the frequency of (c) M1-like CD86+CD206^{neg} and (d) M2-like CD86^{neg}CD206+ macrophages, expressed as a frequency of total macrophages. (e) Representative flow cytometry dot plots from day 14 of MerTK+CD64+ macrophages showing expression of CD86 and CD206. Data expressed as mean ± S.E.M. ^p<0.05 compared to unloaded RGD hydrogel by one-way ANOVA at the indicated time point. n=3-11 animals per group.

6.3.4 Intravital imaging of myeloid cell migration around VEGF-releasing hydrogels

In order to explore the migration patterns of myeloid cells around engineered hydrogels, we performed intravital confocal microscopy in CX3CR1$^{GFP/+}$ mice (**Figure 40a; Chapter 6, Figure 33**). Mice underwent dorsal skinfold window chamber surgery and, immediately after surgery, we placed a pre-cast hydrogel functionalized with RDG or RGD on the exposed subcutaneous layer of the dermis. Each animal received two hydrogels that were either unloaded or loaded with 150ng of VEGF. Utilizing 3D image processing, we tracked the migration of CX3CR1+ cells in real time around hydrogels functionalized with adhesive ligands and/or VEGF (**Figure 40b**). No gross differences in

the frequency of CX3CR1+ cells were observed between different hydrogel formulations, which is consistent with the flow cytometry analysis of monocyte subsets from subcutaneously implanted hydrogels (**Figure 39a,b**).

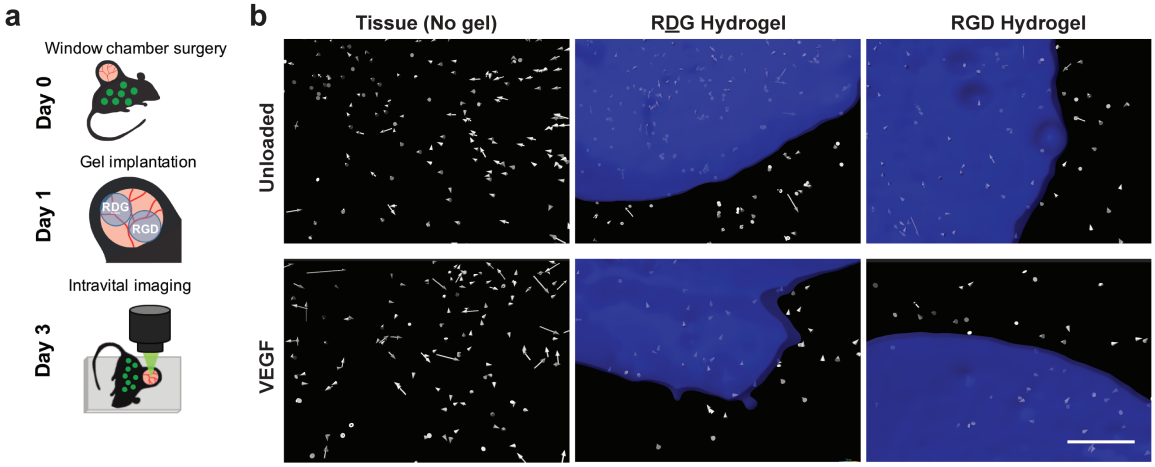

Figure 40. Intravital imaging of CX3CR1+ myeloid cell migration around PEG hydrogels delivering VEGF. (a) Dorsal skinfold window chambers were performed in CX3CR1$^{GFP/+}$ mice. One RDG- and one RGD-functionalized hydrogel was placed on the exposed subcutaneous layer 1 day after surgery. Each animal received either unloaded or VEGF-loaded hydrogels. At 3 days post-injury, intravital confocal microscopy was performed. (b) Time-lapse images were acquired at the edge of each hydrogel and in tissue distal to both hydrogels. Representative renderings of cell displacement vectors generated during image processing to track cell migration. Scale bars, 100μm.

In tissue distal to implanted hydrogels, CX3CR1+ cells displayed a greater average track length in animals that received VEGF-loaded hydrogels (57.7±30.6μm) compared to unloaded hydrogels (40.4±22.0μm) (**Figure 41a**). Interestingly, in images taken at the hydrogel edge, CX3CR1+ cells displayed a lower track distance around VEGF-loaded hydrogels compared to unloaded hydrogels regardless of RGD functionalization (**Figure 41a**). The mean velocity of CX3CR1+ cells moving through tissue far away from the hydrogels was also greater in animals receiving VEGF gels, but decreased when cells were

in close proximity to VEGF gels (**Figure 41b**). No differences in mean velocity were detected between RDG- and RGD-functionalized VEGF hydrogels. The path straightness, which is the track displacement normalized to the track length, was lower in distal tissue of animals receiving VEGF gels, but increased as cells moved closer to VEGF hydrogels (**Figure 41c**). These measurements indicate that VEGF delivery from PEG hydrogels causes myeloid cells far away from the material to migrate faster, but reduces their migration around the hydrogel surface.

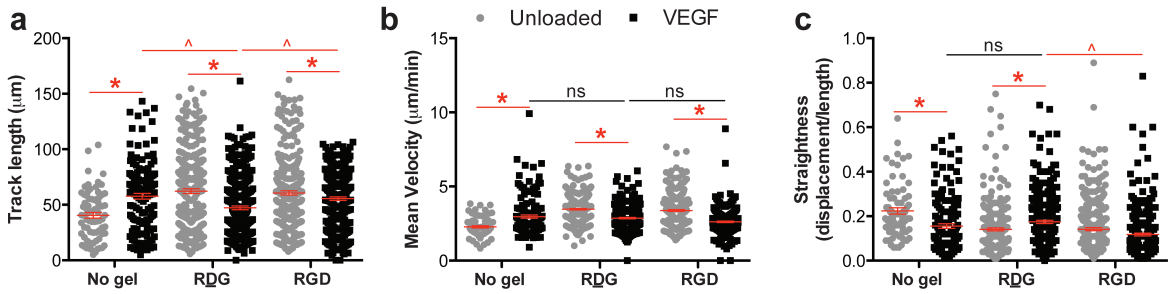

Figure 41. Quantification of myeloid cell migration around PEG hydrogels delivering VEGF. (a) Track length (in μm), (b) mean velocity (in μm/minute), and (c) track straightness (the displacement normalized to the path length) of CX3CR1+ cells moving in tissue without a hydrogel or around hydrogels functionalized with RDG or RGD. Red bar indicates the mean. *p<0.05 compared to unloaded hydrogel or tissue, ^p<0.05 compared to RDG hydrogel by Kruskal-Wallis. n>146 cells across 4 mice (2 mice received unloaded hydrogels, 2 mice received VEGF hydrogels).

6.3.5 Effects of adhesive ligand incorporation on VEGF-induced vascularization

To investigate whether adhesion plays a role in hydrogel vascularization, we co-implanted hydrogels functionalized with VEGF and RDG or RGD immediately adjacent to each other in window chambers. Whole mount immunohistochemistry was used to visualize new microvessels and alternatively activated macrophages via CD31 and CD206 staining, respectively (**Figure 42a**). To quantify the extent of vascularization, we selected

the region of greatest vessel density within each hydrogel and measured the length of CD31+ blood vessels. VEGF hydrogels functionalized with RGD increased the total length of blood vessels associated with implanted hydrogels compared to RDG control gels (**Figure 42b**). In high-power images, we observed that regions of CD206+ cell infiltration were associated with hydrogel degradation and vascular ingrowth into the hydrogel (**Figure 42c**). Consequently, incorporation of integrin ligands into PEG hydrogels delivering VEGF facilitates vessel growth.

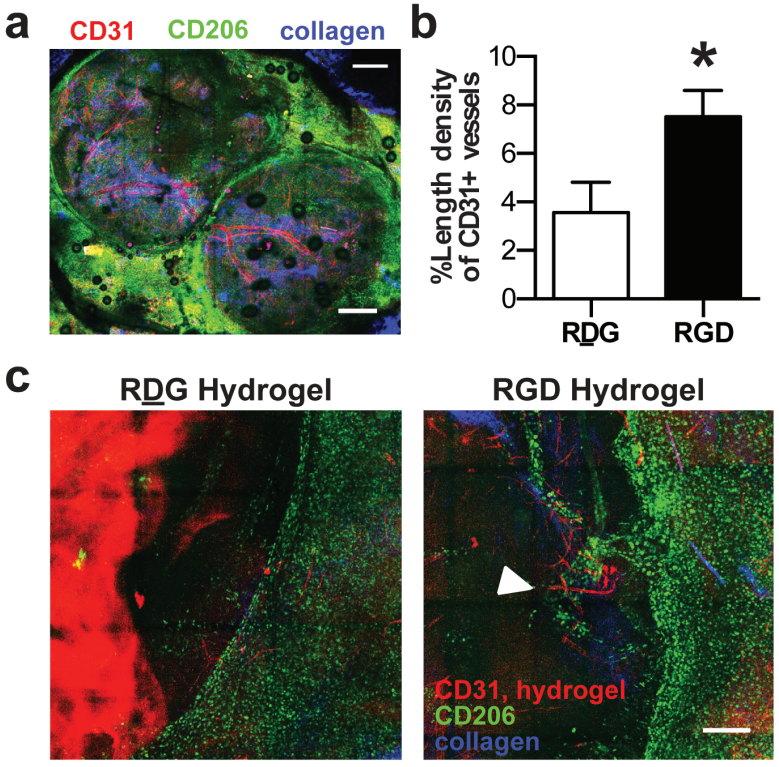

Figure 42. Effect of RGD incorporation on vascularization in response to VEGF delivery from PEG hydrogels. (a) Immunohistochemistry for CD31 (red) and CD206 (green) was performed 7 days after implantation of VEGF-loaded hydrogels in dorsal skinfold window chambers. Collagen was visualized using second harmonic generation with multiphoton microscopy (blue). Scale bar, 1mm. (b) Quantitative analysis of blood vessel length normalized to the analysis region's area. (c) Regions of vascular ingrowth and hydrogel degradation (white arrow). Scale bar, 100μm. Data expressed as mean ± S.E.M. *$p<0.05$ by paired t test. n=6 animals per group.

6.4 Discussion

Cardiovascular diseases are the main source of mortality in the US and around the world, with peripheral arterial disease being present in 12% of the adult population and presenting a major risk factor for adverse cardiovascular events [239]. Delivery of angiogenic growth factors represents a promising strategy to enhance endogenous angiogenic and arteriogenic programs; however, controlled delivery of proteins such as VEGF is critical, as supraphysiological doses can result in pathological vessel formation characterized by excessive leakiness and poor perfusion [229]. Immune cells play key roles in vascularization during development and after injury, both through physical contacts [23, 233] and providing paracrine signals to endothelial cells [55]. In the current study, we examined how VEGF delivery from engineered hydrogels impacts the kinetics of myeloid cell recruitment and migration.

Monocytes express VEGFR1, enabling them to migrate towards gradients of VEGF, and we detected that they also express VEGFR2 (**Chapter 3, Figure 12g**). We explored myeloid cell migration through interstitial space using intravital confocal microscopy of dorsal skinfold window chambers in CX3CR1$^{GFP/+}$ mice. The path length of CX3CR1+ cells was nearly twice as long in tissue distal to VEGF hydrogels compared to unloaded hydrogels (**Figure 41a**). This finding is consistent with cells displaying enhanced migration in response to a chemokine gradient. Interestingly, we detected no difference in the average speed of distal cells. In close proximity to implanted hydrogels, CX3CR1+ cells displayed decrease both in path length and mean velocity near VEGF hydrogels, regardless of RGD incorporation (**Figure 41a,b**). Previous work has demonstrated that neutrophils migrating towards a site of infection slow down as they approach the infection

loci [240]. Our findings suggest that myeloid cells similarly slow down and move shorter distances in close proximity to exogenously delivered VEGF. During VEGF delivery, path length was greater around PEG hydrogels functionalized with RGD compared to RDG; however, both were lower compared to unloaded hydrogels (**Figure 41a**). Migration speed was insensitive to adhesive ligand functionalization in the presence of VEGF. In the context of vascularization, VEGF and adhesive ligand incorporation into hydrogels has been demonstrated to be synergistic [238], but this effect may not be mediated through leukocyte recruitment. Endothelial cells in particular may be sensitized to VEGF signaling during ligation to integrins $\alpha_v\beta_3$ [241] and $\alpha_1\beta_1$ [242], and thus may be the primary mediators of cooperation between VEGF and integrin signaling.

Transgenic activation of VEGF production by the liver results in recruitment of $Ly6C^{hi}$ monocytes that convert *in situ* to $Ly6C^{lo}$ monocytes within 3 days [56]. In the present work, we saw no differences in the composition of monocytes ($Ly6C^{hi}$ or $Ly6^{lo}$) around VEGF hydrogels (**Figure 39a,b**), despite an increase in the overall frequency of monocytes (**Figure 38d**). These results are particularly surprising given that circulating non-classical monocytes express higher levels of VEGF receptors compared to classical monocytes (**Figure 12g**). We previously demonstrated that non-classical monocytes differentiate into alternatively activated macrophages (**Chapter 3**). We observed parallel increases in the proportion of non-classical $Ly6C^{lo}$ monocytes and $CD86^{neg}CD206+$ alternatively activated macrophages. However, we did not see enhancement of $Ly6C^{lo}$ monocytes around VEGF hydrogels at any time points, which had more $CD86^{neg}CD206+$ macrophages 14 days post-implantation (**Figure 39d**). It is possible that our temporal resolution was not sufficient to detect differences in monocyte recruitment in these studies,

or that changes in macrophage phenotype occurred independently of changes to monocyte recruitment. We also detected an increase in CD11c+ DCs around VEGF hydrogels compared to unloaded hydrogels after 14 days (**Figure 38f**). VEGF inhibits DC maturation and may be a mechanism by which tumors suppress the immune system [243]. Interestingly, tumors also selectively recruit plasmacytoid DCs, but exclude monocyte-derived DCs, which contributes to dysregulated angiogenesis [236]. While we were unable to discriminate DC subsets in the current studies, an interesting future direction would be to investigate whether hydrogel-delivered VEGF recruits DCs that more closely resemble those present during physiological or pathological vascular remodeling.

Consistent with previous work [61], vascularization occurred more robustly when VEGF hydrogels were functionalized with RGD compared to a scrambled peptide control (**Figure 42b**). Regions of vascular ingrowth into the material were associated with infiltration of CD206+ cells and hydrogel degradation (**Figure 42c**). The protease-sensitive crosslinker we used in these studies is degraded by matrix metalloproteinase (MMP)-1 and MMP-2 [139], which can be produced by myeloid cells, including macrophages [244]. In addition to matrix remodeling, macrophages may support stabilization of vasculature induced by biomaterial-delivered VEGF. Encapsulation of VEGF within PEG hydrogels generates disorganized and leaky blood vessels, but co-delivery of macrophage colony-stimulate factor 1 (M-CSF1) promotes vascular stabilization [143]. The current work seeks to limit the side effects of VEGF by tethering it to the matrix, and delivering low doses during the course of inflammation; however, incorporation of macrophage-targeted factors could further enhance or improve the quality of vascularization induced by VEGF in our system.

This work demonstrates that VEGF delivery from protease-degradable PEG hydrogels alters bulk myeloid cell recruitment, particularly at later time points. Following subcutaneous hydrogel implantation, we detected an increase in monocytes and dendritic cells, but a decrease in macrophages during VEGF delivery, regardless of incorporation of RGD adhesive ligands. Monocyte phenotype was unaffected, but an increase in the proportion of $CD86^{neg}CD206+$ alternatively activated macrophages occurred in the presence of VEGF. In dorsal skinfold window chambers, we observed that myeloid cells move greater distances in tissue far from VEGF hydrogels compared to unloaded hydrogels. However, myeloid cells move slower and shorter distances near the source of VEGF. These findings demonstrate the impact that VEGF incorporation and adhesive ligand functionalization have on the inflammatory response to hydrogel implantation, which will likely be important to the translation of angiogenic therapies.

6.5 Materials and Methods

6.5.1 Hydrogel fabrication

Four-arm poly(ethylene glycol) (PEG, 20 kDA molecular weight) end-functionalized with maleimide (>95% purity, Laysan Bio) at 4.5% weight/volume was used for all hydrogel formulations. Recombinant human VEGF-A_{165} (Invitrogen) was covalently tethered to PEG macromers for 30 minutes on ice in PBS, pH 7.4. PEG macromers were also functionalized with RGD peptide (GRGDSPC) or RDG scrambled peptide control (GRDGSPC), and crosslinked with the cysteine-flanked peptide VPM (GCRDVPMSMRGGDRCG) (AAPPTec) in 0.5M MES buffer, pH 5.5. The final concentration of RGD or RDG was 1.0mM and the final concentration of VEGF was 10μg/mL. Crosslinker concentration was based on the concentration of non-reacted maleimide groups remaining on PEG macromers. To generate pre-formed hydrogels, the hydrogel was cast in a 4mm diameter silicon mold. After crossslinking, hydrogels were incubated at 37˚C for 15 minutes and then swelled in PBS for at least 30 minutes.

6.5.2 Subcutaneous implant model and flow cytometry

All animal procedures were conducted according to protocols approved by the Georgia Institute of Technology Animal Care and Use Committee. Male C57BL/6J mice (8-12 weeks) were used for subcutaneous implant studies. Mice were anesthetized with vaporized isoflurane at 5% concentration and maintained under anesthesia at 1-3%. The animal's dorsal skin was shaved, depilated, and sterilized with chlorhexidine and 70% isopropanol. All animals received a single dose of sustained release buprenorphine (1.2mg/kg injected intraperitoneally) prior to implantation. One hydrogel (25μL volume)

was placed on each side of the spine (two total hydrogels per animal). Each animal received unloaded or VEGF hydrogels, with one hydrogel containing RGD and the other containing RDG. Animals were euthanized by CO_2 inhalation for flow cytometry analysis at 3, 7, or 14 days post-implantation. Hydrogels were explanted from the subcutaneous space, weighed, and washed for 30 minutes in cold PBS containing calcium and magnesium. Adherent cells were isolated by digesting hydrogels with collagenase type 1A (1mg/ml) at 37°C for 30 minutes. Single cell suspensions were stained for flow cytometry analysis in 3% FBS/PBS according to standard procedures and analyzed on a FACS-AriaIIIu flow cytometer (BD Biosciences). Staining using BV dyes was performed in the presence of Brilliant Stain Buffer (BD Biosciences). Positivity was determined by gating on fluorescence minus one controls. Absolute quantification of cell numbers was performed by adding 25µL of AccuCheck counting beads to flow cytometry samples (Thermo Fisher Scientific).

6.5.3 Dorsal skinfold window chamber model

Male B6.129P-Cx3cr1tm1Litt/J mice ($CX3CR1^{GFP/+}$) mice (8-12 weeks) were used for dorsal skinfold window chamber studies. A sterile dorsal skinfold window chambers (APJ Trading Co) was placed on the mouse dorsum as previously described [227]. Briefly, mice were anesthetized with vaporized isoflurane at 5% concentration and maintained under anesthesia at 1-3%. The dorsal skin was shaved, depilated, and sterilized with 70% ethanol and chlorhexidine. One of the window chamber titanium frames was fitted on the underside of a double-layered skin fold on the back of the mouse. A 12mm diameter circular area of epidermis and dermis was removed from the top of the skinfold using surgical microscissors, revealing the underlying vasculature. Sterile saline was superfused

on the exposed tissue throughout surgery to prevent desiccation. The upper titanium frame was placed on the top side of the skinfold, secured to the underlying frame, and sutured to the surrounding tissue. The exposed subreticular dermis was flushed with sterile saline and sealed with a sterile glass window layer (a circular cover slip). One day after surgery (day 1), the cover slip was removed and two hydrogels (unloaded or VEGF-loaded) were placed on top of the exposed tissue. The window chamber was resealed with a new sterile cover slip.

6.5.4 Intravital confocal microscopy and analysis

Mice were anesthetized with vaporized isoflurane at 5% concentration and maintained under anesthesia at 1-3%. The glass cover slip was removed and sterile saline was administered to the exposed dorsal tissue to prevent desiccation. The anesthetized mouse was secured to the microscope stage in a custom adapter placed on top of a heating block to maintain body temperature. Intravital confocal microscopy was performed as described in Chapter 5 with a 20X water immersion objective fixed to an inverter on a Zeiss LSM710 NLO microscope. Time-lapse z-stack images were acquired at each hydrogel edge, with a time step of 30 seconds and a total of 2-3 videos acquired for each hydrogel, and one video acquired in distal tissue without a hydrogel. To track cell migration over time, cells were identified in Imaris software using the spots tool. Estimated diameter was set to 8.00μm with background subtraction enabled and an automatic threshold on quality. Tracks were selected for analysis if they lasted at least 300 seconds. Tracks were set to a maximum distance of 10.0μm and a max gap size of 3μm. Because statistical comparisons were made on a single-cell basis, an equal number of randomly selected cells was selected from each video and used for analysis.

6.5.5 Whole mount immunohistochemistry and quantification

Post-euthanasia, mouse vasculature was perfused with warm saline followed by 4% PFA until tissues were fixed. Dorsal tissue was explanted, leaving implanted hydrogels intact. Tissue was permeabilized overnight with 0.1% saponin and tissues were blocked overnight in 10% mouse serum. Tissues were incubated at 4˚C overnight in solution containing 0.1% saponin, 5% mouse serum, 0.5% bovine serum albumin, and the following conjugated fluorescent antibodies: Alexa Fluor 594 (BioLegend, eBioscience) for blood vessel visualization, Alexa Fluor 647 anti-CD68 (AbD Serotec) for monocyte/macrophage visualization, and Alexa Fluor 647 anti-CD206 (Biolegend). Following immunostaining, tissues were washed 4 times for 30 minutes each, mounted in 50/50 glycerol/phosphate buffered saline and imaged until fluorescence signal was lost on a Zeiss LSM 710 NLO confocal microscope. Acquisition parameters were kept identical across all animals. For quantification of blood vessel density, CD31+ blood vessels were manually traced and analyzed by a blinded observer. Using ImageJ software (NIH), a region of fixed size was selected on the area of greatest vascular density within the hydrogel (identified by incorporation of a fluorescent tag) and the length of blood vessels was normalized to the region's area.

6.5.6 Statistical analysis

Data are presented as mean ± standard error of the mean (S.E.M.), unless otherwise noted. All statistical analysis was performed in GraphPad Prism software. For comparisons of two groups, a two-tailed paired t-test was used. For comparisons of more than two groups analyses, one-way ANOVA with Tukey's post-test was used for multiple

comparisons. For intravital imaging data, a non-parametric Mann-Whitney test (for comparing two groups) or a Kruskal-Wallis test with Dunn's test for multiple comparisons (for comparing more than two groups) was used. $p<0.05$ was considered statistically significant.

7. CONCLUSIONS AND FUTURE DIRECTIONS[5,6]

7.1 Overall Summary

The work presented in this thesis represents a significant contribution to the fields of biomaterials and regenerative medicine by demonstrating that modulation of monocyte and macrophage accumulation around biomaterial implants can enhance vascularization and tissue repair. This work expands understanding of the relationship between blood monocyte subsets and alternatively activated macrophages, as well as identifies potential targets by which to modulate myeloid cell recruitment.

In Aim 1, non-classical monocytes were identified as biased progenitors of alternatively activated macrophages during inflammation induced by cutaneous wounding. Blood monocytes exist in two primary subpopulations, characterized as classical inflammatory or non-classical. Through the use of cell fate tracking techniques, the relationship between circulating monocyte subsets and wound macrophages can be studied. Utilizing fluorescent bead- and CD45.1/CD45.2-based labeling of blood monocyte subsets, we demonstrated that non-classical monocytes are directly recruited to soft tissue injury and selectively give rise to alternatively activated macrophages. Reduction of non-classical monocytes with clodronate liposomes impaired generation of alternatively activated

[5]Portions of this chapter adapted from: Ogle ME, Segar CE, Sridhar S, Botchwey EA, Monocytes and macrophages in tissue repair: Implications for immunoregenerative biomaterial design. Exp Biol Med (241) pp. 1084-97. Copyright © 2016. Reprinted by permission of SAGE publications.

[6]Portions of this chapter adapted from: San Emeterio CL, Olingy CE, Chu Y, Botchwey EA. Selective recruitment of non-classical monocytes promotes skeletal muscle repair. Biomaterials. 2017;117:32-43. License No. 4098910025385

macrophages, while adoptive transfer of non-classical monocytes increased the frequency of donor-derived wound healing macrophages compared to adoptive transfer of classical monocytes.

Taken together, these results highlight a previously unknown role for blood-derived non-classical monocytes as contributors to alternatively activated macrophages. The significance of this work includes identification of a novel therapeutic target for enhancing accumulation of cells that support repair and improve host responses to implanted materials. Harnessing myeloid cell functions for regenerative medicine applications requires an understanding of the cues that direct the localization and fate of these cells. While monocytes and macrophages appear during the first few days after injury, their effects can be long-lived and have critical impacts on tissue repair [147].

In Aim 2, we demonstrated that delivery of FTY720 from polymer films enhances recruitment of alternatively activated macrophages and skeletal muscle repair after ischemic or traumatic injury. Mononuclear phagocytes play key roles in regulating post-injury processes of vascularization, re-organization of tissue architecture, and regulating the activities of stem and parenchymal cells. We used intravital confocal microscopy in dorsal skinfold window chambers to demonstrate that FTY720 delivery promoted perivascular accumulation of non-classical monocytes during the acute inflammatory phase. Immunohistochemistry and flow cytometry were used to demonstrate that FTY720 promoted subsequent accumulation of CD206+ alternatively activated macrophages. Mouse models of ischemic and volumetric muscle injuries were treated with FTY720-loaded materials to investigate how FTY720-mediated immunomodulation impacts revascularization and tissue repair. During early wound healing, FTY720 enhanced the

density of CD31+ blood vessels and collagen within the defect area. In the later stages of repair, FTY720 improved muscle fiber regeneration and reduced fibrotic collagen deposition.

These findings indicate that biomaterials delivering immunomodulatory factors that target S1P receptors, such as FTY720, can enhance accumulation of pro-regenerative myeloid subsets. The significance of this work is demonstration that FTY720-mediated immunomodulation accelerates revascularization and enhances non-fibrotic muscle tissue repair after injury. While granulation tissue formation and its subsequent remodeling into mature extracellular matrix is crucial for the restoration of functional tissue in the volumetric void, a fibrotic response often progresses faster than a myogenic response [245]. Interventions that tune acute inflammatory responses may be more efficacious at enhancing repair than those that directly target parenchymal cells, although this requires further investigation.

In Aim 3, the progression of inflammation around protease-degradable PEG hydrogels functionalized with bioadhesive RGD peptides and vascular endothelial growth factor (VEGF) was explored using high-dimensional flow cytometry data paired with intravital image acquisition. Incorporation of RGD into PEG hydrogels did not impact the overall composition of innate immune cells adherent to the material surface after 1, 3, 7, and 14 days of subcutaneous implantation in mice. Hydrogel implantation significantly altered myeloid cell composition compared to uninjured tissue: during the acute inflammatory phase, monocytes and neutrophils were the primary cell type recruited to subcutaneously implanted hydrogels, while macrophages and dendritic cells predominated the later stages. Using intravital confocal microscopy, we visualized real-time myeloid cell

interactions with hydrogels implanted in dorsal skinfold window chambers. Myeloid cells moved at greater velocities around hydrogels compared to distal tissue, and velocity was further increased by RGD functionalization.

While synthetic hydrogels such as those derived from PEG are extensively used throughout the biomaterials field for cell and growth factor delivery, the innate immune response to engineered hydrogel matrices remains incompletely understood. The significance of this work is demonstration that degradable PEG hydrogels induce recruitment of anti-inflammatory myeloid populations without exogenous biomolecule delivery. Delivery of VEGF alters myeloid cell recruitment and further enhances accumulation of alternatively activated macrophages, which could have important implications for the clinical translation of pro-angiogenic therapies. Additionally, these findings shed light on how myeloid cells interpret signals presented by engineered hydrogels, included covalently-tethered VEGF and RGD presentation.

7.2 Engineering smarter immunoregenerative materials

In the current work, we explored how biomaterial-based delivery of FTY720 and VEGF impact myeloid cell recruitment into the surrounding tissue. This was motivated in part by the knowledge that monocyte subsets differentially expressed receptors for these chemokines, including S1PR3 and VEGFR2. Future work in this area should focus on the following topics: 1) Optimized delivery vehicle for FTY720 and 2) Delivery of other biomolecules to target monocyte/macrophage activities.

A PLGA thin film was selected for delivery of FTY720 because of our extensive experience with encapsulating sphingolipid signaling molecules and controlling release

kinetics *in vivo* [9, 53, 246]. Additionally, PLGA is approved by the FDA for various drug delivery and biomedical applications [247], and can be readily combined with other therapies such as in coatings on bone allografts [192]. However, other biomaterial delivery vehicles may provide enhanced support of vascularization and tissue repair, as well as greater control over the kinetics and mechanism of delivery. While PLGA promotes production of inflammatory mediators such as TNF-α by macrophages [248] and impairs early revascularization of muscle defects [72], we observed that non-classical monocytes and alternatively activated macrophages accumulate around degradable PEG hydrogels in the absence of additional biomolecules. To incorporate the small molecule FTY720 into a porous matrix, our lab has recently utilized heparin-PEG hydrogels loaded with albumin that sequesters FTY720 within the material [249]. The use of aqueous materials would also enable co-delivery of proteins and cells. An immediate future direction would be to explore how co-delivery of FTY720 and VEGF from hydrogel materials impacts vascular remodeling. These studies would be particularly interesting from both an immunology perspective, in which FTY720-mediated monocyte/macrophage recruitment could help stabilize VEGF-induced vascularization [23], and a vascular biology perspective, in which extensive literature has documented the role of sphingolipid signaling in vascular maturation through direct signaling on endothelial cells [250, 251].

Generally, biomolecules can regulate monocyte and macrophage function by modulating the following biological processes: 1) recruitment of monocytes and macrophages from blood or surrounding tissue, 2) monocyte/macrophage polarization state, and 3) macrophage proliferation. In addition to FTY720 or S1P, recruitment can be controlled by local delivery of chemokines that selectively target monocytes and

macrophages, such as MCP-1, SDF-1, or CX3CL1. For example, SDF-1 delivery from heparin-PEG hydrogels can selectively enhance recruitment of non-classical monocytes, but not classical monocytes, by exploiting their relative overexpression of CXCR4 [54]. Given our findings regarding the localization of $CX3CR1^{hi}$ cells near the endothelium, it would be extremely interesting to explore the effect of CX3CL1 (fractalkine) delivery on monocyte recruitment and tissue repair. Delivery of M-CSF, which promotes monocyte/macrophage proliferation, from PEG hydrogels enhances macrophage accumulation in the cornea and supports more mature vascularization than VEGF [143]. Release of polarizing cytokines such as IL-4 enhances M2 macrophage generation and promotes peripheral nerve regeneration [144]. While a strong therapeutic benefit on vascularization was not observed, sequential delivery of IFN-γ and IL-4 was used to guide the kinetics of macrophage polarization *in vivo* [57]. As more strategies emerge to target myeloid cells, it will be of interest for the field to identify which approaches (such as targeting recruitment, polarization, or proliferation) generate the most robust functional outcomes in the context of a specific therapeutic application.

7.3 Expansion of macrophage classifications

Biomaterial-mediated delivery of FTY720 promoted accumulation of CD206+ macrophages in injured skin and muscle, which correlated with tissue repair outcomes such as vascularization and muscle regrowth. While our studies were an informative first step, futures studies should focus on expanding our characterization of macrophage subsets. Given the extreme heterogeneity of macrophages and the many different factors to which they can respond, single surface markers are likely insufficient to accurately distinguish macrophage subsets. Incorporation of additional analysis techniques such as cytokine

production, transcription factor dependence, and gene expression would enable better assessment of the roles specific macrophages play in repair [210].

In addition to the phenotypic complexity presented by the wide range of polarizing cues, macrophages have different developmental origins, which can contribute to heterogeneity between organs [21]. While some macrophages are the descendants of circulating monocytes and are replenished at steady state and during inflammation by blood-derived monocytes [13, 26], other macrophages are derived from embryonic sources and self-maintain locally in tissues throughout adulthood in a manner analogous to stem cells [14, 27, 28]. Specifically, populations of tissue macrophages of the heart, lung, brain, skin, and liver are derived prenatally [14, 29-31]. Some injury contexts, such as T_H2-linked infection, can increase local tissue macrophage populations specifically through proliferation as opposed to monocyte recruitment from the blood [27].

Monocyte-derived alternatively activated macrophages have a unique gene expression profile compared to tissue resident alternatively activated macrophages, upregulating genes important during inflammation such as *Socs2, IL-31ra, Ccl17, Ch25h, Jag2,* and *Ccl22* [252]. Monocyte-derived alternatively activated macrophages also specifically drive the differentiation of CD4+ T cells to Foxp3+ regulatory T cells [252]. These observations could have particular importance for skeletal muscle repair, in which Foxp3+ regulatory T cells are crucial to healing [253]. While distinguishing monocyte-derived and tissue resident populations is challenging, this may be critical to understanding the phenotypic and functional diversity of macrophages.

7.4 Innate immune cell interactions with adaptive immunity

Most of the literature exploring host response to biomaterials has focused on innate immunity because these constitute the majority of cells that are recruited to implanted materials [85]. However, a role for adaptive immune responses to material implantation and tissue repair is being increasingly appreciated [97]. For example, implantation of alginate microspheres induces recruitment of B cells within the first week of implantation [223]. While macrophages are sufficient for the complete fibrotic response, macrophage paracrine factors are responsible for recruiting B cells that potentiated fibrosis [223]. Additionally, loss of T cells increased fibrosis, suggesting they may play a regulatory role in preventing implant fibrous encapsulation. Recent work indicated that implantation of scaffolds derived from extracellular matrix modify systemic immune homeostasis by inducing expression of IL-4 in lymph nodes [97]. Macrophage polarization towards a regenerative phenotype did not occur in the absence of T_H2 signals derived from T cells, which functionally impaired regeneration of volumetric muscle injury. Future work should more closely examine the interplay between the innate and adaptive branches of immunity in tissue repair and host responses to material implantation in order to better understand whether macrophages are absolutely required, or just participate, in these processes.

7.5 Extension of findings to other medical applications

The work presented in this thesis investigated myeloid cell trafficking during soft tissue injury and material implantation. Given the broad roles that myeloid cells play in injury and pathology, investigation of the presented immunomodulatory materials for treatment of other injuries and disease contexts is of great interest. We found differences

in the effects of FTY720 on myeloid cells between ischemic and traumatic injuries within the same tissue, so it is likely that different tissues undergoing injury will have unique immunological responses and needs.

Given the promising results we reported in the spinotrapezius arteriole ligation model, future studies could explore FTY720-mediated immunomodulation in the murine hindlimb ischemia model, which is the most common preclinical model of peripheral arterial disease (PAD). PAD is present in 12% of the adult population and represents a major risk factor for cardio- and cerebrovascular events [239]. Pro-angiogenic therapies have been largely unsuccessful in clinical translation in part due to the high doses required for effect and the pathophysiological side effects on the vasculature [229]. Delivery of factors such as FTY720 alone or in combination with VEGF in a mouse model of hindlimb ischemia would provide important insights into whether simultaneous targeting of the immune system can enhance the efficacy of therapies for treatment of vascular diseases.

Another application that would be extremely interesting to investigate modulation of monocyte/macrophage activities is during cancer progression. Non-classical monocytes have been shown to restrict cancer metastasis by ingesting tumor material [254], while tumor-associated macrophages display an alternatively activated phenotype that supports dysfunctional tumor angiogenesis and deactivation of anti-tumor adaptive immune responses [255]. Consequently, tumors represent a context where the anti-inflammatory activities of mononuclear phagocytes may be overactive. While biomaterials-based approaches to anti-cancer therapy have focused on nanoparticle-based drug delivery, particles have previously been used to modulate monocyte trafficking, with success in treatment of inflammatory diseases [127]. Perturbing monocyte and macrophage function

in the context of cancer could reveal unexpected functions that would guide the design of future therapies.

7.6 Conclusions

By investigating the recruitment of myeloid cells to implanted biomaterials, we revealed several key findings: 1) Non-classical monocytes differentiate into wound healing macrophages within cutaneous wounds, 2) Biomaterial-delivered FTY720 enhances wound healing macrophage accumulation, vascularization, and non-fibrotic repair during muscle injury, 3) Both PEG hydrogel implantation and RGD functionalization enhance the speed of myeloid cells migrating within skin injuries, and 4) Degradable PEG hydrogels promote accumulation of alternatively activated macrophages, which is further enhanced by VEGF delivery. These findings identify non-classical monocytes and alternatively activated macrophages as therapeutic targets for strategies attempting to overcome challenges facing biomaterials, including proper integration into host tissue, vascularization, and circumventing fibrosis. Taken together, these results provide previously unknown insight into the value of leveraging endogenous populations of pro-regenerative monocytes and macrophages during tissue repair.

REFERENCES

[1] Shi C, Pamer EG. Monocyte recruitment during infection and inflammation. Nature reviews Immunology. 2011;11:762-74.

[2] Godwin JW, Pinto AR, Rosenthal NA. Macrophages are required for adult salamander limb regeneration. Proc Natl Acad Sci U S A. 2013;110:9415-20.

[3] Li L, Yan B, Shi YQ, Zhang WQ, Wen ZL. Live imaging reveals differing roles of macrophages and neutrophils during zebrafish tail fin regeneration. The Journal of biological chemistry. 2012;287:25353-60.

[4] Arnold L, Henry A, Poron F, Baba-Amer Y, van Rooijen N, Plonquet A, et al. Inflammatory monocytes recruited after skeletal muscle injury switch into antiinflammatory macrophages to support myogenesis. J Exp Med. 2007;204:1057-69.

[5] van Amerongen MJ, Harmsen MC, van Rooijen N, Petersen AH, van Luyn MJ. Macrophage depletion impairs wound healing and increases left ventricular remodeling after myocardial injury in mice. Am J Pathol. 2007;170:818-29.

[6] Schlundt C, El Khassawna T, Serra A, Dienelt A, Wendler S, Schell H, et al. Macrophages in bone fracture healing: Their essential role in endochondral ossification. Bone. 2015.

[7] Bergmann CE, Hoefer IE, Meder B, Roth H, van Royen N, Breit SM, et al. Arteriogenesis depends on circulating monocytes and macrophage accumulation and is severely depressed in op/op mice. J Leukoc Biol. 2006;80:59-65.

[8] Nahrendorf M, Swirski FK, Aikawa E, Stangenberg L, Wurdinger T, Figueiredo JL, et al. The healing myocardium sequentially mobilizes two monocyte subsets with divergent and complementary functions. J Exp Med. 2007;204:3037-47.

[9] Awojoodu AO, Ogle ME, Sefcik LS, Bowers DT, Martin K, Brayman KL, et al. Sphingosine 1-phosphate receptor 3 regulates recruitment of anti-inflammatory monocytes to microvessels during implant arteriogenesis. Proc Natl Acad Sci U S A. 2013;110:13785-90.

[10] Mosser DM, Edwards JP. Exploring the full spectrum of macrophage activation. Nature reviews Immunology. 2008;8:958-69.

[11] Edwards JP, Zhang X, Frauwirth KA, Mosser DM. Biochemical and functional characterization of three activated macrophage populations. J Leukoc Biol. 2006;80:1298-307.

[12] Nassiri S, Zakeri I, Weingarten MS, Spiller KL. Relative Expression of Proinflammatory and Antiinflammatory Genes Reveals Differences between Healing and Nonhealing Human Chronic Diabetic Foot Ulcers. J Invest Dermatol. 2015;135:1700-3.

[13] van Furth R, Cohn ZA. The origin and kinetics of mononuclear phagocytes. The Journal of experimental medicine. 1968;128:415-35.

[14] Yona S, Kim KW, Wolf Y, Mildner A, Varol D, Breker M, et al. Fate mapping reveals origins and dynamics of monocytes and tissue macrophages under homeostasis. Immunity. 2013;38:79-91.

[15] Slaney CY, Toker A, La Flamme A, Backstrom BT, Harper JL. Naive blood monocytes suppress T-cell function. A possible mechanism for protection from autoimmunity. Immunol Cell Biol. 2011;89:7-13.

[16] Geissmann F, Jung S, Littman DR. Blood monocytes consist of two principal subsets with distinct migratory properties. Immunity. 2003;19:71-82.

[17] Goncalves R, Zhang X, Cohen H, Debrabant A, Mosser DM. Platelet activation attracts a subpopulation of effector monocytes to sites of Leishmania major infection. The Journal of experimental medicine. 2011;208:1253-65.

[18] Carlin LM, Stamatiades EG, Auffray C, Hanna RN, Glover L, Vizcay-Barrena G, et al. Nr4a1-dependent Ly6C(low) monocytes monitor endothelial cells and orchestrate their disposal. Cell. 2013;153:362-75.

[19] Dal-Secco D, Wang J, Zeng Z, Kolaczkowska E, Wong CH, Petri B, et al. A dynamic spectrum of monocytes arising from the in situ reprogramming of CCR2+ monocytes at a site of sterile injury. The Journal of experimental medicine. 2015;212:447-56.

[20] Nahrendorf M, Pittet MJ, Swirski FK. Monocytes: protagonists of infarct inflammation and repair after myocardial infarction. Circulation. 2010;121:2437-45.

[21] Gautier EL, Shay T, Miller J, Greter M, Jakubzick C, Ivanov S, et al. Gene-expression profiles and transcriptional regulatory pathways that underlie the identity and diversity of mouse tissue macrophages. Nat Immunol. 2012;13:1118-28.

[22] Wu AC, Raggatt LJ, Alexander KA, Pettit AR. Unraveling macrophage contributions to bone repair. Bonekey Rep. 2013;2:373.

[23] Fantin A, Vieira JM, Gestri G, Denti L, Schwarz Q, Prykhozhij S, et al. Tissue macrophages act as cellular chaperones for vascular anastomosis downstream of VEGF-mediated endothelial tip cell induction. Blood. 2010;116:829-40.

[24] Lavine KJ, Epelman S, Uchida K, Weber KJ, Nichols CG, Schilling JD, et al. Distinct macrophage lineages contribute to disparate patterns of cardiac recovery and remodeling in the neonatal and adult heart. Proc Natl Acad Sci U S A. 2014;111:16029-34.

[25] Lu H, Huang D, Saederup N, Charo IF, Ransohoff RM, Zhou L. Macrophages recruited via CCR2 produce insulin-like growth factor-1 to repair acute skeletal muscle injury. FASEB journal : official publication of the Federation of American Societies for Experimental Biology. 2011;25:358-69.

[26] Ginhoux F, Schultze JL, Murray PJ, Ochando J, Biswas SK. New insights into the multidimensional concept of macrophage ontogeny, activation and function. Nature immunology. 2016;17:34-40.

[27] Jenkins SJ, Ruckerl D, Cook PC, Jones LH, Finkelman FD, van Rooijen N, et al. Local macrophage proliferation, rather than recruitment from the blood, is a signature of TH2 inflammation. Science. 2011;332:1284-8.

[28] Hashimoto D, Chow A, Noizat C, Teo P, Beasley MB, Leboeuf M, et al. Tissue-resident macrophages self-maintain locally throughout adult life with minimal contribution from circulating monocytes. Immunity. 2013;38:792-804.

[29] Epelman S, Lavine KJ, Beaudin AE, Sojka DK, Carrero JA, Calderon B, et al. Embryonic and adult-derived resident cardiac macrophages are maintained through distinct mechanisms at steady state and during inflammation. Immunity. 2014;40:91-104.

[30] Hoeffel G, Chen J, Lavin Y, Low D, Almeida FF, See P, et al. C-Myb(+) erythro-myeloid progenitor-derived fetal monocytes give rise to adult tissue-resident macrophages. Immunity. 2015;42:665-78.

[31] Gomez Perdiguero E, Klapproth K, Schulz C, Busch K, Azzoni E, Crozet L, et al. Tissue-resident macrophages originate from yolk-sac-derived erythro-myeloid progenitors. Nature. 2015;518:547-51.

[32] Spiller KL, Wrona EA, Romero-Torres S, Pallotta I, Graney PL, Witherel CE, et al. Differential Gene Expression in Human, Murine, and Cell Line-derived Macrophages upon Polarization. Exp Cell Res. 2015.

[33] Gordon S, Taylor PR. Monocyte and macrophage heterogeneity. Nature reviews Immunology. 2005;5:953-64.

[34] Lavin Y, Winter D, Blecher-Gonen R, David E, Keren-Shaul H, Merad M, et al. Tissue-resident macrophage enhancer landscapes are shaped by the local microenvironment. Cell. 2014;159:1312-26.

[35] Passlick B, Flieger D, Ziegler-Heitbrock HW. Identification and characterization of a novel monocyte subpopulation in human peripheral blood. Blood. 1989;74:2527-34.

[36] Yrlid U, Jenkins CD, MacPherson GG. Relationships between distinct blood monocyte subsets and migrating intestinal lymph dendritic cells in vivo under steady-state conditions. Journal of immunology. 2006;176:4155-62.

[37] Sunderkotter C, Nikolic T, Dillon MJ, Van Rooijen N, Stehling M, Drevets DA, et al. Subpopulations of mouse blood monocytes differ in maturation stage and inflammatory response. Journal of immunology. 2004;172:4410-7.

[38] Hettinger J, Richards DM, Hansson J, Barra MM, Joschko AC, Krijgsveld J, et al. Origin of monocytes and macrophages in a committed progenitor. Nature immunology. 2013;14:821-30.

[39] Varol C, Landsman L, Fogg DK, Greenshtein L, Gildor B, Margalit R, et al. Monocytes give rise to mucosal, but not splenic, conventional dendritic cells. The Journal of experimental medicine. 2007;204:171-80.

[40] Ruparelia N, Godec J, Lee R, Chai JT, Dall'Armellina E, McAndrew D, et al. Acute myocardial infarction activates distinct inflammation and proliferation pathways in circulating monocytes, prior to recruitment, and identified through conserved transcriptional responses in mice and humans. Eur Heart J. 2015;36:1923-34.

[41] Spiller KL, Anfang RR, Spiller KJ, Ng J, Nakazawa KR, Daulton JW, et al. The role of macrophage phenotype in vascularization of tissue engineering scaffolds. Biomaterials. 2014;35:4477-88.

[42] Mantovani A, Sica A, Sozzani S, Allavena P, Vecchi A, Locati M. The chemokine system in diverse forms of macrophage activation and polarization. Trends Immunol. 2004;25:677-86.

[43] Martinez FO, Gordon S, Locati M, Mantovani A. Transcriptional profiling of the human monocyte-to-macrophage differentiation and polarization: new molecules and patterns of gene expression. Journal of immunology. 2006;177:7303-11.

[44] Sironi M, Martinez FO, D'Ambrosio D, Gattorno M, Polentarutti N, Locati M, et al. Differential regulation of chemokine production by Fcgamma receptor engagement in human monocytes: association of CCL1 with a distinct form of M2 monocyte activation (M2b, Type 2). J Leukoc Biol. 2006;80:342-9.

[45] Knipper JA, Willenborg S, Brinckmann J, Bloch W, Maass T, Wagener R, et al. Interleukin-4 Receptor alpha Signaling in Myeloid Cells Controls Collagen Fibril Assembly in Skin Repair. Immunity. 2015;43:803-16.

[46] Swirski FK, Nahrendorf M, Etzrodt M, Wildgruber M, Cortez-Retamozo V, Panizzi P, et al. Identification of splenic reservoir monocytes and their deployment to inflammatory sites. Science. 2009;325:612-6.

[47] Rzeniewicz K, Newe A, Rey Gallardo A, Davies J, Holt MR, Patel A, et al. L-selectin shedding is activated specifically within transmigrating pseudopods of monocytes to regulate cell polarity in vitro. Proceedings of the National Academy of Sciences of the United States of America. 2015;112:E1461-70.

[48] Collison JL, Carlin LM, Eichmann M, Geissmann F, Peakman M. Heterogeneity in the Locomotory Behavior of Human Monocyte Subsets over Human Vascular Endothelium In Vitro. Journal of immunology. 2015;195:1162-70.

[49] Auffray C, Fogg D, Garfa M, Elain G, Join-Lambert O, Kayal S, et al. Monitoring of blood vessels and tissues by a population of monocytes with patrolling behavior. Science. 2007;317:666-70.

[50] Tacke F, Alvarez D, Kaplan TJ, Jakubzick C, Spanbroek R, Llodra J, et al. Monocyte subsets differentially employ CCR2, CCR5, and CX3CR1 to accumulate within atherosclerotic plaques. J Clin Invest. 2007;117:185-94.

[51] Hanna RN, Carlin LM, Hubbeling HG, Nackiewicz D, Green AM, Punt JA, et al. The transcription factor NR4A1 (Nur77) controls bone marrow differentiation and the survival of Ly6C- monocytes. Nature immunology. 2011;12:778-85.

[52] Ancuta P, Rao R, Moses A, Mehle A, Shaw SK, Luscinskas FW, et al. Fractalkine preferentially mediates arrest and migration of CD16+ monocytes. The Journal of experimental medicine. 2003;197:1701-7.

[53] Ogle ME, Sefcik LS, Awojoodu AO, Chiappa NF, Lynch K, Peirce-Cottler S, et al. Engineering in vivo gradients of sphingosine-1-phosphate receptor ligands for localized microvascular remodeling and inflammatory cell positioning. Acta biomaterialia. 2014;10:4704-14.

[54] Krieger JR, Ogle ME, McFaline-Figueroa J, Segar CE, Temenoff JS, Botchwey EA. Spatially localized recruitment of anti-inflammatory monocytes by SDF-1alpha-releasing hydrogels enhances microvascular network remodeling. Biomaterials. 2016;77:280-90.

[55] Grunewald M, Avraham I, Dor Y, Bachar-Lustig E, Itin A, Jung S, et al. VEGF-induced adult neovascularization: recruitment, retention, and role of accessory cells. Cell. 2006;124:175-89.

[56] Avraham-Davidi I, Yona S, Grunewald M, Landsman L, Cochain C, Silvestre JS, et al. On-site education of VEGF-recruited monocytes improves their performance as angiogenic and arteriogenic accessory cells. J Exp Med. 2013;210:2611-25.

[57] Spiller KL, Nassiri S, Witherel CE, Anfang RR, Ng J, Nakazawa KR, et al. Sequential delivery of immunomodulatory cytokines to facilitate the M1-to-M2 transition of macrophages and enhance vascularization of bone scaffolds. Biomaterials. 2015;37:194-207.

[58] Crane MJ, Daley JM, van Houtte O, Brancato SK, Henry WL, Jr., Albina JE. The monocyte to macrophage transition in the murine sterile wound. PloS one. 2014;9:e86660.

[59] Misharin AV, Cuda CM, Saber R, Turner JD, Gierut AK, Haines GK, 3rd, et al. Nonclassical Ly6C(-) monocytes drive the development of inflammatory arthritis in mice. Cell Rep. 2014;9:591-604.

[60] Griffith CK, Miller C, Sainson RC, Calvert JW, Jeon NL, Hughes CC, et al. Diffusion limits of an in vitro thick prevascularized tissue. Tissue Eng. 2005;11:257-66.

[61] Lee TT, Garcia JR, Paez JI, Singh A, Phelps EA, Weis S, et al. Light-triggered in vivo activation of adhesive peptides regulates cell adhesion, inflammation and vascularization of biomaterials. Nat Mater. 2015;14:352-60.

[62] Nickerson MM, Burke CW, Meisner JK, Shuptrine CW, Song J, Price RJ. Capillary arterialization requires the bone-marrow-derived cell (BMC)-specific expression of chemokine (C-C motif) receptor-2, but BMCs do not transdifferentiate into microvascular smooth muscle. Angiogenesis. 2009;12:355-63.

[63] Ito WD, Arras M, Winkler B, Scholz D, Schaper J, Schaper W. Monocyte chemotactic protein-1 increases collateral and peripheral conductance after femoral artery occlusion. Circulation research. 1997;80:829-37.

[64] Hoefer IE, van Royen N, Rectenwald JE, Deindl E, Hua J, Jost M, et al. Arteriogenesis proceeds via ICAM-1/Mac-1- mediated mechanisms. Circulation research. 2004;94:1179-85.

[65] Heil M, Ziegelhoeffer T, Pipp F, Kostin S, Martin S, Clauss M, et al. Blood monocyte concentration is critical for enhancement of collateral artery growth. Am J Physiol Heart Circ Physiol. 2002;283:H2411-9.

[66] Melgar-Lesmes P, Edelman ER. Monocyte-endothelial cell interactions in the regulation of vascular sprouting and liver regeneration in mouse. J Hepatol. 2015;63:917-25.

[67] Heil M, Ziegelhoeffer T, Wagner S, Fernandez B, Helisch A, Martin S, et al. Collateral artery growth (arteriogenesis) after experimental arterial occlusion is impaired in mice lacking CC-chemokine receptor-2. Circulation research. 2004;94:671-7.

[68] Moldovan NI, Goldschmidt-Clermont PJ, Parker-Thornburg J, Shapiro SD, Kolattukudy PE. Contribution of monocytes/macrophages to compensatory neovascularization: the drilling of metalloelastase-positive tunnels in ischemic myocardium. Circulation research. 2000;87:378-84.

[69] Willenborg S, Lucas T, van Loo G, Knipper JA, Krieg T, Haase I, et al. CCR2 recruits an inflammatory macrophage subpopulation critical for angiogenesis in tissue repair. Blood. 2012;120:613-25.

[70] Madsen DH, Leonard D, Masedunskas A, Moyer A, Jurgensen HJ, Peters DE, et al. M2-like macrophages are responsible for collagen degradation through a mannose receptor-mediated pathway. J Cell Biol. 2013;202:951-66.

[71] Deng B, Wehling-Henricks M, Villalta SA, Wang Y, Tidball JG. IL-10 triggers changes in macrophage phenotype that promote muscle growth and regeneration. Journal of immunology. 2012;189:3669-80.

[72] San Emeterio CL, Olingy CE, Chu Y, Botchwey EA. Selective recruitment of non-classical monocytes promotes skeletal muscle repair. Biomaterials. 2017;117:32-43.

[73] Saclier M, Yacoub-Youssef H, Mackey AL, Arnold L, Ardjoune H, Magnan M, et al. Differentially activated macrophages orchestrate myogenic precursor cell fate during human skeletal muscle regeneration. Stem cells. 2013;31:384-96.

[74] Sinder BP, Pettit AR, McCauley LK. Macrophages: Their Emerging Roles in Bone. J Bone Miner Res. 2015.

[75] Chang MK, Raggatt LJ, Alexander KA, Kuliwaba JS, Fazzalari NL, Schroder K, et al. Osteal tissue macrophages are intercalated throughout human and mouse bone lining tissues and regulate osteoblast function in vitro and in vivo. J Immunol. 2008;181:1232-44.

[76] Winkler IG, Sims NA, Pettit AR, Barbier V, Nowlan B, Helwani F, et al. Bone marrow macrophages maintain hematopoietic stem cell (HSC) niches and their depletion mobilizes HSCs. Blood. 2010;116:4815-28.

[77] Cho SW, Soki FN, Koh AJ, Eber MR, Entezami P, Park SI, et al. Osteal macrophages support physiologic skeletal remodeling and anabolic actions of parathyroid hormone in bone. Proc Natl Acad Sci U S A. 2014;111:1545-50.

[78] Vi L, Baht GS, Whetstone H, Ng A, Wei Q, Poon R, et al. Macrophages promote osteoblastic differentiation in-vivo: implications in fracture repair and bone homeostasis. J Bone Miner Res. 2015;30:1090-102.

[79] Champagne CM, Takebe J, Offenbacher S, Cooper LF. Macrophage cell lines produce osteoinductive signals that include bone morphogenetic protein-2. Bone. 2002;30:26-31.

[80] Xie H, Cui Z, Wang L, Xia Z, Hu Y, Xian L, et al. PDGF-BB secreted by preosteoclasts induces angiogenesis during coupling with osteogenesis. Nat Med. 2014;20:1270-8.

[81] Xing Z, Lu C, Hu D, Yu YY, Wang X, Colnot C, et al. Multiple roles for CCR2 during fracture healing. Dis Model Mech. 2010;3:451-8.

[82] Raggatt LJ, Wullschleger ME, Alexander KA, Wu AC, Millard SM, Kaur S, et al. Fracture healing via periosteal callus formation requires macrophages for both initiation and progression of early endochondral ossification. Am J Pathol. 2014;184:3192-204.

[83] Alexander KA, Chang MK, Maylin ER, Kohler T, Muller R, Wu AC, et al. Osteal macrophages promote in vivo intramembranous bone healing in a mouse tibial injury model. J Bone Miner Res. 2011;26:1517-32.

[84] Goodman SB. Wear particles, periprosthetic osteolysis and the immune system. Biomaterials. 2007;28:5044-8.

[85] Anderson JM, Rodriguez A, Chang DT. Foreign body reaction to biomaterials. Semin Immunol. 2008;20:86-100.

[86] Ogle ME, Segar CE, Sridhar S, Botchwey EA. Monocytes and macrophages in tissue repair: Implications for immunoregenerative biomaterial design. Exp Biol Med (Maywood). 2016;241:1084-97.

[87] Nygren H, Tengvall P, Lundstrom I. The initial reactions of TiO2 with blood. J Biomed Mater Res. 1997;34:487-92.

[88] Wilson CJ, Clegg RE, Leavesley DI, Pearcy MJ. Mediation of biomaterial-cell interactions by adsorbed proteins: a review. Tissue Eng. 2005;11:1-18.

[89] Swartzlander MD, Barnes CA, Blakney AK, Kaar JL, Kyriakides TR, Bryant SJ. Linking the foreign body response and protein adsorption to PEG-based hydrogels using proteomics. Biomaterials. 2015;41:26-36.

[90] Tang L, Jennings TA, Eaton JW. Mast cells mediate acute inflammatory responses to implanted biomaterials. Proc Natl Acad Sci U S A. 1998;95:8841-6.

[91] Jhunjhunwala S, Aresta-DaSilva S, Tang K, Alvarez D, Webber MJ, Tang BC, et al. Neutrophil Responses to Sterile Implant Materials. PLoS One. 2015;10:e0137550.

[92] Soehnlein O, Lindbom L. Phagocyte partnership during the onset and resolution of inflammation. Nat Rev Immunol. 2010;10:427-39.

[93] Patel JD, Krupka T, Anderson JM. iNOS-mediated generation of reactive oxygen and nitrogen species by biomaterial-adherent neutrophils. J Biomed Mater Res A. 2007;80:381-90.

[94] Taekema-Roelvink ME, Kooten C, Kooij SV, Heemskerk E, Daha MR. Proteinase 3 enhances endothelial monocyte chemoattractant protein-1 production and induces increased adhesion of neutrophils to endothelial cells by upregulating intercellular cell adhesion molecule-1. J Am Soc Nephrol. 2001;12:932-40.

[95] Geissmann F, Manz MG, Jung S, Sieweke MH, Merad M, Ley K. Development of monocytes, macrophages, and dendritic cells. Science. 2010;327:656-61.

[96] Fadok VA, Bratton DL, Konowal A, Freed PW, Westcott JY, Henson PM. Macrophages that have ingested apoptotic cells in vitro inhibit proinflammatory cytokine production through autocrine/paracrine mechanisms involving TGF-beta, PGE2, and PAF. J Clin Invest. 1998;101:890-8.

[97] Sadtler K, Estrellas K, Allen BW, Wolf MT, Fan H, Tam AJ, et al. Developing a pro-regenerative biomaterial scaffold microenvironment requires T helper 2 cells. Science. 2016;352:366-70.

[98] DeFife KM, Jenney CR, McNally AK, Colton E, Anderson JM. Interleukin-13 induces human monocyte/macrophage fusion and macrophage mannose receptor expression. J Immunol. 1997;158:3385-90.

[99] Hernandez-Pando R, Bornstein QL, Aguilar Leon D, Orozco EH, Madrigal VK, Martinez Cordero E. Inflammatory cytokine production by immunological and foreign body multinucleated giant cells. Immunology. 2000;100:352-8.

[100] McNally AK, Anderson JM. Complement C3 participation in monocyte adhesion to different surfaces. Proc Natl Acad Sci U S A. 1994;91:10119-23.

[101] Franz S, Rammelt S, Scharnweber D, Simon JC. Immune responses to implants - a review of the implications for the design of immunomodulatory biomaterials. Biomaterials. 2011;32:6692-709.

[102] Berton G, Lowell CA. Integrin signalling in neutrophils and macrophages. Cell Signal. 1999;11:621-35.

[103] Chan JR, Hyduk SJ, Cybulsky MI. Chemoattractants induce a rapid and transient upregulation of monocyte alpha4 integrin affinity for vascular cell adhesion molecule 1 which mediates arrest: an early step in the process of emigration. J Exp Med. 2001;193:1149-58.

[104] Sumagin R, Prizant H, Lomakina E, Waugh RE, Sarelius IH. LFA-1 and Mac-1 define characteristically different intralumenal crawling and emigration patterns for monocytes and neutrophils in situ. J Immunol. 2010;185:7057-66.

[105] Abram CL, Lowell CA. The ins and outs of leukocyte integrin signaling. Annu Rev Immunol. 2009;27:339-62.

[106] Zhang Z, Vuori K, Reed JC, Ruoslahti E. The alpha 5 beta 1 integrin supports survival of cells on fibronectin and up-regulates Bcl-2 expression. Proc Natl Acad Sci U S A. 1995;92:6161-5.

[107] Keselowsky BG, Collard DM, Garcia AJ. Surface chemistry modulates fibronectin conformation and directs integrin binding and specificity to control cell adhesion. J Biomed Mater Res A. 2003;66:247-59.

[108] Lammermann T, Bader BL, Monkley SJ, Worbs T, Wedlich-Soldner R, Hirsch K, et al. Rapid leukocyte migration by integrin-independent flowing and squeezing. Nature. 2008;453:51-5.

[109] Zaveri TD, Lewis JS, Dolgova NV, Clare-Salzler MJ, Keselowsky BG. Integrin-directed modulation of macrophage responses to biomaterials. Biomaterials. 2014;35:3504-15.

[110] McNally AK, Anderson JM. Beta1 and beta2 integrins mediate adhesion during macrophage fusion and multinucleated foreign body giant cell formation. Am J Pathol. 2002;160:621-30.

[111] Podolnikova NP, Kushchayeva YS, Wu Y, Faust J, Ugarova TP. The Role of Integrins alphaMbeta2 (Mac-1, CD11b/CD18) and alphaDbeta2 (CD11d/CD18) in Macrophage Fusion. Am J Pathol. 2016;186:2105-16.

[112] Reid B, Gibson M, Singh A, Taube J, Furlong C, Murcia M, et al. PEG hydrogel degradation and the role of the surrounding tissue environment. J Tissue Eng Regen Med. 2015;9:315-8.

[113] Rettig L, Haen SP, Bittermann AG, von Boehmer L, Curioni A, Kramer SD, et al. Particle size and activation threshold: a new dimension of danger signaling. Blood. 2010;115:4533-41.

[114] Veiseh O, Doloff JC, Ma M, Vegas AJ, Tam HH, Bader AR, et al. Size- and shape-dependent foreign body immune response to materials implanted in rodents and non-human primates. Nat Mater. 2015;14:643-51.

[115] Tabata Y, Ikada Y. Effect of the size and surface charge of polymer microspheres on their phagocytosis by macrophage. Biomaterials. 1988;9:356-62.

[116] Champion JA, Mitragotri S. Role of target geometry in phagocytosis. Proceedings of the National Academy of Sciences of the United States of America. 2006;103:4930-4.

[117] Underhill DM, Goodridge HS. Information processing during phagocytosis. Nature reviews Immunology. 2012;12:492-502.

[118] Padmanabhan J, Kinser ER, Stalter MA, Duncan-Lewis C, Balestrini JL, Sawyer AJ, et al. Engineering cellular response using nanopatterned bulk metallic glass. ACS Nano. 2014;8:4366-75.

[119] Chen S, Jones JA, Xu Y, Low HY, Anderson JM, Leong KW. Characterization of topographical effects on macrophage behavior in a foreign body response model. Biomaterials. 2010;31:3479-91.

[120] Garg K, Pullen NA, Oskeritzian CA, Ryan JJ, Bowlin GL. Macrophage functional polarization (M1/M2) in response to varying fiber and pore dimensions of electrospun scaffolds. Biomaterials. 2013;34:4439-51.

[121] Sanders JE, Stiles CE, Hayes CL. Tissue response to single-polymer fibers of varying diameters: evaluation of fibrous encapsulation and macrophage density. J Biomed Mater Res. 2000;52:231-7.

[122] Cao H, McHugh K, Chew SY, Anderson JM. The topographical effect of electrospun nanofibrous scaffolds on the in vivo and in vitro foreign body reaction. J Biomed Mater Res A. 2010;93:1151-9.

[123] McWhorter FY, Wang T, Nguyen P, Chung T, Liu WF. Modulation of macrophage phenotype by cell shape. Proc Natl Acad Sci U S A. 2013;110:17253-8.

[124] Feng B, Jinkang Z, Zhen W, Jianxi L, Jiang C, Jian L, et al. The effect of pore size on tissue ingrowth and neovascularization in porous bioceramics of controlled architecture in vivo. Biomed Mater. 2011;6:015007.

[125] Madden LR, Mortisen DJ, Sussman EM, Dupras SK, Fugate JA, Cuy JL, et al. Proangiogenic scaffolds as functional templates for cardiac tissue engineering. Proc Natl Acad Sci U S A. 2010;107:15211-6.

[126] Bota PC, Collie AM, Puolakkainen P, Vernon RB, Sage EH, Ratner BD, et al. Biomaterial topography alters healing in vivo and monocyte/macrophage activation in vitro. J Biomed Mater Res A. 2010;95:649-57.

[127] Getts DR, Terry RL, Getts MT, Deffrasnes C, Muller M, van Vreden C, et al. Therapeutic inflammatory monocyte modulation using immune-modifying microparticles. Sci Transl Med. 2014;6:219ra7.

[128] Brodbeck WG, Patel J, Voskerician G, Christenson E, Shive MS, Nakayama Y, et al. Biomaterial adherent macrophage apoptosis is increased by hydrophilic and anionic substrates in vivo. Proceedings of the National Academy of Sciences of the United States of America. 2002;99:10287-92.

[129] Gref R, Luck M, Quellec P, Marchand M, Dellacherie E, Harnisch S, et al. 'Stealth' corona-core nanoparticles surface modified by polyethylene glycol (PEG): influences of the corona (PEG chain length and surface density) and of the core composition on phagocytic uptake and plasma protein adsorption. Colloids Surf B Biointerfaces. 2000;18:301-13.

[130] Mutsaers SE, Papadimitriou JM. Surface charge of macrophages and their interaction with charged particles. J Leukoc Biol. 1988;44:17-26.

[131] Patel NR, Bole M, Chen C, Hardin CC, Kho AT, Mih J, et al. Cell elasticity determines macrophage function. PLoS One. 2012;7:e41024.

[132] Blakney AK, Swartzlander MD, Bryant SJ. The effects of substrate stiffness on the in vitro activation of macrophages and in vivo host response to poly(ethylene glycol)-based hydrogels. J Biomed Mater Res A. 2012;100:1375-86.

[133] Fereol S, Fodil R, Labat B, Galiacy S, Laurent VM, Louis B, et al. Sensitivity of alveolar macrophages to substrate mechanical and adhesive properties. Cell Motil Cytoskeleton. 2006;63:321-40.

[134] Riedel T, Riedelova-Reicheltova Z, Majek P, Rodriguez-Emmenegger C, Houska M, Dyr JE, et al. Complete identification of proteins responsible for human blood plasma fouling on poly(ethylene glycol)-based surfaces. Langmuir. 2013;29:3388-97.

[135] Lynn AD, Bryant SJ. Phenotypic changes in bone marrow-derived murine macrophages cultured on PEG-based hydrogels activated or not by lipopolysaccharide. Acta Biomater. 2011;7:123-32.

[136] Lynn AD, Kyriakides TR, Bryant SJ. Characterization of the in vitro macrophage response and in vivo host response to poly(ethylene glycol)-based hydrogels. J Biomed Mater Res A. 2010;93:941-53.

[137] Wolf MT, Dearth CL, Ranallo CA, LoPresti ST, Carey LE, Daly KA, et al. Macrophage polarization in response to ECM coated polypropylene mesh. Biomaterials. 2014;35:6838-49.

[138] Lutolf MP, Weber FE, Schmoekel HG, Schense JC, Kohler T, Muller R, et al. Repair of bone defects using synthetic mimetics of collagenous extracellular matrices. Nat Biotechnol. 2003;21:513-8.

[139] Patterson J, Hubbell JA. SPARC-derived protease substrates to enhance the plasmin sensitivity of molecularly engineered PEG hydrogels. Biomaterials. 2011;32:1301-10.

[140] Phelps EA, Headen DM, Taylor WR, Thule PM, Garcia AJ. Vasculogenic bio-synthetic hydrogel for enhancement of pancreatic islet engraftment and function in type 1 diabetes. Biomaterials. 2013;34:4602-11.

[141] Hoffman AS. Stimuli-responsive polymers: biomedical applications and challenges for clinical translation. Adv Drug Deliv Rev. 2013;65:10-6.

[142] Jay SM, Shepherd BR, Andrejecsk JW, Kyriakides TR, Pober JS, Saltzman WM. Dual delivery of VEGF and MCP-1 to support endothelial cell transplantation for therapeutic vascularization. Biomaterials. 2010;31:3054-62.

[143] Hsu CW, Poche RA, Saik JE, Ali S, Wang S, Yosef N, et al. Improved Angiogenesis in Response to Localized Delivery of Macrophage-Recruiting Molecules. PLoS One. 2015;10:e0131643.

[144] Mokarram N, Merchant A, Mukhatyar V, Patel G, Bellamkonda RV. Effect of modulating macrophage phenotype on peripheral nerve repair. Biomaterials. 2012;33:8793-801.

[145] Reeves AR, Spiller KL, Freytes DO, Vunjak-Novakovic G, Kaplan DL. Controlled release of cytokines using silk-biomaterials for macrophage polarization. Biomaterials. 2015;73:272-83.

[146] Jenkins SJ, Ruckerl D, Thomas GD, Hewitson JP, Duncan S, Brombacher F, et al. IL-4 directly signals tissue-resident macrophages to proliferate beyond homeostatic levels controlled by CSF-1. The Journal of experimental medicine. 2013;210:2477-91.

[147] Wynn TA, Vannella KM. Macrophages in Tissue Repair, Regeneration, and Fibrosis. Immunity. 2016;44:450-62.

[148] Ginhoux F, Jung S. Monocytes and macrophages: developmental pathways and tissue homeostasis. Nature reviews Immunology. 2014;14:392-404.

[149] Qu C, Edwards EW, Tacke F, Angeli V, Llodra J, Sanchez-Schmitz G, et al. Role of CCR8 and other chemokine pathways in the migration of monocyte-derived dendritic cells to lymph nodes. J Exp Med. 2004;200:1231-41.

[150] Wong KL, Tai JJ, Wong WC, Han H, Sem X, Yeap WH, et al. Gene expression profiling reveals the defining features of the classical, intermediate, and nonclassical human monocyte subsets. Blood. 2011;118:e16-31.

[151] Jakubzick C, Gautier EL, Gibbings SL, Sojka DK, Schlitzer A, Johnson TE, et al. Minimal differentiation of classical monocytes as they survey steady-state tissues and transport antigen to lymph nodes. Immunity. 2013;39:599-610.

[152] Zigmond E, Varol C, Farache J, Elmaliah E, Satpathy AT, Friedlander G, et al. Ly6C hi monocytes in the inflamed colon give rise to proinflammatory effector cells and migratory antigen-presenting cells. Immunity. 2012;37:1076-90.

[153] Okuno Y, Nakamura-Ishizu A, Kishi K, Suda T, Kubota Y. Bone marrow-derived cells serve as proangiogenic macrophages but not endothelial cells in wound healing. Blood. 2011;117:5264-72.

[154] Takeda Y, Costa S, Delamarre E, Roncal C, Leite de Oliveira R, Squadrito ML, et al. Macrophage skewing by Phd2 haplodeficiency prevents ischaemia by inducing arteriogenesis. Nature. 2011;479:122-6.

[155] Kigerl KA, Gensel JC, Ankeny DP, Alexander JK, Donnelly DJ, Popovich PG. Identification of two distinct macrophage subsets with divergent effects causing either neurotoxicity or regeneration in the injured mouse spinal cord. The Journal of neuroscience : the official journal of the Society for Neuroscience. 2009;29:13435-44.

[156] Ramachandran P, Pellicoro A, Vernon MA, Boulter L, Aucott RL, Ali A, et al. Differential Ly-6C expression identifies the recruited macrophage phenotype, which orchestrates the regression of murine liver fibrosis. Proc Natl Acad Sci U S A. 2012;109:E3186-95.

[157] Girgis NM, Gundra UM, Ward LN, Cabrera M, Frevert U, Loke P. Ly6C(high) monocytes become alternatively activated macrophages in schistosome granulomas with help from CD4+ cells. PLoS pathogens. 2014;10:e1004080.

[158] Denney L, Kok WL, Cole SL, Sanderson S, McMichael AJ, Ho LP. Activation of invariant NKT cells in early phase of experimental autoimmune encephalomyelitis results in differentiation of Ly6Chi inflammatory monocyte to M2 macrophages and improved outcome. J Immunol. 2012;189:551-7.

[159] Ogle ME, Sefcik LS, Awojoodu AO, Chiappa NF, Lynch K, Peirce-Cottler S, et al. Engineering in vivo gradients of sphingosine-1-phosphate receptor ligands for localized microvascular remodeling and inflammatory cell positioning. Acta biomaterialia. 2014.

[160] Tacke F, Ginhoux F, Jakubzick C, van Rooijen N, Merad M, Randolph GJ. Immature monocytes acquire antigens from other cells in the bone marrow and present them to T cells after maturing in the periphery. J Exp Med. 2006;203:583-97.

[161] Potteaux S, Gautier EL, Hutchison SB, van Rooijen N, Rader DJ, Thomas MJ, et al. Suppressed monocyte recruitment drives macrophage removal from atherosclerotic plaques of Apoe-/- mice during disease regression. J Clin Invest. 2011;121:2025-36.

[162] Shook B, Xiao E, Kumamoto Y, Iwasaki A, Horsley V. CD301b+ Macrophages Are Essential for Effective Skin Wound Healing. Journal of Investigative Dermatology. 2016;136:1885-91.

[163] Shook B, Xiao E, Kumamoto Y, Iwasaki A, Horsley V. CD301b+ Macrophages Are Essential for Effective Skin Wound Healing. J Invest Dermatol. 2016;136:1885-91.

[164] Leuschner F, Rauch PJ, Ueno T, Gorbatov R, Marinelli B, Lee WW, et al. Rapid monocyte kinetics in acute myocardial infarction are sustained by extramedullary monocytopoiesis. J Exp Med. 2012;209:123-37.

[165] Stein M, Keshav S, Harris N, Gordon S. Interleukin 4 potently enhances murine macrophage mannose receptor activity: a marker of alternative immunologic macrophage activation. The Journal of experimental medicine. 1992;176:287-92.

[166] Bao P, Kodra A, Tomic-Canic M, Golinko MS, Ehrlich HP, Brem H. The role of vascular endothelial growth factor in wound healing. J Surg Res. 2009;153:347-58.

[167] Cyster JG. Chemokines, sphingosine-1-phosphate, and cell migration in secondary lymphoid organs. Annu Rev Immunol. 2005;23:127-59.

[168] Barleon B, Sozzani S, Zhou D, Weich HA, Mantovani A, Marme D. Migration of human monocytes in response to vascular endothelial growth factor (VEGF) is mediated via the VEGF receptor flt-1. Blood. 1996;87:3336-43.

[169] Briquez PS, Clegg LE, Martino MM, Mac Gabhann F, Hubbell JA. Design principles for therapeutic angiogenic materials. Nat Rev Mater. 2016;1.

[170] Forbes SJ, Rosenthal N. Preparing the ground for tissue regeneration: from mechanism to therapy. Nat Med. 2014;20:857-69.

[171] Aurora AB, Porrello ER, Tan W, Mahmoud AI, Hill JA, Bassel-Duby R, et al. Macrophages are required for neonatal heart regeneration. The Journal of clinical investigation. 2014;124:1382-92.

[172] Jaipersad AS, Lip GY, Silverman S, Shantsila E. The role of monocytes in angiogenesis and atherosclerosis. Journal of the American College of Cardiology. 2014;63:1-11.

[173] Varga T, Mounier R, Horvath A, Cuvellier S, Dumont F, Poliska S, et al. Highly Dynamic Transcriptional Signature of Distinct Macrophage Subsets during Sterile Inflammation, Resolution, and Tissue Repair. The Journal of Immunology. 2016.

[174] Jetten N, Verbruggen S, Gijbels MJ, Post MJ, De Winther MP, Donners MM. Anti-inflammatory M2, but not pro-inflammatory M1 macrophages promote angiogenesis in vivo. Angiogenesis. 2014;17:109-18.

[175] Takeda Y, Costa S, Delamarre E, Roncal C, Leite de Oliveira R, Squadrito ML, et al. Macrophage skewing by Phd2 haplodeficiency prevents ischaemia by inducing arteriogenesis. Nature. 2011;479:122-6.

[176] Summan M, Warren GL, Mercer RR, Chapman R, Hulderman T, Van Rooijen N, et al. Macrophages and skeletal muscle regeneration: a clodronate-containing liposome depletion study. American Journal of Physiology - Regulatory, Integrative and Comparative Physiology. 2006;290:R1488-R95.

[177] Wang H, Melton DW, Porter L, Sarwar ZU, McManus LM, Shireman PK. Altered macrophage phenotype transition impairs skeletal muscle regeneration. The American journal of pathology. 2014;184:1167-84.

[178] Guihard P, Danger Y, Brounais B, David E, Brion R, Delecrin J, et al. Induction of osteogenesis in mesenchymal stem cells by activated monocytes/macrophages depends on oncostatin M signaling. Stem Cells. 2012;30:762-72.

[179] Ludin A, Itkin T, Gur-Cohen S, Mildner A, Shezen E, Golan K, et al. Monocytes-macrophages that express alpha-smooth muscle actin preserve primitive hematopoietic cells in the bone marrow. Nat Immunol. 2012;13:1072-82.

[180] Song E, Ouyang N, Horbelt M, Antus B, Wang M, Exton MS. Influence of alternatively and classically activated macrophages on fibrogenic activities of human fibroblasts. Cellular immunology. 2000;204:19-28.

[181] Lemos DR, Babaeijandaghi F, Low M, Chang CK, Lee ST, Fiore D, et al. Nilotinib reduces muscle fibrosis in chronic muscle injury by promoting TNF-mediated apoptosis of fibro/adipogenic progenitors. Nature medicine. 2015;21:786-94.

[182] Garg K, Ward CL, Hurtgen BJ, Wilken JM, Stinner DJ, Wenke JC, et al. Volumetric muscle loss: Persistent functional deficits beyond frank loss of tissue. Journal of Orthopaedic Research. 2015;33:40-6.

[183] Rivera J, Proia RL, Olivera A. THE ALLIANCE OF SPHINGOSINE-1-PHOSPHATE AND ITS RECEPTORS IN IMMUNITY. Nature reviews Immunology. 2008;8:753-63.

[184] Das A, Segar CE, Hughley BB, Bowers DT, Botchwey EA. The promotion of mandibular defect healing by the targeting of S1P receptors and the recruitment of alternatively activated macrophages. Biomaterials. 2013;34:9853-62.

[185] He H, Xu J, Warren CM, Duan D, Li X, Wu L, et al. Endothelial cells provide an instructive niche for the differentiation and functional polarization of M2-like macrophages. Blood. 2012;120:3152-62.

[186] Ryu JC, Davidson BP, Xie A, Qi Y, Zha D, Belcik JT, et al. Molecular imaging of the paracrine proangiogenic effects of progenitor cell therapy in limb ischemia. Circulation. 2013;127:710-9.

[187] Guendel AM, Martin KS, Cutts J, Foley PL, Bailey AM, Mac Gabhann F, et al. Murine spinotrapezius model to assess the impact of arteriolar ligation on microvascular function and remodeling. J Vis Exp. 2013:e50218.

[188] Bailey AM, O'Neill TJt, Morris CE, Peirce SM. Arteriolar remodeling following ischemic injury extends from capillary to large arteriole in the microcirculation. Microcirculation (New York, NY : 1994). 2008;15:389-404.

[189] Awojoodu AO, Ogle ME, Sefcik LS, Bowers DT, Martin K, Brayman KL, et al. Sphingosine 1-phosphate receptor 3 regulates recruitment of anti-inflammatory monocytes to microvessels during implant arteriogenesis. Proceedings of the National Academy of Sciences. 2013.

[190] Bruce AC, Kelly-Goss MR, Heuslein JL, Meisner JK, Price RJ, Peirce SM. Monocytes are recruited from venules during arteriogenesis in the murine spinotrapezius ligation model. Arteriosclerosis, thrombosis, and vascular biology. 2014;34:2012-22.

[191] McDougall S, Dallon J, Sherratt J, Maini P. Fibroblast migration and collagen deposition during dermal wound healing: mathematical modelling and clinical implications. Philosophical transactions Series A, Mathematical, physical, and engineering sciences. 2006;364:1385-405.

[192] Das A, Segar CE, Chu Y, Wang TW, Lin Y, Yang C, et al. Bioactive lipid coating of bone allografts directs engraftment and fate determination of bone marrow-derived cells in rat GFP chimeras. Biomaterials. 2015;64:98-107.

[193] Rodriguez A, Macewan SR, Meyerson H, Kirk JT, Anderson JM. The foreign body reaction in T-cell-deficient mice. J Biomed Mater Res A. 2009;90:106-13.

[194] Jung S, Aliberti J, Graemmel P, Sunshine MJ, Kreutzberg GW, Sher A, et al. Analysis of fractalkine receptor CX(3)CR1 function by targeted deletion and green fluorescent protein reporter gene insertion. Mol Cell Biol. 2000;20:4106-14.

[195] He L, Marneros AG. Doxycycline inhibits polarization of macrophages to the proangiogenic M2-type and subsequent neovascularization. The Journal of biological chemistry. 2014;289:8019-28.

[196] Zajac E, Schweighofer B, Kupriyanova TA, Juncker-Jensen A, Minder P, Quigley JP, et al. Angiogenic capacity of M1- and M2-polarized macrophages is determined by the levels of TIMP-1 complexed with their secreted proMMP-9. Blood. 2013;122:4054-67.

[197] Olingy CE, San Emeterio CL, Ogle ME, Krieger JR, Bruce AC, Pfau DD, et al. Non-classical monocytes are biased progenitors of wound healing macrophages during soft tissue injury. Sci Rep. 2017;7:447.

[198] Troidl C, Jung G, Troidl K, Hoffmann J, Mollmann H, Nef H, et al. The temporal and spatial distribution of macrophage subpopulations during arteriogenesis. Current vascular pharmacology. 2013;11:5-12.

[199] Tonkin J, Temmerman L, Sampson RD, Gallego-Colon E, Barberi L, Bilbao D, et al. Monocyte/Macrophage-derived IGF-1 Orchestrates Murine Skeletal Muscle Regeneration and Modulates Autocrine Polarization. Mol Ther. 2015;23:1189-200.

[200] Annabi N, Tamayol A, Uquillas JA, Akbari M, Bertassoni LE, Cha C, et al. 25th anniversary article: Rational design and applications of hydrogels in regenerative medicine. Adv Mater. 2014;26:85-123.

[201] Zisch AH, Lutolf MP, Ehrbar M, Raeber GP, Rizzi SC, Davies N, et al. Cell-demanded release of VEGF from synthetic, biointeractive cell ingrowth matrices for vascularized tissue growth. FASEB J. 2003;17:2260-2.

[202] DeForest CA, Polizzotti BD, Anseth KS. Sequential click reactions for synthesizing and patterning three-dimensional cell microenvironments. Nat Mater. 2009;8:659-64.

[203] Mothe AJ, Tam RY, Zahir T, Tator CH, Shoichet MS. Repair of the injured spinal cord by transplantation of neural stem cells in a hyaluronan-based hydrogel. Biomaterials. 2013;34:3775-83.

[204] Kloxin AM, Kasko AM, Salinas CN, Anseth KS. Photodegradable hydrogels for dynamic tuning of physical and chemical properties. Science. 2009;324:59-63.

[205] Chatterjee K, Lin-Gibson S, Wallace WE, Parekh SH, Lee YJ, Cicerone MT, et al. The effect of 3D hydrogel scaffold modulus on osteoblast differentiation and mineralization revealed by combinatorial screening. Biomaterials. 2010;31:5051-62.

[206] Phelps EA, Enemchukwu NO, Fiore VF, Sy JC, Murthy N, Sulchek TA, et al. Maleimide cross-linked bioactive PEG hydrogel exhibits improved reaction kinetics and cross-linking for cell encapsulation and in situ delivery. Adv Mater. 2012;24:64-70, 2.

[207] Gajanayake T, Olariu R, Leclere FM, Dhayani A, Yang Z, Bongoni AK, et al. A single localized dose of enzyme-responsive hydrogel improves long-term survival of a vascularized composite allograft. Sci Transl Med. 2014;6:249ra110.

[208] Sharma B, Fermanian S, Gibson M, Unterman S, Herzka DA, Cascio B, et al. Human cartilage repair with a photoreactive adhesive-hydrogel composite. Sci Transl Med. 2013;5:167ra6.

[209] Vegas AJ, Veiseh O, Gurtler M, Millman JR, Pagliuca FW, Bader AR, et al. Long-term glycemic control using polymer-encapsulated human stem cell-derived beta cells in immune-competent mice. Nat Med. 2016;22:306-11.

[210] Murray PJ, Allen JE, Biswas SK, Fisher EA, Gilroy DW, Goerdt S, et al. Macrophage activation and polarization: nomenclature and experimental guidelines. Immunity. 2014;41:14-20.

[211] Xue J, Sharma V, Hsieh MH, Chawla A, Murali R, Pandol SJ, et al. Alternatively activated macrophages promote pancreatic fibrosis in chronic pancreatitis. Nat Commun. 2015;6:7158.

[212] Ernst PB, Gold BD. The disease spectrum of Helicobacter pylori: the immunopathogenesis of gastroduodenal ulcer and gastric cancer. Annu Rev Microbiol. 2000;54:615-40.

[213] Zhao QH, McNally AK, Rubin KR, Renier M, Wu Y, Rose-Caprara V, et al. Human plasma alpha 2-macroglobulin promotes in vitro oxidative stress cracking of Pellethane 2363-80A: in vivo and in vitro correlations. J Biomed Mater Res. 1993;27:379-88.

[214] Hern DL, Hubbell JA. Incorporation of adhesion peptides into nonadhesive hydrogels useful for tissue resurfacing. J Biomed Mater Res. 1998;39:266-76.

[215] Lutolf MP, Lauer-Fields JL, Schmoekel HG, Metters AT, Weber FE, Fields GB, et al. Synthetic matrix metalloproteinase-sensitive hydrogels for the conduction of tissue regeneration: engineering cell-invasion characteristics. Proc Natl Acad Sci U S A. 2003;100:5413-8.

[216] Kao WJ, McNally AK, Hiltner A, Anderson JM. Role for interleukin-4 in foreign-body giant cell formation on a poly(etherurethane urea) in vivo. J Biomed Mater Res. 1995;29:1267-75.

[217] Pfaff M, Tangemann K, Muller B, Gurrath M, Muller G, Kessler H, et al. Selective recognition of cyclic RGD peptides of NMR defined conformation by alpha IIb beta 3, alpha V beta 3, and alpha 5 beta 1 integrins. J Biol Chem. 1994;269:20233-8.

[218] Amir el AD, Davis KL, Tadmor MD, Simonds EF, Levine JH, Bendall SC, et al. viSNE enables visualization of high dimensional single-cell data and reveals phenotypic heterogeneity of leukemia. Nat Biotechnol. 2013;31:545-52.

[219] Cobelli N, Scharf B, Crisi GM, Hardin J, Santambrogio L. Mediators of the inflammatory response to joint replacement devices. Nat Rev Rheumatol. 2011;7:600-8.

[220] Steiert AE, Boyce M, Sorg H. Capsular contracture by silicone breast implants: possible causes, biocompatibility, and prophylactic strategies. Med Devices (Auckl). 2013;6:211-8.

[221] Hannan MA, Mutashar S, Samad SA, Hussain A. Energy harvesting for the implantable biomedical devices: issues and challenges. Biomed Eng Online. 2014;13:79.

[222] Slaughter BV, Khurshid SS, Fisher OZ, Khademhosseini A, Peppas NA. Hydrogels in regenerative medicine. Adv Mater. 2009;21:3307-29.

[223] Doloff JC, Veiseh O, Vegas AJ, Tam HH, Farah S, Ma M, et al. Colony stimulating factor-1 receptor is a central component of the foreign body response to biomaterial implants in rodents and non-human primates. Nat Mater. 2017.

[224] Shekaran A, Garcia AJ. Nanoscale engineering of extracellular matrix-mimetic bioadhesive surfaces and implants for tissue engineering. Biochim Biophys Acta. 2011;1810:350-60.

[225] Barczyk M, Carracedo S, Gullberg D. Integrins. Cell Tissue Res. 2010;339:269-80.

[226] De Jong WH, Dormans JA, Van Steenbergen MJ, Verharen HW, Hennink WE. Tissue response in the rat and the mouse to degradable dextran hydrogels. J Biomed Mater Res A. 2007;83:538-45.

[227] !!! INVALID CITATION !!! [57].

[228] Lovett M, Lee K, Edwards A, Kaplan DL. Vascularization strategies for tissue engineering. Tissue Eng Part B Rev. 2009;15:353-70.

[229] Weis SM, Cheresh DA. Pathophysiological consequences of VEGF-induced vascular permeability. Nature. 2005;437:497-504.

[230] Silva EA, Mooney DJ. Spatiotemporal control of vascular endothelial growth factor delivery from injectable hydrogels enhances angiogenesis. J Thromb Haemost. 2007;5:590-8.

[231] Olsson AK, Dimberg A, Kreuger J, Claesson-Welsh L. VEGF receptor signalling - in control of vascular function. Nat Rev Mol Cell Biol. 2006;7:359-71.

[232] Casazza A, Laoui D, Wenes M, Rizzolio S, Bassani N, Mambretti M, et al. Impeding macrophage entry into hypoxic tumor areas by Sema3A/Nrp1 signaling blockade inhibits angiogenesis and restores antitumor immunity. Cancer Cell. 2013;24:695-709.

[233] Liu C, Wu C, Yang Q, Gao J, Li L, Yang D, et al. Macrophages Mediate the Repair of Brain Vascular Rupture through Direct Physical Adhesion and Mechanical Traction. Immunity. 2016;44:1162-76.

[234] Hilgendorf I, Gerhardt LM, Tan TC, Winter C, Holderried TA, Chousterman BG, et al. Ly-6Chigh monocytes depend on Nr4a1 to balance both inflammatory and reparative phases in the infarcted myocardium. Circ Res. 2014;114:1611-22.

[235] Christoffersson G, Vagesjo E, Vandooren J, Liden M, Massena S, Reinert RB, et al. VEGF-A recruits a proangiogenic MMP-9-delivering neutrophil subset that induces angiogenesis in transplanted hypoxic tissue. Blood. 2012;120:4653-62.

[236] Curiel TJ, Cheng P, Mottram P, Alvarez X, Moons L, Evdemon-Hogan M, et al. Dendritic cell subsets differentially regulate angiogenesis in human ovarian cancer. Cancer Res. 2004;64:5535-8.

[237] Garcia JR, Clark AY, Garcia AJ. Integrin-specific hydrogels functionalized with VEGF for vascularization and bone regeneration of critical-size bone defects. J Biomed Mater Res A. 2016;104:889-900.

[238] Phelps EA, Landazuri N, Thule PM, Taylor WR, Garcia AJ. Bioartificial matrices for therapeutic vascularization. Proc Natl Acad Sci U S A. 2010;107:3323-8.

[239] Olin JW, Sealove BA. Peripheral artery disease: current insight into the disease and its diagnosis and management. Mayo Clin Proc. 2010;85:678-92.

[240] Sarris M, Masson JB, Maurin D, Van der Aa LM, Boudinot P, Lortat-Jacob H, et al. Inflammatory chemokines direct and restrict leukocyte migration within live tissues as glycan-bound gradients. Curr Biol. 2012;22:2375-82.

[241] Somanath PR, Malinin NL, Byzova TV. Cooperation between integrin alphavbeta3 and VEGFR2 in angiogenesis. Angiogenesis. 2009;12:177-85.

[242] Senger DR, Claffey KP, Benes JE, Perruzzi CA, Sergiou AP, Detmar M. Angiogenesis promoted by vascular endothelial growth factor: regulation through alpha1beta1 and alpha2beta1 integrins. Proc Natl Acad Sci U S A. 1997;94:13612-7.

[243] Oyama T, Ran S, Ishida T, Nadaf S, Kerr L, Carbone DP, et al. Vascular endothelial growth factor affects dendritic cell maturation through the inhibition of nuclear factor-kappa B activation in hemopoietic progenitor cells. J Immunol. 1998;160:1224-32.

[244] Galis ZS, Khatri JJ. Matrix metalloproteinases in vascular remodeling and atherogenesis: the good, the bad, and the ugly. Circ Res. 2002;90:251-62.

[245] Garg K, Corona BT, Walters TJ. Therapeutic strategies for preventing skeletal muscle fibrosis after injury. Frontiers in pharmacology. 2015;6:87.

[246] Sefcik LS, Aronin CE, Awojoodu AO, Shin SJ, Mac Gabhann F, MacDonald TL, et al. Selective activation of sphingosine 1-phosphate receptors 1 and 3 promotes local microvascular network growth. Tissue Eng Part A. 2011;17:617-29.

[247] Lu JM, Wang X, Marin-Muller C, Wang H, Lin PH, Yao Q, et al. Current advances in research and clinical applications of PLGA-based nanotechnology. Expert Rev Mol Diagn. 2009;9:325-41.

[248] Lee Y, Kwon J, Khang G, Lee D. Reduction of inflammatory responses and enhancement of extracellular matrix formation by vanillin-incorporated poly(lactic-co-glycolic acid) scaffolds. Tissue Eng Part A. 2012;18:1967-78.

[249] Ogle ME, Krieger JR, Tellier LE, McFaline-Figueroa J, Temenoff JS, Botchwey EA. Dual Affinity Heparin-Based Hydrogels Achieve Pro-Regenerative Immunomodulation and Microvascular Remodeling. ACS Biomaterials Science & Engineering. 2017.

[250] Allende ML, Yamashita T, Proia RL. G-protein-coupled receptor S1P1 acts within endothelial cells to regulate vascular maturation. Blood. 2003;102:3665-7.

[251] Kono M, Mi Y, Liu Y, Sasaki T, Allende ML, Wu YP, et al. The sphingosine-1-phosphate receptors S1P1, S1P2, and S1P3 function coordinately during embryonic angiogenesis. J Biol Chem. 2004;279:29367-73.

[252] Gundra UM, Girgis NM, Ruckerl D, Jenkins S, Ward LN, Kurtz ZD, et al. Alternatively activated macrophages derived from monocytes and tissue macrophages are phenotypically and functionally distinct. Blood. 2014;123:e110-22.

[253] Burzyn D, Kuswanto W, Kolodin D, Shadrach JL, Cerletti M, Jang Y, et al. A special population of regulatory T cells potentiates muscle repair. Cell. 2013;155:1282-95.

[254] Hanna RN, Cekic C, Sag D, Tacke R, Thomas GD, Nowyhed H, et al. Patrolling monocytes control tumor metastasis to the lung. Science. 2015;350:985-90.

[255] Sica A, Schioppa T, Mantovani A, Allavena P. Tumour-associated macrophages are a distinct M2 polarised population promoting tumour progression: potential targets of anti-cancer therapy. Eur J Cancer. 2006;42:717-27.